DRIVERS AND VARIABILITY OF IRON REDUCTION IN UPLAND SOILS

by

CAITLIN HODGES

(Under the Direction of Aaron Thompson)

ABSTRACT

Soil iron reduction influences ecosystems by altering the cycling of carbon, nutrients, and trace elements. Much of our understanding of soil iron reduction stems from in-lab investigations of wetland soils. However, recent work indicates iron reduction can occur in a range of upland soils, with clear implications for soil carbon dynamics. To better elucidate Fe redox in upland soils, two experiments were conducted in the Southeastern Piedmont of South Carolina and across age and climate gradients of Hawaii. In the piedmont soils, we found the potential for Fe reduction to vary with intensity and depth over a year, dependent upon soil moisture and carbon. In Hawaii, potential for Fe reduction increased with precipitation, with no effect of parent material age. These results provide strong *in situ* evidence of Fe reduction in soils previously considered to be redox inactive, and indicate environmental factors and inputs necessary to foster upland Fe reduction.

INDEX WORDS: Soil Iron; Electromagnetic Induction; Calhoun Critical Zone Observatory; Long Substrate Age Gradient; Maui Climate Gradient; Carbon Cycle; Anaerobic Respiration; Hawaiian Islands; Piedmont Soil

DRIVERS AND VARIABILITY OF IRON REDOX IN UPLAND SOILS

by

CAITLIN HODGES

BSES, University of Georgia, 2014

A Thesis Submitted to the Graduate Faculty of the University of Georgia in Partial Fulfillment of the Requirements for the Degree

MASTER OF SCIENCE

ATHENS, GA

2017

DRIVERS AND VARIABILITY OF IRON REDUCTION IN UPLAND SOILS

by

CAITLIN HODGES

Major Professor: Aaron Thompson

Committee: Daniel Markewitz

Ford Ballantyne

Electronic Version Approved:

Suzanne Barbour

Dean of the Graduate School

The University of Georgia

May, 2017

TABLE OF CONTENTS

LIST OF TABLES

Page

LIST OF FIGURES

Page

CHAPTER 1

INTRODUCTION AND LITERATURE REVIEW

Iron minerals play a key role in governing biogeochemical cycles in soils. Plant nutrients, like phosphorus and molybdenum, are bound to high surface area, poorly crystalline Fe(III) minerals, while the use of Fe(III) as a terminal electron acceptor, or Fe(II) as an electron donor, by microbial populations tightly links Fe to the soil carbon cycle (Stumm and Sulzberger, 1992; Goldberg and Forster, 1996; Li et al., 2012). Under low-oxygen conditions (i.e. when biological oxygen demand is high) microbes seek out alternate electron acceptors (Sexstone and Parkin, 1985). Elements with high affinities for electrons, like NO_3^- and $Mn^{(IV)}$, are quickly depleted from soil upon the onset of low oxygen conditions conditions. This drives microbes to utilize Fe(III) in short-range ordered minerals as a terminal electron acceptor, according to energy yield (Peters and Conrad, 1996). Fe(III) respiration is particularly prevalent in older soils of humid climates that are leached of other potential electron acceptors (like Mn(IV)) (Küsel et al., 2002). When microbes utilize Fe(III)-minerals during respiration, the minerals undergo reductive dissolution and release any bound minerals, nutrients, trace metals, and carbon, with important effects on nutrient availability, contaminant mobility, and soil carbon flux (Miller et al., 2001; Peretyazhko and Sposito, 2005; Chacon et al., 2006; Borch et al., 2009) .

Environments that undergo frequent fluctuations in soil oxygen, or are anoxic for the majority of the time, like wetlands, sediments, and rainforest soils, have been the focus of the majority of the research on Fe redox (Lovley and Phillips, 1988; Roden et al., 2004; Pett-Ridge et al., 2006; Fakih et al., 2008; Dubinsky et al., 2010). However, recent work has found that

upland soils that do not regularly experience anoxia have a high capacity for iron reduction (De-Campos et al., 2012; Yang and Liptzin, 2015). In some upland soils nearly half of total respiration is attributed to Fe reduction during particularly "hot" moments, like spring/summer ice melt or extreme precipitation events (Lipson et al., 2013; McNicol and Silver, 2014). Upland, well-drained soils are known to form anoxic microsites that produce high levels of the reduced species N_20, Fe^{+2}, Mn^{+2}, S, and CH_4 (Küsel et al., 2002; Megonigal and Guenther, 2008). During times that oxygen diffusion is limited, these alternate respiration pathways become particularly important in terms of nutrient and carbon flux.

In upland soils with fluctuating oxygen status, microbial populations are replete with facultative aerobes that have the capacity to utilize alternate electron acceptors under low-oxygen conditions (Pett-Ridge et al., 2006; DeAngelis et al., 2010). Research indicates, however, that not just soils with fluctuating Eh have populations of bacteria that can readily utilize Fe(III) as a terminal electron acceptor. Indeed, in-lab incubations of predominately oxic upland soils that rarely undergo redox fluctuations have demonstrated that nearly all soils have the capacity to undergo significant iron reduction under low-oxygen conditions (De-Campos et al., 2012; McNicol and Silver, 2014; Yang and Liptzin, 2015). Additionally, even soils that seem inhospitable towards iron reduction in terms of iron and carbon concentrations host populations of bacteria that have the potential to reduce Fe(III) (Fimmen et al., 2008; Yang and Liptzin, 2015). Fe reduction in upland soils is most likely pervasive in many ecosystems, and plays a widespread role in soil biogeochemistry.

The mechanistic understanding of Fe reduction has not been applied successfully to characterizing the process (Hall et al., 2013). It is challenging to measure iron redox *in situ*. Platinum electrodes measure soil redox potential, but present certain problems when used in the

field; they are strongly affected by the immediate surrounding soil and solution chemistry, are very sensitive to minute changes in the environment, and only make point observations that rarely represent the overall condition of the soil (Mansfeldt, 2003; Vorenhout et al., 2004). Some suggest that soil redox potential measurements are only useful when made repeatedly, in replicate, over extended periods of months to years (Rabenhorst and Hively, 2009). To circumvent the problems with platinum probes, researchers have developed passive probes, which have principally been used in wetland soils to examine high water table dynamics (Bridgham and Faulkner, 1991; Castenson and Rabenhorst, 2006; Jenkinson and Franzmeier, 2006; Rabenhorst and Burch, 2006; Fakih et al., 2008; Owens et al., 2008; Rabenhorst and Hively, 2009; Stiles et al., 2010; Dorau and Mansfeldt, 2015). These passive probes track the changes and dissolution of a redox-sensitive species, like Fe or Mn oxides, affixed to a probe. While passive probes are more or less effective at characterizing hydric soils, they are still quite delicate and may not be suited to the purpose of characterizing upland soil iron reduction (Stiles et al., 2010).

When viewing iron reduction within and across landscapes, it is useful to take into account hydrologic regimes and vadose zone water relations, as iron reduction is favored under higher precipitation conditions in convergent landscape positions, and areas of low relief, like upland flats and riparian zones, which retain water for prolonged periods of time (Yesavage et al., 2012; Jackson et al., 2014). High precipitation facilitates the presence of more frequent and prolonged microsites, and flat landscape positions provide for slower water movement, giving microbes an opportunity to deplete the rainwater of oxygen (Zaslavsky and Rogowski 1969).

Using information on site soil moisture and precipitation, in conjunction with passive redox probes, I sought to characterize the *in situ* potential for iron redox in an upland humid

temperate forest, and across the Hawaiian Islands at sites that vary in climate. With respect to the humid, temperate forest I sought to answer two questions: 1) What is the variability of iron reduction in first-order watersheds of a humid, temperate, forested ecosystem. and 2) What are the drivers of that observed variability? Across the Hawaiian sites, I asked, how does soil iron reduction respond to increases in mean annual precipitation and parent material age. Answers to these questions will provide critical information on the role of soil iron minerals in controlling the biogeochemical cycling of elements (most importantly C and P) in humid, forested, systems.

REQUIREMENTS FOR SOIL IRON REDUCTION

There are four main requirements for Fe reduction in soils: (1) Fe-reducing bacteria, (2) an electron donor, (3) adequate Fe^{III} concentrations, (4) and conditions excluding oxygen from the preceding three (Lovley et al., 2004). 1) Studies have shown that many soil bacteria, not just those typically considered as "Fe-reducers," have the ability to reduce Fe^{III} when it is energetically favorable (Pett-Ridge et al., 2006; DeAngelis et al., 2010). Once high-energy terminal electron acceptors, like oxygen, nitrate, and Mn^{IV}, have been consumed, many soil bacteria will automatically switch to Fe respiration (Patrick and Jugsujinda, 1992; Peters and Conrad, 1996). Therefore, most of the soil, particularly horizons that already host large populations of soil bacteria, have the potential to foster Fe-reducing microbes. 2) Typically, the electron donor of choice for microbe-mediated Fe reduction is organic carbon. Most soils decrease in organic carbon with depth, but roots, their exudates, and other biomass at depth can foster microbial biomass deep in the soil environment. Although, soils and horizons that are poor in terms of organic carbon can have a high potential to reduce Fe if reduced forms of carbon become available (Hong et al., 2010; Yang and Liptzin, 2015). 3) Fe minerals are ubiquitous in

nearly all upland soils. Well-drained soils mostly contain crystalline Fe^{III}, soils with fluctuating water tables contain a mix of ordered and short-range-ordered Fe^{III} minerals, and poorly drained soils either contain unordered Fe^{II} minerals or are depleted in all forms of Fe (Kämpf and Schwertmann, 1983; Maxbauer et al., 2016). While Fe-reducing microorganisms have the ability to reduce Fe^{III} in most minerals, short-range-ordered minerals are most easily and quickly reduced, so that soils with less-structured minerals are more likely to have a high potential for Fe reduction.

4) In the presence of oxygen, soil Fe reduction is thermodynamically unfavorable. For this reason, factors affecting soil oxygen have been well studied with respect to Fe reduction. Soil moisture is thought to be an important control of oxygen concentrations in soils, as the diffusion of oxygen through water is much slower than through air-filled pores. Early laboratory studies of soils in labs found that following soil flooding, utilization of terminal electron acceptors followed the thermodynamic stability of the redox couple, with oxygen, NO_3^-, Mn^{IV}, and then Fe^{III} subsequently reduced from the substrate (Peters and Conrad, 1996; Küsel et al., 2002; De-Campos et al., 2012). However, studies of less-disturbed soil samples (either in laboratory or field settings) indicate that multiple redox couples operate simultaneously as pores of different sizes deliver oxygen at different rates, with the least amount of oxygen reaching the interior of a ped, to which oxygen must follow a tortuous path of mostly micropores (Sexstone and Parkin, 1985; Roy et al., 1997; van der Lee et al., 1999; Parry et al., 1999; Rabot et al., 2014). The second part of these findings from the less-disturbed soils is that soil moisture still plays a large role in determining which redox couples proceed. Generally, wetter soils host a wider range of redox couples, while in drier soils, only oxygen and denitrification take place. However, this does not mean that saturation is a necessity, as Fe reduction has been found to

occur in soils under ambient conditions that are at 50% water filled pore space (Sexstone and Parkin, 1985). Soil carbon also plays a large, if less straightforward, role in the oxygen concentration of soil, because pulses of labile carbon stimulate microbial activity so that the rate of oxygen consumption outpaces the rate of diffusion. If oxygen diffusion is not meeting the respiration needs of the soil bacteria, they will switch to alternate terminal electron acceptors, like Fe^{III} (Hall et al., 2016).

FE REDOX AND BIOGEOCHEMICAL CYCLING

Fe minerals exert strong controls on the mobility and plant availability of important soil constituents including C, plant macronutrients (especially P), many micronutrients, and other potentially toxic trace metals (Nealson and Saffarini, 1994; Borch et al., 2009; Li et al., 2012; Colombo et al., 2014). Multiple factors determine how Fe minerals control soil biogeochemical conditions. High surface-area Fe minerals act as strong sorption sites and retain soil constituents within the solum. Under low-oxygen conditions, Fe(III) reduction readily proceeds, and Fe acts as a common terminal electron acceptor in anaerobic respiration. Additionally, Fe is one of the most abundant elements in soils, and generally is retained as mass is lost through weathering and pedogenesis, resulting in many Fe-rich soils throughout upland systems. These factors - high surface area, redox activity, and ubiquity of Fe minerals in soils - makes them strong regulators of soil biogeochemistry across a range of soils (Colombo et al., 2014).

When soil microorganisms use Fe as a terminal electron acceptor for respiration, they mineralize soil C, thereby releasing CO_2 along with any potential elements in the organic material (like N, and S) (Li et al., 2012). This respiration under low oxygen conditions drives a potentially unaccounted for carbon and nutrient flux during periods of a perceived deceleration

of soil microorganism activity (Davidson et al., 1998; Scott-Denton et al., 2003; Lipson et al., 2010; McNicol and Silver, 2014; Hall and Silver, 2015). Carbon and Fe often co-precipitate in soils to form mineral-organic-associations. The carbon in these coprecipitates is released and mobilized when Fe(III) in the mineral association is reduced (Lundström et al., 2000; Buurman and Jongmans, 2005; Buettner et al., 2014) . On the other hand, many have found that Fe^{III} minerals control the retention of terrestrial carbon in soils and sediments, acting as a means of preventing DOC transport to surface waters through sorption and coprecipitation (Knorr, 2013; Gannon et al., 2015; Ekström et al., 2016; Linkhorst et al., 2016).

When Fe minerals undergo reductive dissolution, they release sorbed and otherwise associated constituents into the pedosphere (Li et al., 2012). This release can act as a means of remobilizing important nutrients for trees and soil organisms. In acidic, highly weathered soils, periodic reduction can act as an important source of P that would otherwise be strongly bound to Fe minerals (Hutchison and Hesterberg, 2004; Peretyazhko and Sposito, 2005; Chacon et al., 2006; Henderson et al., 2012). However, over geologic timescales, frequent or prolonged reducing conditions (and as a result Fe reduction) can potentially lead to a loss of key nutrients from the system, as mobilized nutrients are transported out of the regolith to groundwater instead of being re-captured by minerals or organisms (Miller et al., 2001).

SOIL IRON REDUCTION IN DIFFERENT ECOSYSTEMS

Recently, soil iron has come into greater focus as an important driver of terrestrial biogeochemical cycles. Initial research on soil iron reduction was conducted mainly in wetlands (hydric soils), and then tropical soils. Only recently have reducing processes in well-drained, upland soils, come to be seen as potentially important to a wide range of ecosystems. While

wetlands, tropical and sub-tropical rainforests, and temperate uplands are fundamentally different systems, it is useful to build a conceptual model, and then adjust that model as needed for each particular ecosystem's differences.

Wetlands

In wetland soils, redox processes are driven by microbial populations that use oxidized chemical species as a terminal electron acceptor during respiration. When soils flood, oxygen diffusion is limited, and microbial populations shift to the next most energetically favorable redox couple. This sequence of energetic favorability is as follows: aerobic respiration, denitrification, Mn^{IV} reduction, Fe^{III} reduction, and finally methanogenesis (Patrick and Jugsujinda, 1992; Peters and Conrad, 1996). The differences in thermodynamic favorability and limited oxygen diffusion creates redox gradients across the macroscale as redox potential decreases with depth, and across the meso and micro scale as redox potential decreases towards the center of a soil aggregate (Kögel-Knabner et al., 2010).

Tropical and Sub-Tropical Rainforest Soils

Warm rainforest soils have also been a focus with respect to Fe reduction because they have been documented to undergo frequent shifts in soil oxygen/redox potential. These shifts to low oxygen necessitate the use of alternate electron acceptors. However, studying these systems has presented greater challenges than wetlands, because upland soils encompass a wider range of soil texture, moisture, and nutrient inputs. This variation in spatial and temporal soil conditions increases the complexity of soil biogeochemical processes. While this site variability has presented some problems to characterization of this process, some have been successful. To this

point, we know that tropical and sub-tropical rainforests experience frequent Fe reduction events that are tied to soil oxygen, water, and carbon. These Fe reduction events have been tied to soil phosphorus release, and changes in soil carbon (Peretyazhko and Sposito, 2005; Chacon et al., 2006).

Other Soils

While iron reduction in systems other than warm rainforests has not been studied as closely, there has been a growing interest in upland reduction processes. This research has been spurred by findings that point to the capacity for predominately oxic soils to reduce iron (Fimmen et al., 2008; Li et al., 2008; Fuss et al., 2010; Hong et al., 2010; De-Campos et al., 2012; Yang and Liptzin, 2015). Additional investigation has uncovered high concentrations of Fe^{+2} in soil pore water, surface water, and groundwater after periods of high soil moisture conditions (Lipson et al., 2010; Knorr, 2013; Lipson et al., 2013; Ekström et al., 2016), pointing to Fe reduction under high soil moisture conditions. These in-lab and *in situ* investigations provide strong evidence for upland Fe reduction, but few have characterized the relationship of Fe reduction to varied landscapes and a-seasonality that is common in upland systems.

METHODS OF REDOX MEASUREMENTS

Although many soils indicate reducing conditions in the form of mottling or a reduced matrix, many more may experience reducing conditions without such a clear visual representation. For this reason, and to provide a better means of quantifying reducing conditions in soils, methods have been developed to track soil redox processes. While direct measurements of redox potential seem straightforward and easy to collect and interpret, platinum redox probes

present many difficulties. These platinum redox electrodes are strongly affected by the redox couple with the highest activity in a soil, and therefore skew all measurements toward the redox potential of that couple. Additionally, redox probes only measure the soil with which a platinum tip is in direct contact. This means that a redox measurement, even when taken in replicate, represents an infinitesimally small fraction of soil conditions, which are inherently heterogeneous. To be sure, studies have had the most successes with using platinum electrodes when the electrodes are installed over the course of months to years, and either tracked continuously with dataloggers or measured regularly. These methods present problems to the researcher who has little experience with computer programming, does not have regular access to the field-site, or does not have a large amount of time to devote to redox measurements.

To combat some of these issues with active, platinum redox probes, scientists have developed alternate methods that use passive means (i.e. no electrical current, or need to record with a computer) of measuring soil redox potential. While there are others, the most successful of these methods are those that utilize a redox-active mineral affixed to a passive surface that is inserted into the soil for a predetermined period of time. The incipient examples of these passive probes are zero-valent iron in the form of steel rods inserted into soil to determine water-table depth under varying soil moisture and water table conditions (McKee, 1978; Carnell and Anderson, 1986; Hook et al., 1987; Bridgham and Faulkner, 1991). Zero-valent iron in the rods oxidized to reddish $Fe^{(III)}$ minerals when in the presence of oxygen (low soil water content), and the iron remained gray (Fe^0) under reducing conditions. While water table is sometimes indicative of low redox potential, soil water can still contain oxygen that facilitates oxic processes (Owens et al., 2008). For this reason, Owens et al. (2008) measured soil oxygen over the period of time that the iron rods were installed in soils along a catena sequence, and found

that generation of bright rust was greatest at soil oxygen contents greater than 5%, and no rust formed when soil water dissolved oxygen concentrations were below 2 mg L^{-}.

Other studies have utilized minerals containing oxidized Fe affixed to rods to track iron reduction. These probes work in a similar way to the zero-valent iron rods in that they rely upon the redox reactions of Fe within the soil to indicate the level of oxidation/reduction occurring in the soils, but the focus of these rods is on reducing conditions. For example, Indicator of Reduction in Soils (IRIS) tubes are PVC tubes painted with poorly chrystalline Fe minerals. Fe mineral dissolution using image analysis is performed after installation in the soil for a period of three weeks. Jenkinson and Franzmeier (2006), and Castenson and Rabenhorst (2006), both used IRIS tubes to determine presence/absence of a high water table in hydric soils. Others have used this type of probe to examine the change in Fe minerals subjected to variable redox potentials *in situ*. There has also been work using Mn oxides in conjunction with Fe oxides to provide a more complete picture of soil reducing conditions. Mn oxides are more sensitive than Fe to reducing conditions, and therefore indicate reducing conditions in soils sooner than the ferrihydrite-coated IRIS tubes.

GEOPHYSICAL METHODS OF SOIL CHARACTERIZATION

Geophysical methods have grown in popularity for characterizing spatial and temporal variations in the pedosphere. These methods are useful because they provide a high-resolution characterization of soil texture, moisture, salinity, bulk density, structure, and other characteristics that would traditionally be mapped using intensive, destructive sampling techniques (Samouëlian et al., 2005) . The most apparently useful methods in the geophysical toolbox are those that utilize an electrical current or field that is sent into the soil, as soils, being

comprised of charged particles, air, and water, are inherently responsive to electricity (Tabbagh et al., 2000; Samouëlian et al., 2005). These geophysical techniques have been used to successfully locate geologic formations, soil features, permafrost, nutrient content, and contamination plumes (Doolittle et al., 1994; Corwin and Lesch, 2005; Samouëlian et al., 2005). Resistivity or conductivity is measured and recorded as a georeferenced data point, and mapped so that interpretations about soil properties can be made.

Two methods that are particularly useful in making high-resolution observations of soil properties over large spatial extents are electromagnetic induction (EMI) and soil electrical resistivity. An EMI probe projects an electromagnetic field to a certain depth into the soil; the ease at which the soil carries the electromagnetic field is recorded as apparent conductance. Apparent conductance is a weighted average of the soil conductivity to the depth of the electromagnetic field (Doolittle et al., 1994). The wetter and finer the soil, the greater the specific conductance (Doolittle et al., 1994; Corwin and Lesch, 2005; Francés and Lubczynski, 2011). Measurements can be collected nearly instantaneously so that measurements across the entirety of the study area can be surveyed with relative ease. The measurements are georeferenced so that a 2D surface conductivity map can be made through interpolation techniques in a geographic information system (GIS) software. With the conductivity map of the study area, locations that that vary in soil moisture, texture, and parent material may be pinpointed for further investigation (Harvey and Morgan, 2009).

Soil resistivity measurements use the same concept as soil electromagnetic induction, but simply measure the difficulty in the movement of an electrical current (Tabbagh et al., 2000; Samouëlian et al., 2005) . These probes are static and are therefore more difficult than EMI to use over large study areas. However, resistivity provides higher resolution depth data than EMI,

and is therefore very helpful in pinpointing soil horizonation and water tables (Corwin and Lesch, 2005; Francés and Lubczynski, 2011) . While EMI is most often used to make a 2D surface map of conductivity, resistivity data is often shown as a 2D "slice" into the earth. Again, like EMI, this method is useful for targeting specific areas of interest for further sampling. While augering and other more destructive methods can never be abandoned, the use of geophysical tools provides a useful means of collecting preliminary site data while preserving the site integrity for more focused destructive methods.

SOILS OF THE CALHOUN CZO

The Calhoun Critical Zone Observatory is located in Union County, South Carolina. The Calhoun Forest is a sub-tropical mixed hardwood-pine forest in the Piedmont of the Southeastern United States. While the majority of the soils of the Calhoun are ultisols derived from granitic gneiss, the soils of the experimental watersheds are mainly Hapludalfs of the Wilkes and Enon Series (Richter et al., 1994; Soil Survey Staff, 2016). Mean annual temperature of the Calhoun Experimental Forest is 16˚ C, and mean annual precipitation is about 1170 mm (Richter et al., 1994).

From European settlement to the 1950s, agriculture was the predominate land-use of the land that is now the Calhoun CZO. After the 1950s, the majority of the site was converted to pine forest, either through planting or secession (Richter et al., 1994) . The effects of agricultural erosion and subsequent reforestation on the biogeochemical cycling of this site has been the subject of many studies (e.g. Richter et al., 1994; Markewitz et al., 1998; Richter et al., 1999; Markewitz and Richter, 2000; Richter et al., 2000; 2006; Li et al., 2008) . From these studies we know that the soils of the Calhoun are depleted of Ca, Mg, N, B, and Mn due to the nutrient

demands from the developing forest and cessation of agricultural fertilization (Richter et al., 1994; 2000; Li et al., 2008). Similarly, the end of agricultural liming, and the increase of organic acid inputs from the newly grown trees, has decreased soil pH over the nearly 50 years of forest development (Richter et al., 1994; Markewitz et al., 1998). Especially relevant is that short-range-ordered Fe in the O and A horizons has increased nearly 10 times more than would be accounted for by accumulations in tree biomass (Li et al., 2008). These results demonstrate an upward translocation of Fe, and point to the importance of Fe in carbon and nutrient cycling in forested systems (Fimmen et al., 2008; Li et al., 2008).

HAWAIIAN LONG SUBSTRATE AGE GRADIENT

The Hawaiian Islands are exceptional in that they encompass a wide range of variation in soil forming processes that manifests systematically over a relatively small area. This is due to the nature of the formation of the Hawaiian archipelago, which is a chain of shield volcanoes originating from one hot spot in the earth's crust. This resulted in mountainous, volcanic islands of uniform parent material that vary in age over a short distance (Macdonald et al., 1983). The combination of the trade winds carrying humid air and the mountainous islands results in strong orographic effects that produce extreme ranges in precipitation. This variation in forming processes, especially climate and parent material age, lends the islands easily to studies focused on changes in soil chemical and physical processes with respect to the state factors of formation.

The great range of studies done on these sites is too large to completely cover in the scope of a short review (e.g. Vitousek and Howarth, 1991; Crews et al., 1995; Torn et al., 1997; Chadwick et al., 1999; Schuur and Matson, 2001; Kurtz et al., 2002; Chadwick et al., 2003; Chorover et al., 2004; Porder et al., 2007a; b; Mikutta et al., 2009; Vitousek et al., 2010;

Vitousek and Chadwick, 2013). Indeed, books have been written on the subject. In short, we know how mineralogy, nutrients, and carbon change with respect to both parent material age and climate on the Hawaiian basalt. The primary minerals of the fresh basalt initially weather to form poorly crystalline secondary minerals in intermediate (120-500 ky) substrates, which then slowly develop into crystalline secondary minerals (Torn et al., 1997; Chorover et al., 2004). It turns out that this intermediate age is important also in terms of nutrient and carbon retention (Torn et al., 1997; Porder and Chadwick, 2009; Vitousek and Chadwick, 2013). As the soils age past this intermediate age they lose rock-derived nutrients in addition to key structural elements Si, Al, and Fe (Chadwick et al., 2003; Vitousek and Chadwick, 2013). Climate works in a similar way as parent material age, as precipitation increases, so too does the initial release and then eventual loss of soil constituents (Vitousek and Chadwick, 2013).

REFERENCES

Borch, T., R. Kretzschmar, and A. Kappler. 2009. Biogeochemical redox processes and their impact on contaminant dynamics. Environmental Science & Technology 44: 15–23.

Bridgham, SD, and SP Faulkner. 1991. Steel rod oxidation as a hydrologic indicator in wetland soils. Soil Sci. Soc. Am. J. (55): 856–862.

Buettner, S., M. Kramer, O. Chadwick, and A. Thompson. 2014. Mobilization of colloidal carbon during iron reduction in basaltic soils. Geoderma (221-222): 139–145.

Buurman, P., and A.G. Jongmans. 2005. Podzolisation and soil organic matter dynamics. Geoderma 125(1-2): 71–83.

Caell, R., and M. Anderson. 1986. A Technique for Extensive Field Measurement of Soil Anaerobism by Rusting of Steel Rods. Forestry 59(2): 129–140.

De-Campos, A., C. Huang, and C. Johnston. 2012. Biogeochemistry of terrestrial soils as influenced by short-term flooding. Biogeochemistry (111): 239–252.

Castenson, K., and M. Rabenhorst. 2006. Indicator of Reduction in Soil (IRIS): Evaluation of a New Approach for Asessing Reduced Conditions in Soil. Soil Science Society of America (70): 1222–1226.

Chacon, N., W. Silver, E. Dubinsky, and D. Cusack. 2006. Iron reduction and soil phosphorus solubilization in humid tropical forests soils: the roles of labile carbon pools and an electron shuttle compound. Biogeochemistry 78: 67–84.

Chadwick O.A., L.A. Derry, P.M. Vitousek, B.T. Huebert, and L.O. Hedin. 1999. Changing sources of nutrients during four million years of ecosystem development. Nature 397(6719): 491–497.

Chadwick, O., R. Gavenda, E. Kelly, K. Ziegler, C. Olson, C. Elliott, and D. Hendricks. 2003. The impact of climate on the biogeochemical functioning of volcanic soils. Chemical Geology 202(3): 195–223.

Chorover, J., M. Amistadi, and O. Chadwick. 2004. Surface charge evolution of mineral-organic complexes during pedogenesis in Hawaiian basalt. Geochimica et Cosmochimica Acta 68(23): 4859–4876.

Colombo, C., G. Palumbo, J. He, and R. Pinton. 2014. Review on iron availability in soil: interaction of Fe minerals, plants, and microbes. Journal of Soils and Sediments 14(3).

Corwin, D., and Lesch. 2005. Characterizing soil spatial variability with apparent soil electrical conductivity: I. Survey protocols. Computers and Electronics in Agriculture (46): 103–133.

Crews, T., K. Kitayama, J. Fownes, R. Riley, D. Herbert, D. Mueller-Dombois, and P. Vitousek. 1995. Changes in Soil Phosphorus Fractions and Ecosystem Dynamics across a Long Chronosequence in Hawaii. Ecology 76(5): 1407–1424.

Davidson, E., E. Belk, and R.D. Boone. 1998. Soil water content and temperature as independent or confounded factors controlling soil respiration in a temperate mixed hardwood forest. Global change biology 4(2): 217–227.

DeAngelis, K., W. Silver, A.W. Thompson, and M.K. Firestone. 2010. Microbial communities acclimate to recurring changes in soil redox potential status. Environmental Microbiology 12(12): 3137–3149.

Doolittle, J., K. Sudduth, and N. Kitchen. 1994. Estimating depths to claypans using electromagnetic induction methods . J. Soil and Water Conservation 49(6): 572–575.

Dorau, K., and T. Mansfeldt. 2015. Manganese-Oxide-Coated Redox Bars as an Indicator of Reducing Conditions in Soils. Journal of Environmental Quality (44): 696–703.

Dubinsky, E., W. Silver, and M. Firestone. 2010. Tropical forest soil microbial communities couple iron and carbon biogeochemistry. Ecology 91(9).

Ekström, S., O. Regnell, H. Reader, A. Nilsson, S. Löfgren, and E. Kritzberg. 2016. Increasing concentrations of iron in surface waters as a consequence of reducing conditions in the catchment area. J Geophys Res Biogeosciences 121(2): 479–493.

Fakih, M., M. Davranche, A. Dia, B. Nowack, P. Petitjean, X. Châtellier, and G. Gruau. 2008. A new tool for in situ monitoring of Fe-mobilization in soils. Applied Geochemistry 23(12): 3372–3383.

Fimmen, R., D. RichterJr., D. Vasudevan, M. Williams, and L. West. 2008. Rhizogenic Fe–C redox cycling: a hypothetical biogeochemical mechanism that drives crustal weathering in upland soils. Biogeochemistry 87(2): 127–141.

Francés, A., and M. Lubczynski. 2011. Topsoil thickness prediction at the catchment scale by integration of invasive sampling, surface geophysics, remote sensing and statistical modeling. Journal of Hydrology 405(1-2): 3147.

Fuss, C., C. Driscoll, C. Johnson, R. Petras, and T. Fahey. 2010. Dynamics of oxidized and reduced iron in a northern hardwood forest. Biogeochemistry 104(1-3): 103–119.

Gannon, J.P., S.W. Bailey, K.J. McGuire, and J.B. Shanley. 2015. Flushing of distal hillslopes as an alternative source of stream dissolved organic carbon in a headwater catchment. Water Resources Research (51): 8114–8128.

Goldberg, S., and H. Forster. 1996. Molybdenum adsorption on oxides, clay minerals, and soils. Soil Science Society of America.

Hall, S., D. Liptzin, H. Buss, K. DeAngelis, and W. Silver. 2016. Drivers and patterns of iron redox cycling from surface to bedrock in a deep tropical forest soil: a new conceptual model. Biogeochemistry 130(1-2): 177–190.

Hall, S., W. McDowell, and W. Silver. 2013. When wet gets wetter: decoupling of moisture, redox biogeochemistry, and greenhouse gas fluxes in a humid tropical forest soil. Ecosystems (16): 576–589.

Hall, S., and W. Silver. 2015. Reducing conditions, reactive metals, and their interactions can explain spatial patterns of surface soil carbon in a humid tropical forest. Biogeochemistry 125: 149–165.

Harvey, O., and C. Morgan. 2009. Predicting regional-scale soil variability using a single calibrated apparent soil electrical conductivity model. Soil Science Society of America.

Henderson, R., N. Kabengi, N. Mantripagada, M. Cabrera, S. Hassan, and A. Thompson. 2012. Anoxia-induced release of colloid-and nanoparticle-bound phosphorus in grassland soils. Environmental Science & Technology 46: 11727–11734.

Hong, H., Y. Gu, K. Yin, K. Zhang, and Z. Li. 2010. Red soils with white net-like veins and their climate significance in south China. Geoderma 160(2): 197–207.

Hook, D.D., M.D. Murray, D.S. DeBell, and B.C. Wilson. 1987. Notes: Variation in Growth of Red Alder Families in Relation to Shallow Water Table Levels. Forest science 33(1): 224–229.

Hutchison, K., and D. Hesterberg. 2004. Dissolution of Phosphate in a Phosphorus-Enriched Ultisol as Affected by Microbial Reduction. J Environ Qual 33(5): 1793.

Jackson, C., M. Bitew, and E. Du. 2014. When interflow also percolates: downslope travel distances and hillslope process zones. Hydrological Processes 28(7): 3195–3200.

Jenkinson, B., and D. Franzmeier. 2006. Development and evaluation of iron-coated tubes that indicate reduction in soils. Soil Science Society of America (70): 183–191.

Knorr, K.-H. 2013. DOC-dynamics in a small headwater catchment as driven by redox fluctuations and hydrological flow paths–are DOC exports mediated by iron reduction/oxidation cycles? Biogeosciences 10(2): 891–904.

Kurtz, A., L. Derry, and O. Chadwick. 2002. Germanium-silicon fractionation in the weathering environment. Geochimica et Cosmochimica Acta 66(9): 1525–1537.

Kämpf, N., and U. Schwertmann. 1983. Goethite and hematite in a climosequence in southern Brazil and their application in classification of kaolinitic soils. Geoderma 29: 27–39.

Kögel-Knabner, I., W. Amelung, Z. Cao, and S. Fiedler. 2010. Biogeochemistry of paddy soils. Geoderma 157: 1–14.

Küsel, K., C. Wagner, T. Trinkwalter, A.S. Gobner, R. Baumler, and H.L. Drake. 2002. Microbial reduction of Fe (III) and turnover of acetate in Hawaiian soils. FEMS Microbiology Ecology 40: 73–81.

Lee, G. van der, B. de Winder, W. Bouten, and A. Tietama. 1999. Anoxic microsites in Douglas fir litter. Soil Biology and Biochemistry 31(9): 1295-1301.

Li, J., D. Richter, A. Mendoza, and P. Heine. 2008. Four-decade responses of soil trace elements to an aggrading old-field forest: B, Mn, Zn, Cu, and Fe. Ecology 891(10): 2911–2923.

Li, Y., S. Yu, J. Strong, and H. Wang. 2012. Are the biogeochemical cycles of carbon, nitrogen, sulfur, and phosphorus driven by the “FeIII–FeII redox wheel” in dynamic redox environments? J Soils Sediments 12(5): 683–693.

Linkhorst, A., T. Dittmar, and H. Waska. 2016. Molecular fractionation of dissolved organic matter in a shallow subterranean estuary: the role of the iron curtain. Environ Sci Technology 51(3): 1312–1320.

Lipson, D., M. Jha, T. Raab, and W.C. Oechel. 2010. Reduction of iron (III) and humic substances plays a major role in anaerobic respiration in an Arctic peat soil. Journal of Geophysical Research 115: 1–13.

Lipson, D., T. Raab, D. Goria, and J. Zlamal. 2013. The contribution of Fe (III) and humic acid reduction to ecosystem respiration in drained thaw lake basins of the Arctic Coastal Plain. Global Biogeochemical Cycles 27: 399–409.

Lovley, D., D. Holmes, and K. Nevin. 2004. Dissimilatory Fe(III) and Mn(IV) reduction. Adv Microb Physiol 49: 219–86.

Lovley D., and E. Phillips. 1988. Novel mode of microbial energy metabolism: organic carbon oxidation coupled to dissimilatory reduction of iron or manganese.Applied and Environmental Microbiology 54(6): 1472-1480.

Lundström, U.S., N. van Breemen, and D. Bain. 2000. The podzolization process. A review. Geoderma 94(2-4): 91-107.

Mansfeldt, T. 2003. In situ long-term redox potential measurements in a dyked marsh soil. Journal of Plant Nutrition and Soil Science 166: 210–219.

Markewitz, D., and D. Richter. 2000. Long-term soil potassium availability from a Kanhapludult to an aggrading loblolly pine ecosystem. Forest Ecology and Management 130: 109–129.

Markewitz, D., D. Richter, and H. Allen. 1998. Three decades of observed soil acidification in the Calhoun Experimental Forest: Has acid rain made a difference? Soil Science Society of America 62: 1428–1439.

Maxbauer, D.P., J.M. Feinberg, and D.L. Fox. 2016. Magnetic mineral assemblages in soils and paleosols as the basis for paleoprecipitation proxies: A review of magnetic methods and challenges. Earth-Science Reviews 155: 28–48.

McKee, W. 1978. Rust on iron rods indicate depth of soil water tables. Proc. Soil Moisture Site Productivity Symposium. US .

McNicol, G., and W. Silver. 2014. Separate effects of flooding and anaerobiosis on soil greenhouse gas emissions and redox sensitive biogeochemistry. Journal of Geophysical Research: Biogeosciences 119(4): 557–566.

Megonigal, J., and A. Guenther. 2008. Methane emissions from upland forest soils and vegetation. Tree Physiology 28: 491–498.

Mikutta, R., G. Schaumann, and D. Gildemeister. 2009. Biogeochemistry of mineral–organic associations across a long-term mineralogical soil gradient (0.3–4100kyr), Hawaiian Islands. Geochimica et Cosmochimica Acta 73: 2034–2060.

Miller, A., E. Schuur, and O. Chadwick. 2001. Redox control of phosphorus pools in Hawaiian montane forest soils. Geoderma 102: 219–237.

Nealson, K., and D. Saffarini. 1994. Iron and manganese in anaerobic respiration: environmental significance, physiology, and regulation. Annual Reviews in Microbiology 48: 311–343.

Owens, P., L. Wilding, W. Miller, and R. Griffin. 2008. Using iron metal rods to infer oxygen status in seasonally saturated soils. Catena 73: 197–203.

Parry, S., P. Renault, C. Chenu, and R. Lensi. 1999. Denitrification in pasture and cropped soil clods as affected by pore space structure. Soil Biol. Biochem.: 493–501.

Patrick, W., and A. Jugsujinda. 1992. Sequential reduction and oxidation of inorganic nitrogen, manganese, and iron in flooded soil. Soil Science Society of America 56: 1071–1073.

Peretyazhko, T., and G. Sposito. 2005. Iron (III) reduction and phosphorous solubilization in humid tropical forest soils. Geochimica et Cosmochimica Acta 69(14): 3643–3652.

Peters, V., and R. Conrad. 1996. Sequential reduction processes and initiation of CH 4 production upon flooding of oxic upland soils. Soil Biology and Biochemistry 28(3): 371–382.

Pett-Ridge, J., W. Silver, and M. Firestone. 2006. Redox Fluctuations Frame Microbial Community Impacts on N-cycling Rates in a Humid Tropical Forest Soil. Biogeochemistry 81(1): 95–110.

Porder, S., and O.A. Chadwick. 2009. Climate and soil age constraints on nutrient uplift and retention by plants. Ecology 90(3): 623–636.

Porder, S., G.E. Hilley, and O.A. Chadwick. 2007a. Chemical weathering, mass loss, and dust inputs across a climate by time matrix in the Hawaiian Islands. Earth and Planetary Science Letters 258(3-4): 414–427.

Porder, S., P. Vitousek, O. Chadwick, and C. Chamberlain. 2007b. Uplift, erosion, and phosphorus limitation in terrestrial ecosystems. Ecosystems 10: 158–170.

Prem, M., H. Hansen, W. Wenzel, L. Heiberg, H. Sørensen, and O. Borggaard. 2014. High Spatial and Fast Changes of Iron Redox State and Phosphorus Solubility in a Seasonally Flooded Temperate Wetland Soil. Wetlands 35(2): 237–246.

Rabenhorst, M., and S. Burch. 2006. Synthetic iron oxides as an indicator of reduction in soils (IRIS). Soil Science Society of America 70: 1227–1236.

Rabenhorst, M., and W. Hively. 2009. Measurements of soil redox potential. Soil Science Society of America Journal 73: 668–674.

Rabot, E., C. Hénault, and I. Cousin. 2014. Temporal Variability of Nitrous Oxide Emissionsby Soils as Affected by Hydric History. Soil Science Society of America 78: 434–444.

Richter, D., H. Allen, J. Li, D. Markewitz, and J. Raikes. 2006. Bioavailability of slowly cycling soil phosphorus: major restructuring of soil P fractions over four decades in an aggrading forest. Oecologia 150: 259–271.

Richter, D., D. Markewitz, P. Heine, and V. Jin. 2000. Legacies of agriculture and forest regrowth in the nitrogen of old-field soils. Forest Ecology and Management 138: 233–248.

Richter, D., D. Markewitz, S. Trumbore, and C. Wells. 1999. Rapid accumulation and turnover of soil carbon in a re-establishing forest. Nature 400: 56–58.

Richter, D.D., D. Markewitz, C. Wells, H. Allen, R. April, P. Heine, and B. Urrego. 1994. Soil chemical change during three decades in an old-field loblolly pine (Pinus taeda L.) ecosystem. Ecology 75(5): 1463–1473.

Roden, E., D. Sobolev, and B. Glazer. 2004. Potential for microscale bacterial Fe redox cycling at the aerobic-anaerobic interface. Geomicrobiology Journal 21(6): 379–391.

Roy, R., H. Klüber, and R. Conrad. 1997. Early initiation of methane production in anoxic rice soil despite the presence of oxidants. FEMS Microbiology Ecology 24: 311–320.

Samouëlian, A., I. Cousin, A. Tabbagh, and A. Bruand. 2005. Electrical resistivity survey in soil science: a review. Soil and Tillage Research 83: 173–193.

Schuur, E., and P. Matson. 2001. Net primary productivity and nutrient cycling across a mesic to wet precipitation gradient in Hawaiian montane forest. Oecologia 128: 431–442.

Scott-Denton, L., K. Sparks, and R. Monson. 2003. Spatial and temporal controls of soil respiration rate in a high-elevation, subalpine forest. Soil Biology Biochem 35(4): 525–534.

Sexstone, A., and T. Parkin. 1985. Temporal response of soil denitrification rates to rainfall and irrigation. Soil Science Society of America Journal 49: 99–103.

Stiles, C., E. Dunkinson, C. Ping, and J. Kidd. 2010. Initial field installation of manganese indicators of reduction in soils, Brooks Range, Alaska. Soil Horizons 51: 102–107.

Stumm, W., and B. Sulzberger. 1992. The cycling of iron in natural environments: considerations based on laboratory studies of heterogeneous redox processes. Geochimica et Cosmochimica Acta 56: 3233–3257.

Tabbagh, A., M. Dabas, A. Hesse, and C. Panissod. 2000. Soil resistivity: a non-invasive tool to map soil structure horizonation. Geoderma 97: 393–404.

Torn, M., S. Trumbore, O. Chadwick, and P. Vitousek. 1997. Mineral control of soil organic carbon storage and turnover. Nature 389: 170–173.

Vitousek, P., and O. Chadwick. 2013. Pedogenic thresholds and soil process domains in basalt-derived soils. Ecosystems 16(8): 1379–1395.

Vitousek, P., and R. Howarth. 1991. Nitrogen limitation on land and in the sea: how can it occur? Biogeochemistry 25: 376–381.

Vitousek, P., S. Porder, and B. Houlton. 2010. Terrestrial phosphorus limitation: mechanisms, implications, and nitrogen–phosphorus interactions. Ecological Applications 20(1): 5–15.

Vorenhout, M., H.G. van der Geest, D. van Marum, K. Wattel, and H.J. Eijsackers. 2004. Automated and continuous redox potential measurements in soil. Journal of environmental quality 33(4): 1562–7.

Yang, W., and D. Liptzin. 2015. High potential for iron reduction in upland soils. Ecology 96(7).

Yesavage, T., M.S. Fantle, J. Vervoort, R. Mathur, L. Jin, L.J. Liermann, and S.L. Brantley. 2012. Fe cycling in the Shale Hills Critical Zone Observatory, Pennsylvania: An analysis of biogeochemical weathering and Fe isotope fractionation. Geochimica et Cosmochimica Acta 99: 18–38.

Zaslavsky, D., and Rogowski. 1969. Hydrologic and Morphologic Implications of Anisotropy and Infiltration in Soil Profile Development1. Soil Science Society of America Journal 33(4): 594.

CHAPTER 2

IRON REDUCTION INCREASES WITH RAINFALL IN PREDOMINATELY OXIC UPLAND SOILS[1]

[1] Hodges, C.A., E. King, J. Pett-Ridge, and A. Thompson. submitted to *Soil Science Society of America Journal*, March 2016

ABSTRACT

Microbe-mediated Fe reduction modulates the role of iron minerals in soil nutrient availability and C cycling. In upland soils, Fe reduction can occur without full profile water-saturation within aggregates, or C and clay-rich sites where O_2 consumption exceeds its diffusive flux. Quantifying the net effect of Fe reduction in low-oxygen sites within oxic soil profiles is challenging, but critical for identifying climatic regions and soil types where Fe reduction plays a role in upland soil biogeochemistry. We used techniques originally developed to delineate wetlands to measure Fe reduction in upland soils, and hypothesized that the potential for Fe reduction would correlate with increasing rainfall. We tested this hypothesis at four sites along a climate gradient in Maui, Hawaii [between 2200 and 4400 mm yr^{-1} mean annual precipitation (MAP)] that had an established inverse correlation between Fe content and rainfall. We measured the potential for Fe reduction by the loss of iron coating from (a) Fe oxide-coated polyvinyl chloride (PVC) tubes (Indicator of Reduction in Soils tubes; "PVC IRIS") and (b) from uniformly rusted steel rods (rusted steel reduction indicators; "Steel IRIS probes") at 7, 11, and 14 d after installation in the soil. In addition, we measured soil redox potential (Eh) and pH using platinum and pH electrodes installed at each site**.** Both the PVC and Steel IRIS probes displayed some coating loss at all sites, with the fraction of coating removed on the Steel IRIS probes (0.13 to 0.67) correlating strongly with rainfall (r^2=0.66, p=0.016). This correlation improved the longer the probes were in the soil, with the best site separation evident after 14 d of exposure. Unexpectedly, Eh remained high (~900-650 mV) throughout all sites, except at deeper depth at the wettest site (45 cm, 4200 mm MAP site), suggesting overall oxidizing conditions within the soil profile. Additional experiments conducted in the lab further bolster our observations from the field, indicating that Fe removal is due to Fe reduction, Fe removal increases with increasing

soil moisture, and Fe reduction occurs in soil without complete saturation. Our findings demonstrate that rainfall abundance increases the prevalence of Fe reduction at oxic sites, which points to the importance of iron redox to the biogeochemistry of soils that receive at least 2200 mm MAP.

Abbreviations: Eh – redox potential; Eh_7 – redox potential standardized to pH 7; MAP – mean annual precipitation; MAT – mean annual temperature; MCG – Maui climate gradient

INTRODUCTION

Until recently dissimilatory Fe^{III} reduction (i.e. microbial respiration using Fe^{III}) was disregarded as an important pathway for C mineralization in upland soils. However, a growing body of evidence suggests Fe reduction is coupled to significant portions of upland CO_2 emissions, with estimates near 40% of total soil respiration for some ecosystems (Lipson et al., 2010; Hall et al., 2013; Lipson et al., 2013; McNicol and Silver, 2014). Given that soil is the largest terrestrial C sink, this understudied process is essential for quantifying the global cycling of C (Lal, 2004; Köchy et al., 2015). Future climate change is likely to shift soil moisture and temperature regimes and therefore impact microbial respiration and soil C cycling. Quantifying Fe^{III}-based microbial respiration as a function of climate at an ecosystem level is imperative for accurate representations of the C cycle in global climate models (Davidson et al., 1998; Davidson and Janssens, 2006). Also, Fe reduction can alter soil biogeochemistry in other ways that have cascading influences at the ecosystem level (Borch et al., 2009; Raiswell and Canfield, 2012; Roden, 2012; Colombo et al., 2013). For instance, Fe reduction can release and mobilize colloids, which might contain carbon, pollutants or nutrients (e.g., P) (Henderson et al., 2012; Buettner et al., 2014; Köhler et al., 2014). Additionally, Fe reduction can speed up the processes of mineral transformations, alter the balance of trace gas fluxes, and bring about the release of nutrients and trace metals (Hansel et al., 2005; Polizzotto et al., 2008; Handler et al., 2009).

Microbes preferentially utilize a sequential pattern of terminal electron acceptors (O_2, NO_3, Mn(IV), Fe(III), SO_4, etc.) according to decreasing energy yield (Patrick and Jugsujinda, 1992; Peters and Conrad, 1996). In highly weathered soils that are often leached of other alternate terminal electron acceptors, microbes resort to Fe reduction quickly after the onset of reducing conditions (Küsel et al., 2002; DeAngelis and Silver, 2010). Researchers have shown

that various well-drained soils have a high potential to reduce Fe when incubated under anoxic conditions (De-Campos et al., 2012; Yang and Liptzin, 2015). High concentrations of ferric iron (Fe^{III}) and C are not necessarily required for high Fe reduction rates (Fimmen et al., 2008; Yang and Liptzin, 2015), suggesting that most upland soils have some potential for Fe reduction as long as O_2 becomes limited.

Even though there is evidence for upland Fe reduction, most of the field research on Fe reduction has focused on wetlands and water table delineation (Bridgham and Faulkner, 1991; Castenson and Rabenhorst, 2006; Rabenhorst and Burch, 2006; Fakih et al., 2008; Owens et al., 2008; Rabenhorst and Hively, 2009; Stiles et al., 2010; Dorau and Mansfeldt, 2015). In those studies, a common method for determining a high water table and Fe reducing conditions is to install PVC pipes painted with a short-range-ordered Fe(III) mineral in the soil and monitor the loss of the coating due to Fe reduction (Castenson and Rabenhorst, 2006; Jenkinson and Franzmeier, 2006; Fakih et al., 2008). These Indicators of Reduction in Soil (IRIS) tubes utilize Fe redox chemistry to determine the presence of wet soils and water tables (Castenson and Rabenhorst, 2006; Jenkinson and Franzmeier, 2006; Rabenhorst and Burch, 2006). In a similar manner, zero-valent Fe (Fe^0) rods have also been used to determine redox status based on the amount of change of the gray zero-valent iron to an oxidized red Fe^{III} (Bridgham and Faulkner, 1991; Owens et al., 2008). Recently, redox processes in upland soils have been contextualized by the persistence of both oxic and anoxic microsites at soil moistures less than saturation, underlining a key difference between wetland and upland soils (Hall et al., 2013).

While the importance of Fe reduction in sediments, wetlands, and hydric soils has been well documented, the same attention has not been paid to upland soils (Kögel-Knabner et al., 2010; Roden, 2012; Keiluweit et al., 2016). In comparison to fully-water saturated soils, upland

soils are subjected to a greater range of spatially and temporally variable conditions. However, the amount of moisture is likely a key parameter determining the rate and potential for iron reduction. Therefore, we hypothesized that the potential for soil Fe reduction in upland (non-flooded) soils will increase with increasing rainfall. We tested this hypothesis along a well-characterized climate gradient that varied in rainfall from 2200 to 4200 mm yr^{-1} on the island of Maui, HI [Maui Climate Gradient (MCG) (Miller et al., 2001; Schuur et al., 2001; Schuur and Matson, 2001)]. At four sites along the MCG we installed two forms of passive soil iron reduction indicators (PVC IRIS probes, and a rusted steel rod "Steel IRIS" probe). We also recorded the platinum electrode potential and pH for 7 to 14 days. Loss of iron coating from the PVC and Steel IRIS probes was used as a proxy for iron reduction. Additional studies in the lab were performed to identify the mechanisms of Fe removal from the Steel IRIS Probe.

METHODS

Field Site Description

The MCG is a well-studied rainfall gradient on Haleakala Mountain in Maui (Fig. A.1), in which all state factors of soil formation are constrained except rainfall. This gradient has a documented increase in rainfall that corresponds with a decrease in mean Eh, total Fe concentration, and increasing Fe isotope fractionation relative to underlying basalt (Miller et al., 2001; Schuur et al., 2001; Schuur and Matson, 2001; Thompson et al., 2007; 2011, see Table 2.1). This site provides unique advantages to studying soil because the location of the mountain with respect to the trade winds creates a gradient in rainfall without a change in elevation (or temperature). The sites were established at 2200 mm yr^{-1}, 2800 mm yr^{-1}, 3500 mm yr^{-1} and 4200 mm yr^{-1} MAP (sites 1, 3, 4, and 5 in Schuur and Matson, 2001, see Fig. 2.1)

Steel IRIS Redox Probes

Rusted steel rods were utilized as passive redox probes at the four field sites. These probes are uniformly rusted, 90 cm long, low carbon alloy "1018" steel rods. The low carbon rods have the highest amount of Fe and are therefore the easiest to rust. The rods were wiped thoroughly with an orange degreaser to remove any oil added during machining to retard oxidation. After cleaning, the rods were sprayed with 0.1 M HCl and allowed to dry (Fig. 2.2). This process dissolves some of the zero-valent Fe from the rod, and as the HCl dries the iron re-precipitates as an $Fe^{(III)}$ oxyhydroxide (rust). This spray and dry cycle was repeated two times until the Fe(III) on a rod was a bright orange or red color that would not flake off after brushing of the rod surface. Steel IRIS probes and coatings were characterized with Mossbauer spectroscopy to determine crystallinity, and mineralogy. A scanning electron microscope was used to determine coating thickness.

Twenty of the passive Steel IRIS Probes were installed at each of the four sites. The probes were divided into four sub-sites at each location so that there were five probes in each sub-site. We removed one probes from each sub-site after 7 days (four rods per site) and then two probes from each sub-site after 11 and 14 days (eight rods per site). The passive probes were then immediately washed of soil and root material in a nearby stream. After washing, the rods were imaged in quarters of circumference such that four composite pictures were collected that could be combined to represent the entire surface area of the rod.

PVC IRIS Redox Probes

Polyvinyl chloride pipe coated in Fe oxides was used as another passive redox probe. We followed the construction methods developed by Jenkinson (2002). Ninety centimeter "Schedule 40", ½ inch PVC was cleaned and sanded with fine grit sandpaper. The paint was prepared by dissolving ferric chloride salt in deionized water. One molar KOH was added to sufficiently raise the pH and precipitate the ferrihydrite. The solution was centrifuged, and the solids were transferred to dialysis tubing and suspended in deionized water. After three days, the Fe oxides were removed from the dialysis tubing, and left in a refrigerator until use. Optimum paint viscosity was attained by adding or evaporating water. The Fe oxides were then painted onto the rods evenly in two coats so that the minerals would not flake off when firm pressure was applied across the pipe. The PVC pipes were deployed, collected, and imaged in the same way as the rusted steel rods.

In Lab Studies of Fe Removal from Steel IRIS Probes

Experiments were performed in the lab to examine the mechanisms of Fe removal from the Steel and PVC IRIS Probes. The IRIS probes were cut into 5 cm-long pieces, and placed in 15 mL plastic test tubes for the studies.

In experiment 1, soil from the A horizon of site 3 was packed into the test tubes to a uniform bulk density of ~1.2 g cm^{-3}, Steel IRIS probes were installed, and water was added to achieve 25, 50, or 100% water-filled pore space (WFPS). All water treatments were then either left live or were autoclaved, and then were either left in ambient conditions, or placed in an anoxic glovebox. All anoxic treatments were allowed to de-gas in the anoxic chamber for 36 hours prior to Steel IRIS Probe installation to ensure low levels of oxygen. Soil moisture,

ambient condition, and autoclaved/live treatment was performed in 10 replications. Steel IRIS probes were left in the soil columns for 2 weeks. After the two weeks the rods were removed from the columns, washed, and then each ¼ of the rod circumference was imaged. The quarter images of the Steel IRIS probes were used to create a single composite image of each rod in Photoshop CS6 (Adobe Systems, San Jose, California). The color range associated with reduced regions of the probes was identified manually and then all pixel colors within that range were automatically selected by Photoshop (select color range tool). The fraction of reduced pixels to total pixels was calculated for each rod quarter. The fractions for each rod quarter were standardized and summed to generate the fraction reduced of the whole rod.

In experiment 2 we also used 5 cm-long Steel IRIS Probe pieces in the 15 mL plastic test tubes, but instead placed the probes in live and autoclaved Oi-horizon extracts of varying concentrations. We used a base of a 1:10, 2 hour water extract of the Oi horizon, and then performed serial dilutions to achieve additional 1:100, 1:1000, and 1:10000 dilutions. Each DOM dilution and autoclave treatment was performed in 10 replications. The columns were left capped under ambient conditions, but were uncapped for a minute, re-capped, and shaken every day of the experiment. After the two weeks, some of the DOM solution was sampled and acidified in a 1:1 ratio with 1 M HCL for total Fe, and Fe^{+2} determination. The rods were then removed from the columns, washed, and then imaged in the same way done after the initial experiment.

Finally, an experiment was conducted with Steel IRIS Probes with exposed Fe^{0} (unrusted steel) on the ends, Steel IRIS Probes with rusted ends, and PVC IRIS Probes. All three rod types were exposed to six different treatments: autoclaved and live 100% WFPS soil, autoclaved and live 25% WFPS soil, and autoclaved and live water. All probes remained in oxic conditions

throughout the two week experiment. The water treatments were uncapped for a minute, recapped, and shaken twice daily to maintain dissolved oxygen within the water.

Hydrogen peroxide assays were performed at hour 0, 6, 18, 45, 72, 120, 168, 216, 288, and 336 to determine whether the formation and perpetuation of a hydroxyl or hydroperoxyl free radical is a mechanisms of Fe removal from the Steel IRIS Probes. These free radicals potentially form when in the presence of water, oxygen, and multiple redox states of Fe (Pignatello et al., 2006). They are strong oxidants that go on to take part in other oxidation reactions. The hydroperoxyl free radical can be quenched through reduction of Fe^{III} to Fe^{+2} and the production of oxygen and a proton (Pignatello et al., 2006). The continuous creation and then quenching of free radicals could be driving Fe removal from the Steel IRIS Probes as both Fe^{+2} and Fe^{III} redox states are present.

All hydrogen peroxide assays were performed using Amplex UltraRed Reagent (Thermo Scientific). Soil treatments were extracted with water at 1:10 ratio, and water treatments were diluted 1:10 with phosphate buffer. Hydrogen peroxide assays were performed as specified by Amplex UltraRed guides. Reactions were allowed to proceed for 30 minutes and were then analyzed for absorbance at 560 nm. After two weeks, the probes were removed from the treatments, cleaned, and then imaged in quarters. Photoshop analysis was performed as in the other experiments.

Platinum Electrode Installation

Platinum redox electrodes were installed at the four sites to measure redox potential relative to a Calomel reference electrode (Paleo Terra, Amsterdam, Netherlands). The electrodes were constructed of epoxy with a platinum sensor installed along half of the circumference at a certain

location (2 cm from tip for the shallow electrodes, 5 cm for the deep electrodes). Six electrodes were installed at each site (three electrodes each at 15 cm and 45 cm depth below the soil surface). The electrodes were allowed to equilibrate with the soil for three days before readings were taken, after which Eh measurements were recorded every 15 minutes over the following five days, which corresponded with the last five days the the Steel and PVC IRIS Probes were installed. Eh measurements were logged by a Campbell Scientific CR10X datalogger. All Eh values were standardized to pH 7 using the soil pH measured in the surface soil with a Thermo Scientific Orion pH electrode (Thermo Fisher Scientific, Waltham, Massachusetts) installed at each site.

Image Collection and Analysis

The quarter images of the Steel and PVC and IRIS probes were used to create a single composite image of each rod or pipe in Photoshop CS6 (Adobe Systems, San Jose, California). The color range associated with reduced regions of the probes was identified manually and then all pixel colors within that range were automatically selected by Photoshop (magic wand tool feature). The fraction of reduced pixels to total pixels was calculated for each rod quarter. The fractions for each rod quarter were standardized and summed to generate the fraction reduced of the whole rod. Regressions and all other analyses relating fraction reduced to time and precipitation were performed in R (R Core Team, 2013).

RESULTS and DISCUSSION

Eh Data

Previous work along the MCG has documented decreasing, but highly variable, soil Eh with increasing rainfall (Miller et al., 2001; Schuur and Matson, 2001). High variability in soil oxygen is typical of redox active upland soils (Silver et al., 1999). Our data collected continuously for five days along the same gradient as Schuur and Matson's study (2001) supports this view of a variable redox environment. Over the monitoring period, mean Eh_7 decreased with depth in the soil profile. While mean of Eh values at the 2200, 2800, and 3500 mm yr^{-1} were about 900 mV at 15 cm and 800 mV at 45 cm, the mean Eh at the wettest site (4200 mm yr^{-1}) was 860 mV at 15 cm and it was 595 mV at 30cm. All probes recorded Eh values within the oxidizing Eh range (Eh_7 > 500 mV) (Fig. 2.8) based on prior literature (Husson, 2013). It must be noted that our 5-day Eh_7 data depict a much more oxic environment than Schuur's long-term data set collected over one full year would suggest. Even with all variation taken into account, our Eh_7 values at both depths are greater than the upper quartile of Schuur and Matson's long-term Eh data (Schuur and Matson, 2001). However, this is not completely unexpected, as Eh measurements made with platinum electrodes are highly variable over space and time (Vorenhout et al., 2004; Rabenhorst and Hively, 2009).

Steel IRIS Redox Probes

The fraction of total pixels removed from Steel IRIS probes increased with rainfall at each time point (Fig. 2.10). At 14 days, the fraction of iron removed significantly increased from 0.21±0.05 to 0.53±0.07 over the rainfall gradient (a p-value of 0.016 and an r^2 of 0.66, Fig. 2.9). This points to the importance of rain creating low-O_2 (and low Eh) microsites by filling pores

and limiting O_2 diffusion, which facilitates Fe reduction in upland soils. While the soil as a whole remains within an oxidizing Eh range, there are microsites with sufficient electron donors (e.g., C) and a lack of O_2 such that if Fe^{III} is supplied in a labile form it will be rapidly reduced.

In general, the longer the probes remained exposed in the soil at the 2800, 3500, and 4200 mm yr^{-1} sites, the more Fe coating was removed (i.e., more pixels were considered "reduced", Figs. 2.9, 2.10, and 2.11). The fractional loss of Fe from the steel IRIS probe from day 7 to day 14 increased from 0.18±0.07 to 0.33±0.09 at the 2800 mm yr^{-1} site, from 0.27±0.02 to 0.47±0.11 at the 3500 mm yr^{-1} site, and from 0.34±0.07 to 0.53±0.07 at the 4200 mm yr^{-1} site. In contrast, the fraction of Fe removed at the 2200 mm yr^{-1} site (site 1) were equal within error from day 7 through 14 (Figure 2.10).

Any of the factors limiting Fe reduction could be responsible for a stagnation over time in indicator iron loss as observed at site 1. The four factors driving iron reduction include, (1) availability of soil carbon; (2) the availability of anoxic sites; and(3) the availability of microbes capable of reducing Fe^{III} (or generating reduced chemical compounds, i.e., H_2S, that can reduce Fe^{III}). That said, there is no indication that soil C at site 1 is sufficiently low to inhibit Fe reduction, or that the microbial population is incapable of reducing Fe, or generating any other reduced compounds (Thompson et al., 2011; Table 2.1, Figs. 2.9 and 2.11). Perhaps the most reasonable explanation is that site 1 undergoes active reduction and re-oxidation of the Steel IRIS probes so that only 0.20 of the total surface remains reduced, despite more active Fe redox cycling at the probe surface.

PVC IRIS Redox Probes

PVC IRIS probes indicated Fe reduction at all sites, but the measurements were highly variable (Fig. 2.10). Additionally, the measurements were generally lower than the Steel IRIS probes in terms of fraction of Fe removed (Fig. 2.10). However, comparing the fractional removal between the two types of probes may be inconsequential as thickness and makeup of the two passive probes is different. When averaged, some measurements of fraction of Fe removed generated standard deviations greater than 90% of the mean. In the past, PVC IRIS tubes have been used for coarse-resolution depictions of the redox status of soils (Castenson and Rabenhorst, 2006; Jenkinson and Franzmeier, 2006). These studies focused on bulk soil conditions and water table fluctuations, not the dynamics of rainfall-created microsites and hotspots of reduction, although they did often note hotpots of reduction above the water table (Castenson and Rabenhorst, 2006; Jenkinson and Franzmeier, 2006).

Comparison of PVC and Steel IRIS Probes

The Steel IRIS probes responded more uniformly to mean annual rainfall than the PVC IRIS Probes (Fig. 2.10). As noted earlier, the PVC IRIS Probes were developed to examine hydric soils with Fe reduction due to fluctuating water tables (Castenson and Rabenhorst, 2006; Jenkinson and Franzmeier, 2006). This mode of Fe reduction from low-oxygen groundwater is somewhat different from that of rainfall-induced reduction observed at our MCG sites, and perhaps this is why the PVC IRIS probe resolution was not as high as the steel IRIS probe. The steel rod provides a continuous source of Fe, and once the rust coating is removed, the underlying Fe can be re-oxidized if O_2 or NO_3^- become available as an oxidant. If the ferrihydrite on the PVC IRIS probe is reduced to $Fe^{(+2)}$, it likely diffuses away from the tube and thus the

PVC IRIS tube will indicate the iron reducing conditions, even if the soil becomes oxic again. In this way, the Steel IRIS Probe may provide an average of the iron redox dynamics over the installation time, while the PVC IRIS probes may provide a measure of the presence/absence of reducing conditions during the installation period.

Steel IRIS Characterization and In-Lab Studies

Mossbauer Spectroscopy of the Fe-oxide coating from the Steel IRIS Probes indicates that the coating is comprised of a 50:50 ratio of nano-goethite and ferrihydrite (Appendix C). SEM imaging confirms this result, and also provides confirmation of a relatively uniformly coated surface (Appendix C).

From the first in-lab experiment, we observed an increase in Fe removal from the Steel IRIS Probes with increases in soil moisture (Fig. 2.3). Fe removal was highest at 100% WFPS with (value here), but was also high at 50% WFPS (value here) in the live oxic and anoxic treatments. This indicates Fe reduction at water contents lower than saturation, probably inside aggregates that experience slower oxygen diffusion rates (Horn and Smucker, 2005). At 25% WFPS there was very little Fe removal across all treatments (about 0.02 across all treatments), which is to be expected (Zausig et al., 1993; Küsel et al., 2002).

We did record some Fe removal from the autoclaved treatments (Fig. 2.3). This abiotic removal of Fe oxides is about 30% of the samples that were not autoclaved, and can be attributed to other redox couples that use Fe^{III} as a terminal electron acceptor either through interactions with soil organic matter or other electron-rich soil constituents that couple their oxidation to Fe reduction. To this point, it is important to underline that Steel IRIS Probes are not biotic Fe reduction selective, and that biotic and abiotic Fe reduction have different implications on the

soil environment. While both pathways of Fe reduction lead to dissolution of Fe minerals, and consequent release of associated constituents into the soil environment, there is no respiration component of abiotic Fe reduction. Meaning that a reduction event will always mobilize P, C, and other trace metals, but may not generate a corresponding CO_2 release (Nealson and Myers, 1992; Colombo et al., 2014). When using Steel IRIS Probes to make inferences about biogeochemical processes, it is important to take these results into account so as to not overestimate the carbon mineralization attributed to Fe-Reducing bacteria.

The lab experiments in which we varied DOM concentrations addressed the potential role of chelation and other modes of Fe removal not related to redox reactions. We found no effect of live vs. autoclaved extract and no effect of DOM concentration on Fe removal from the Steel IRIS Probes (Fig. 2.4). All treatments recorded about 0.15 fraction of Fe removed from the Steel IRIS Probes. We also found that nearly all of the Fe in solution (greater than 90% for all treatments) was Fe^{+2} (Fig. 2.4). Together, these results point to reduction of Fe oxides on the Steel IRIS Probes by DOM functional groups, not chelation. If chelation were a main driver of Fe removal from the Steel IRIS Probes, we would have observed more removal with greater DOM concentrations, and the HCl extractable Fe in solution would be Fe^{III}, not Fe^{+2}. Again, with these results, we see the potential signature of abiotic processes in removing Fe^{III} from the Steel IRIS Probes.

In the final experiment we assessed the potential for the Steel IRIS Probes to produce free radicals that strip Fe-oxides from the rods, and we compared the Fe removal from Steel and PVC IRIS Probes subjected to the same soil and water conditions. Under both 100% and 25% WFPS, we observed no difference in Fe removal from the Steel (with and without rusted ends) and PVC IRIS probes (Fig 2.5). This result suggests that Steel and PVC IRIS probes are recording the

same soil processes. Further to this point, all of the types of IRIS Probes indicated the same amount of Fe removal in the 100% WFPS autoclaved treatments. From these results, we are confident that the mechanisms that act to remove Fe from both the Steel and PVC IRIS Probes are the same, and that the measurements made with the two methods are comparable (Figure 2.4 and 2.5).

Hydrogen peroxide was near-continuously detected within both the autoclaved and live water treatments of the Steel IRIS Probe treatments with and without rusted ends. Despite the presence of H_2O_2, Fe removal was low and the same across all treatments in the live water, indicating that Fenton Chemistry did not play a large role in Fe removal in the live water treatment (Fig. 2.6). In the autoclaved treatment, Fe removal from the Steel IRIS Probe without the rusted ends was higher than the Steel and PVC IRIS Probes (Fig. 2.7).

At some sample points hydrogen peroxide was detected in the 100% WFPS treatments containing both types of Steel IRIS Probes (Fig. 2.6 and 2.7). At the same time, the Fe removal from the two different steel and the one type of PVC IRIS Probes was the same at this treatment (Fig 2.5). Hydroxyl or hydroperoxyl free radicals may have been generated, but they were quenched by organic matter, or some other soil constituent, before acting as a means of Fe removal from the Steel IRIS Probes. We can conclude that under well-drained conditions that provide for the movement of the free radicals away from the steel IRIS probe, or under poorly-drained conditions in the presence of some DOC to quench the free radicals, Fenton Chemistry is not a driver of Fe removal from the Steel IRIS Probes. Further supporting this point is that Fe removal from the rods in oxic DOC solution in the previous experiment was relatively low. Additionally, we can conclude that only Steel IRIS Probes with exposed Fe^0 are susceptible to Fenton Chemistry as a mechanism of Fe removal. The Steel IRIS Probes installed across the

MCG did not have exposed unrusted steel on the ends, and were placed in soils high in OC (table 2.1), so we conclude that Fenton Chemistry did not exert a strong influence on the Fe removal that we observed across the sites.

Microsites and Iron Reduction

Previous studies that utilized *in situ* redox measurements suggest Fe reduction can occur within micro-sites that persist in predominately oxic bulk soil conditions; soil aggregates are known to foster reducing conditions despite unsaturated bulk soil and readings of $Eh_7 > 500mV$ at the aggregate surface (Sexstone and Parkin, 1985; Zausig et al., 1993). Indeed, our in-lab results support this view of reducing conditions in soils, as we observed significant Fe reduction from the Steel IRIS probes under unsaturated soil condtions (Figs. A.3, A.6, and A.7). Furthermore, field studies reveal that terminal electron acceptors are not always reduced in bulk soil according to their sequentially decreasing energy yield as observed in lab incubations (e.g. (Peters and Conrad, 1996)). Soils are a mosaic of redox conditions, with many electron acceptors operating simultaneously (Flessa and Fischer, 1992; Roy et al., 1997) . Our data from the MCG support this view of soil as spatially variable; the Steel IRIS probes and platinum Eh electrodes demonstrate high potential for Fe reduction within an oxic bulk soil (Figs. 2.8, 2.9, and 2.11). The high rainfall at our sites evidently generates many persistent low-oxygen microsites with a high capacity for Fe reduction situated in a matrix of well-drained, oxic soil. Soils typically considered “oxic” likely foster Fe reduction processes (Hall et al., 2013).

Our findings corroborate well with other studies that have used passive redox probes for characterizing soil redox potential. For example, Jenkinson and Franzmeier (2006) recorded significant iron coating loss from IRIS tubes and bulk soil Eh values in the typical iron reducing

range (Eh ~300 mV), but they also observed partial loss of Fe coatings above saturated soil, which they attributed to distributed anoxic microsites. Similarly, when unrusted, Fe^0 rods were installed into soils with fluctuating shallow water tables—suggesting a dynamic redox environment—both rust and reduced iron were observed in the zone of fluctuation (Bridgham and Faulkner, 1991).

While no linear relationship exists, the PVC IRIS probe data also suggest iron reduction occurs in upland soils (Fig. 2.10). Castenson and Rabenhorst (2006) categorize sites with more than 0.3 iron loss from PVC IRIS tubes as sites with bulk soil "reducing conditions". In our study, all sites had one or more PVC IRIS probes with greater than 0.3 fractional iron loss, suggesting all sites reached "reducing conditions" over the two week study period. However, more than 75% of the PVC IRIS tubes have less than 0.25 fractional iron loss (Fig 2.10), suggesting Fe reduction was not widespread across the landscape.

Implications

Our data indicate that the potential for Fe reduction increases with rainfall (Fig. 2.9), and suggests that Fe reduction is an important process on an ecosystem-scale for fine-textured soils. However, since even our lowest rainfall site (2200mm MAP) had fractional iron loss of 0.21±0.09 (Fig. 2.9) our study does not delineate the minimum required rainfall for iron reduction in the a-seasonal climate of the MCG (Giambelluca et al., 2013). In upland soils that are wet only part of the year—such as those with seasonal rainfall (Knorr and Blodau, 2009; Hong et al., 2010), seasonal high/low transpirational demand (Fimmen et al., 2008; Fuss et al., 2010; Bourgault et al., 2015), or a spring snowmelt (Lipson et al., 2010; Knorr, 2013)—Fe reduction is probably also an important process at the ecosystem scale. For example, Lipson et

al. (2010) found that during summer thaw of an arctic soil, Fe reduction became a major component of total soil respiration.

Presence of water in the solum is essential for creating reducing conditions, but it is clear that bulk soil saturation is not necessary (Fig. 2.8), Soil Fe reduction probably becomes an important soil process (when other antecedent requirements are met) at 50% WFPS in these fine-texture volcanic soils. Similarly, both NO_3^- reduction and CH_4 production have been shown to occur across a wide range of upland soils at varying O_2 and water contents (Smith and Tiedje, 1979; Parry et al., 1999; Teh et al., 2005; Megonigal and Guenther, 2008; Jarecke et al., 2016). It follows then, that Fe reduction, a process that's energy yield is intermediate to NO_3^- reduction and CH_4 production, occurs broadly in many types of soils and ecosystems that foster these "anaerobic" reduction reactions. For instance, methane production is now well known to occur in dessert biological crusts (Angel et al., 2011); Fe reduction may also occur in these systems. Similarly Fe reduction is evident in vernal pools (Clausnitzer et al., 2003), but may also occur in moderately wet seasonal systems such as coarse-textured soils in a Mediterranean climate or in irrigated croplands (Davidson, 1992; Priemé and Christensen, 2001; Barton et al., 2008; Ambus and Christensen, 1994). These examples significantly broaden our outlook on Fe reduction at the ecosystem-scale, suggesting that it is important across most humid sites, and is not limited to tropical or wetlandsoils.

CONCLUSIONS

We used two passive (Steel and PVC IRIS probes) and one active redox characterization method to study Fe reduction along a well-constrained climate gradient that varies in rainfall. While the active platinum electrodes that measured bulk soil Eh suggested all sites were

oxidizing (>500 mean Eh_7), our passive probes indicated Fe reduction increased with site rainfall after two weeks. Of the two passive methods, the Steel IRIS probes separated the sites better in terms of the potential Fe reduction than the PVC IRIS probes. From our results, we conclude that in well-drained upland soils, bulk soil Eh is a poor predictor of Fe reduction potential. Our study provides field-based evidence for recent findings that indicate a high potential for Fe reduction in upland soils (De-Campos et al., 2012; Yang and Liptzin, 2015), further emphasizing that microsite-driven redox processes occur in predominately oxic soil matrices. We conclude that the potential for Fe reduction is high in upland soils with high precipitation, and could be important in all soils that experience periodically high soil moisture.

REFERENCES

Ambus, P., and S. Christensen. Spatial and seasonal nitrous oxide and methane fluxes in Danish forest-, grassland-, and agroecosystems. J. Environ. Qual. 24(5):993-1001. doi: 10.2134/jeq1995.00472425002400050031x.

Angel, R., D. Matthies, and R. Conrad. 2011. Activation of methanogenesis in arid biological soil crusts despite the presence of oxygen. PLoS ONE 6(5): e20453. doi: 10.1371/journal.pone.0020453.

Borch, T, R Kretzschmar, and A Kappler. 2009. Biogeochemical redox processes and their impact on contaminant dynamics. 44:15-2. Environ. Sci. Technol. doi: 10.1021/es9026248.

Bourgault, R., D. Ross, and S. Bailey. 2015. Chemical and morphological distinctions between vertical and lateral podzolization at hubbard brook. Soil Sci. Soc. Am. J. 79(2): 428-439. doi: 10.2136/sssaj2014.05.0190.

Bridgham, SD, and SP Faulkner. 1991. Steel rod oxidation as a hydrologic indicator in wetland soils. Soil Sci. Soc. Am. J. 55:856–862.

Buettner, S., M. Kramer,O. Chadwick, and A. Thompson. 2014. Mobilization of colloidal carbon during iron reduction in basaltic soils. Geoderma. 221-222:139-145. doi: 10.1016/j.geoderma.2014.01.012.

Castenson, K., and M. Rabenhorst. 2006. Indicator of Reduction in Soil (IRIS). Soil. Sci. Soc. Am. J. 70:1222-1226. doi: 10.2136/sssaj2005.0130.

Clausnitzer, D., J. Huddleston, E. Horn, M. Keller, and C. Leet. 2003. Hydric soils in a Southeastern Oregon vernal pool. Soil Sci Soc Am J. 67(3): 951. 10.2136/sssaj2003.0951.

Colombo, C., G. Palumbo, J.-Z. He, R. Pinton, and S. Cesco. 2013. Review on iron availability in soil: interaction of Fe minerals, plants, and microbes. J. Soils Sediments. 14(3):538-548. doi: 10.1007/511368-013-0814-z.

Davidson, E.A. 1992. Sources of Nitric Oxide and Nitrous Oxide following Wetting of Dry Soil. Soil Sci. Soc. Am. J. 56:95-102. doi: 10.2136/sssaj1992.03615995005600010015x.

Davidson, E., E. Belk, and R. Boone. 1998. Soil water content and temperature as independent or confounded factors controlling soil respiration in a temperate mixed hardwood forest. Glob. Change Biol. 4:217-227. doi:10.1046/j.1365-2486.1998.00128.x.

Davidson, E.A. and I.A. Janssens. 2006. Temperature sensitivity of soil carbon decomposition and feedbacks to climate change. Nature 440:165-173.

De-Campos, A.B., C. Huang and C.T. Johnston. 2012. Biogeochemistry of terrestrial soils as influenced by short-term flooding. Biogeochemistry. 111:239-252.

DeAngelis, K.M., W.L. Silver, A.W. Thompson and M.K. Firestone. 2010. Microbial communities acclimate to recurring changes in soil redox potential status. Environ. Microbiol. 12:3137-3149.

Dorau, C., and T. Mansfeldt. 2015. Manganese-oxide-coated redox bars as an indicator of reducing conditions in soils. J. Environ. Qual. 44:696-703

Fakih, M., M. Davranche, A. Dia, B. Nowack, P. Petitjean, X. Châtellier, and G. Gruau. 2008. A new tool for in situ monitoring of Fe-mobilization in soils. Appl. Geochem. 23(12): 3372–3383.

Fimmen, R., D. Richter, D. Vasudevan, M. Williams, and L. West. 2008. Rhizogenic Fe–C redox cycling: a hypothetical biogeochemical mechanism that drives crustal weathering in upland soils. Biogeochemistry. 87(2): 127–141.

Flessa, H, and WR Fischer. 1992. Plant-induced changes in the redox potentials of rice rhizospheres. Plant Soil. 143:55-60.

Fuss, C., C. Driscoll, C. Johnson, R. Petras, and T. Fahey. 2010. Dynamics of oxidized and reduced iron in a northern hardwood forest. Biogeochemistry 104(1-3): 103–119.

Giambelluca, T.W., Q. Chen, A.G. Frazier, J.P. Price, Y.-L. Chen, P.-S. Chu, J.K. Eischeid, and D.M. Delparte, 2013: Online Rainfall Atlas of Hawai'i. Bull. Amer. Meteor. Soc. 94, 313-316.

Hall, S.J., W.H. McDowell and W.L. Silver. 2013. When wet gets wetter: Decoupling of moisture, redox biogeochemistry, and greenhouse gas fluxes in a humid tropical forest soil. Ecosystems 16:576-589.

Handler, RM, BL Beard, and CM Johnson. 2009. Atom exchange between aqueous Fe (II) and goethite: An Fe isotope tracer study. Environ. Sci. Technol. 43: 1102-1107. doi: 10.1021/es802402m.

Hansel, CM, SG Benner, and S Fendorf. 2005. Competing Fe (II)-induced mineralization pathways of ferrihydrite. Environ. Sci. Technol. 39: 7147-7153. doi: 10.1021/es050666z.

Henderson, R., N. Kabengi, N. Mantripagada, M. Cabrera, S. Hassan, and A. Thompson. 2012. Anoxia-induced release of colloid-and nanoparticle-bound phosphorus in grassland soils. Environ. Sci. Technol. 46: 11727–11734.

Hong, H., Y. Gu, K. Yin, K. Zhang, and Z. Li. 2010. Red soils with white net-like veins and their climate significance in south China. Geoderma 160(2): 197–207.

Husson, O. 2013. Redox potential (Eh) and pH as drivers of soil/plant/microorganism systems: a transdisciplinary overview pointing to integrative opportunities for agronomy. Plant Soil. 362:398-417.

Jarecke, KM, TD Loecke, and AJ Burgin. 2016. Coupled soil oxygen and greenhouse gas dynamics under variable hydrology. Soil Biol. and Biochem. 95:164-172. doi: 10.1016/j.soilbio.2015.12.018.

Jenkinson, B. 2002. Indicators of reduction in soils (IRIS): A visual method for the identification of hydric soils. Ph.D. dis. Purdue Univ., West Lafayette, IN.

Jenkinson, B.J. and D.P. Franzmeier. 2006. Development and evaluation of iron-coated tubes that indicate reduction in soils. Soil Sci. Soc. Am. J. 70:183-191.

Keiluweit, M, PS Nico, M Kleber, and S Fendorf. 2016. Are oxygen limitations under recognized regulators of organic carbon turnover in upland soils? Biogeochemistry. doi: 10.1007/s10533-015-0180-6.

Knorr, K.-H. 2013. DOC-dynamics in a small headwater catchment as driven by redox fluctuations and hydrological flow paths: are DOC exports mediated by iron reduction/oxidation cycles? Biogeosciences. 10(2): 891–904.

Knorr, KH, and C Blodau. 2009. Impact of experimental drought and rewetting on redox transformations and methanogenesis in mesocosms of a northern fen soil. Soil Biol. Biochem. 41:1187-1198. doi: 10.1016/j.soilbio.2009.02.030.

Köchy, M., R. Hiederer, and A. Freibauer. 2015. Global distribution of soil organic carbon – Part 1: Masses and frequency distributions of SOC stocks for the tropics, permafrost regions, wetlands, and the world. Soil. 1(1): 351–365. doi: 10.5194/soil-1-351-2015.

Kögel-Knabner, I, W Amelung, Z Cao, and S Fiedler. 2010. Biogeochemistry of paddy soils. Geoderma. 157: 1-14.

Köhler, SJ, F Lidman, and H Laudon. 2014. Landscape types and pH control organic matter mediated mobilization of Al, Fe, U and La in boreal catchments. Geochim. Cosmochim. Acta. 135:190-202.

Küsel, K, C Wagner, and T Trinkwalter. 2002. Microbial reduction of Fe (III) and turnover of acetate in Hawaiian soils. FEMS Microbiol. Ecol. 40:73-81.

Lal, R. 2004. Soil carbon sequestration impacts on global climate change and food security. Science 304:1623-1627.

Lipson, D.A., M. Jha, T.K. Raab and W.C. Oechel. 2010. Reduction of iron (III) and humic substances plays a major role in anaerobic respiration in an arctic peat soil. J. Geophys. Res.:Biogeosciences. 115:G00I06. doi: 10.1029/2009JG001147.

Lipson, D.A., T.K. Raab, D. Goria and J. Zlamal. 2013. The contribution of fe(III) and humic acid reduction to ecosystem respiration in drained thaw lake basins of the arctic coastal plain. Global Biogeochem. Cycles 27:399-409.

McNicol, G., and W. Silver. 2014. Separate effects of flooding and anaerobiosis on soil greenhouse gas emissions and redox sensitive biogeochemistry. J. Geophys. Res.: Biogeosciences. 119(4): 557–566. doi: 100.1002/2013JG002433.

Megonigal J.P., and Guenther, A.B. 2008. Methane emissions from upland forest soils and vegetation. Tree Physiol. 28:491-498.

Miller, A.J., E.A.G. Schuur and O.A. Chadwick. 2001. Redox control of phosphorus pools in hawaiian montane forest soils. Geoderma 102:219-237.

Owens, P.R., L.P. Wilding, W.M. Miller and R.W. Griffin. 2008. Using iron metal rods to infer oxygen status in seasonally saturated soils. Catena 73:197-203.

Parry, S., P. Renault, C. Chenu, and R. Lensi. 1999. Denitrification in pasture and cropped soil clods as affected by pore space structure. Soil Biol. Biochem.: 493–501.

Patrick, W.H. and A. Jugsujinda. 1992. Sequential reduction and oxidation of inorganic nitrogen, manganese, and iron in flooded soil. Soil Sci. Soc. Am. J. 56:1071-1073.

Peters, V., and R. Conrad. 1996. Sequential reduction processes and initiation of CH 4 production upon flooding of oxic upland soils. Soil Biol. Biochem. 28(3): 371–382.

Pignatello, J.J., E. Oliveros, and A. MacKay. 2006. Advanced oxidation processes for organic contaminant destruction based on the Fenton reaction and related chemistry. Critical reviews in environmental science and technology 36(1): 1–84.

Polizzotto, ML, BD Kocar, SG Benner, and M Sampson. 2008. Near-surface wetland sediments as a source of arsenic release to ground water in Asia. Nature. 454:505-508.

Priemé, A, and S Christensen. 2001. Natural perturbations, drying–wetting and freezing–thawing cycles, and the emission of nitrous oxide, carbon dioxide and methane from farmed organic soils. Soil Biol. Biochem. 33(15): 2083-2091. doi: 10.1016/S0038-0717(01)00140-7.

Rabenhorst, M.C. and S.N. Burch. 2006. Synthetic iron oxides as an indicator of reduction in soils (IRIS). Soil Sci. Soc. Am. J. 70:1227-1236.

Rabenhorst, and Hively. 2009. Measurements of soil redox potential. Soil Sci. Soc. Am. J. 73:668-674.

Raiswell, R, and DE Canfield. 2012. The iron biogeochemical cycle past and present. Geochem. Persp. 1(1):1-220. doi:10.7185/geochempersp.1.1.

Roden, EE. 2012. Microbial iron-redox cycling in subsurface environments. Biochem. Soc. Trans. 40:1249-1256.

Roy, R, HD Klüber, and R Conrad. 1997. Early initiation of methane production in anoxic rice soil despite the presence of oxidants. FEMS Microbiol. 24:311-320.

Barton, L., R. Kiese, D. Gatter, K. Butterbach-Bahl, R. Buck, C. hinz, and D. V. Murphy. 2008. Nitrous oxide emissions from a cropped soil in a semi-arid climate. Glob. Chang. Biol. 14(1): 177–192.

Schuur, E.A.G., O.A. Chadwick and P.A. Matson. 2001. Carbon cycling and soil carbon storage in mesic to wet hawaiian montane forests. Ecology 82:3182-3196.

Schuur E., and P. Matson. 2001. Net primary productivity and nutrient cycling across a mesic to wet precipitation gradient in Hawaiian montane forest. Oecologia. 128:431-442. doi: 10.1007/s004420100671.

Sexstone, AJ, TB Parkin, JM Tiedje. 1985. Temporal response of soil denitrification rates to rainfall and irrigation. Soil Sci. Soc. Am. J. 49:99-103.

Silver, W.L., A.E. Lugo and M. Keller. 1999. Soil oxygen availability and biogeochemistry along rainfall and topographic gradients in upland wet tropical forest soils. Biogeochemistry. 44:301-328.

Smith, MS, and JM Tiedje. 1979. Phases of denitrification following oxygen depletion in soil. Soil Biol. Biochem. 11:261-267. doi: 10.1016/0038-0717(79)90071-3.

Stiles, CA, ET Dunkinson, CL Ping, and J Kidd. 2010. Initial field installation of manganese indicators of reduction in soils, Brooks Range, Alaska. Soil Surv. Horiz. 51:102-107.

Teh, Y., W. Silver, and M. Conrad. 2005. Oxygen effects on methane production and oxidation in humid tropical forest soils. Glob. Chang. Biol. 114(3):331-345. doi: 10.1111/j.1365-2486.2005.00983.x.

Thompson, A., D.G. Rancourt, O.A. Chadwick and J. Chorover. 2011. Iron solid-phase differentiation along a redox gradient in basaltic soils. Geochim. Cosmochim. Acta 75:119-133.

Thompson, A., J. Ruiz, O.A. Chadwick, M. Titus and J. Chorover. 2007. Rayleigh fractionation of iron isotopes during pedogenesis along a climate sequence of hawaiian basalt. Chem. Geol. 238:72-83.

Yang, W., and D. Liptzin. 2015. High potential for iron reduction in upland soils. Ecology. 96(7):2015-2020.

Zausig, J., W. Stepniewski, and R. Horn. 1993. Oxygen Concentration and Redox Potential Gradients in Unsaturated Model Soil Aggregates. Soil Sci. Soc. Am. J. 57: 908–916.

FIGURES and TABLES

Table 2.1. MCG site characteristics (adapted from Miller et al., 2001; Thompson et al., 2007, 2011)

Site Number	MAP (mm)	Elevation (m)	MAT (˚C)	Taxonomic Class	Total Fe† (g kg^{-1})	Total Organic Carbon† (g kg^{-1})
1	2200	1370	16	hydrous, ferrihydritic, isomesic Andic Dystrudept	283.0 (198)	108 (4)
3	2800	1370	16	hydrous, ferrihydritic, isomesic Andic Dystrudept	156.0 (109)	218 (2)
4	3500	1320	16	hydrous, ferrihydritic, isomesic Acrudoxic Hydrudand	97.0 (68)	107 (3)
5	4200	1300	16	very-fine, isotic, isomesic Aquandic Epiaquept	6.2 (4)	478 (5)

†Error of one standard deviation in parentheses

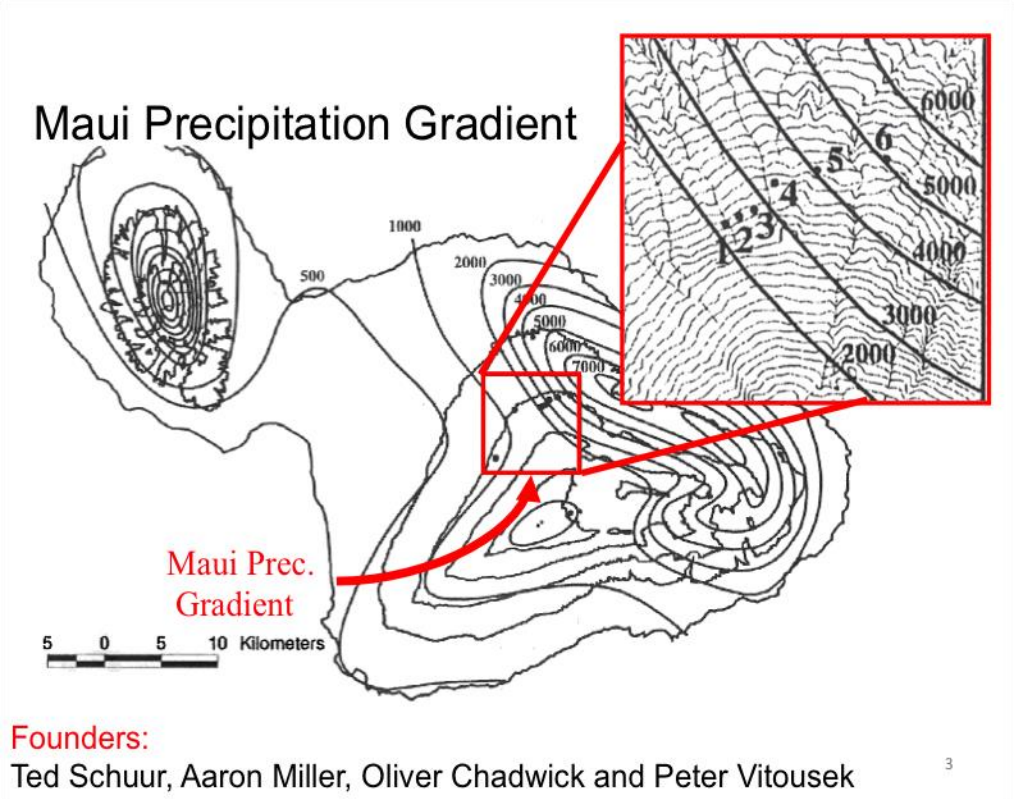

Fig. 2.1. The Maui Climate gradient with sites and corresponding mean annual precipitation isohyets. We included sites 1, 3, 4, and 5 in our study. (Reprinted from Thompson et al 2007).

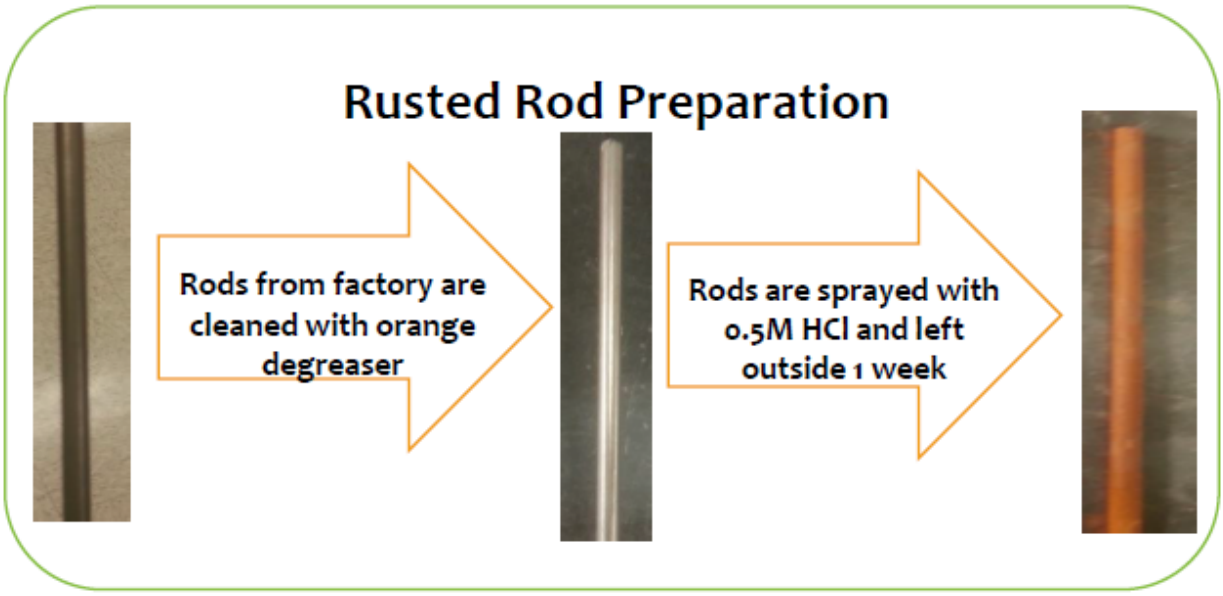

Fig. 2.2. Flow chart depicting the processes for producing the rusted steel reduction indicators. Rods are cleaned with citrus degreaser and then sprayed with dilute HCl.

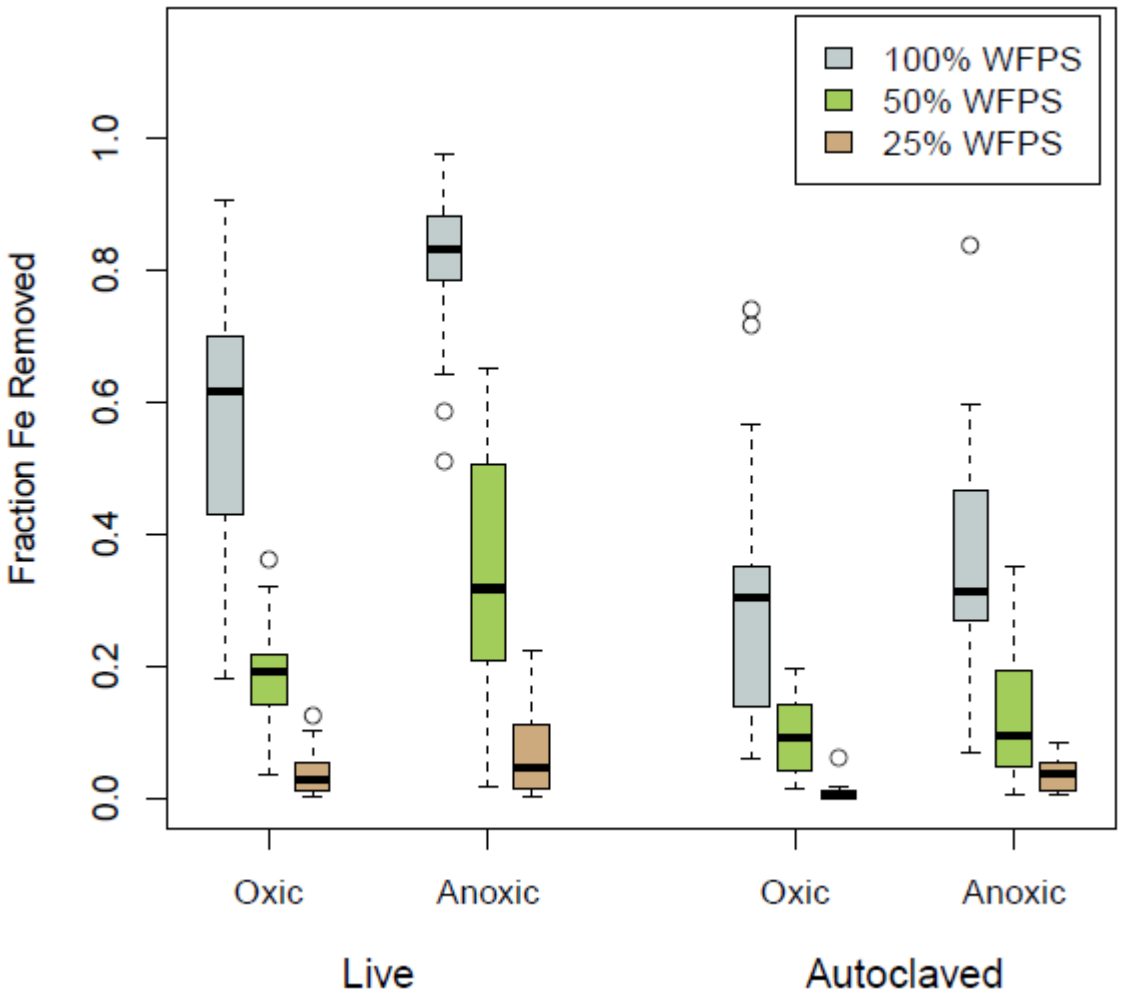

Figure 2.3: Results from the second experiment examining the effect of soil water content (WFPS), soil microorganisms, and ambient oxygen conditions on Fe removal from the steel IRIS probes. Blue represents 100% WFPS (saturation), the green represents 50% WFPS, and the pink represents 25% WFPS. The box represents the middle 25-75% of the distribution, the outer whiskers represent the minimum and maximum, and the heavy middle line represents the median. Circles represent outliers. Generally, the anoxic, wetter, and live treatments generated more Fe removal than the other treatments.

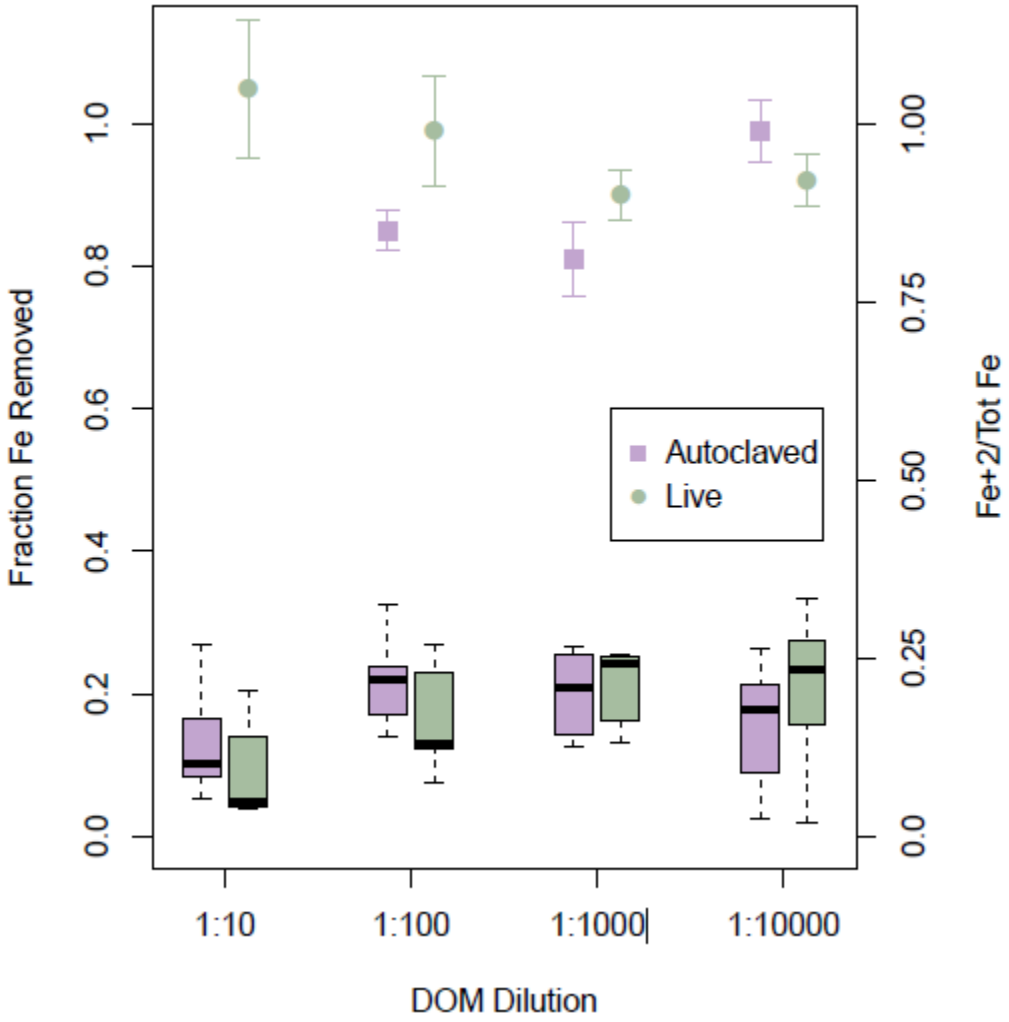

Figure 2.4: Next experiment examining the effect of DOM concentration on Fe removal from Steel IRIS rods along with Fe redox state in solution after removal. Boxplots represent the fraction of Fe removed from the Steel IRIS probes, and the points represent the average Fe^{+2}/Fe^{tot} ratio of the DOM solutions after the two week experimental period. . The box represents the middle 25-75% of the distribution, the outer whiskers represent the minimum and maximum, and the heavy middle line represents the median. Whiskers out of the Fe redox state points represent one standard error from the mean. There was no treatment effect with DOM concentration, and all measured treatment Fe ratios indicate predominately Fe^{+2} in solution.

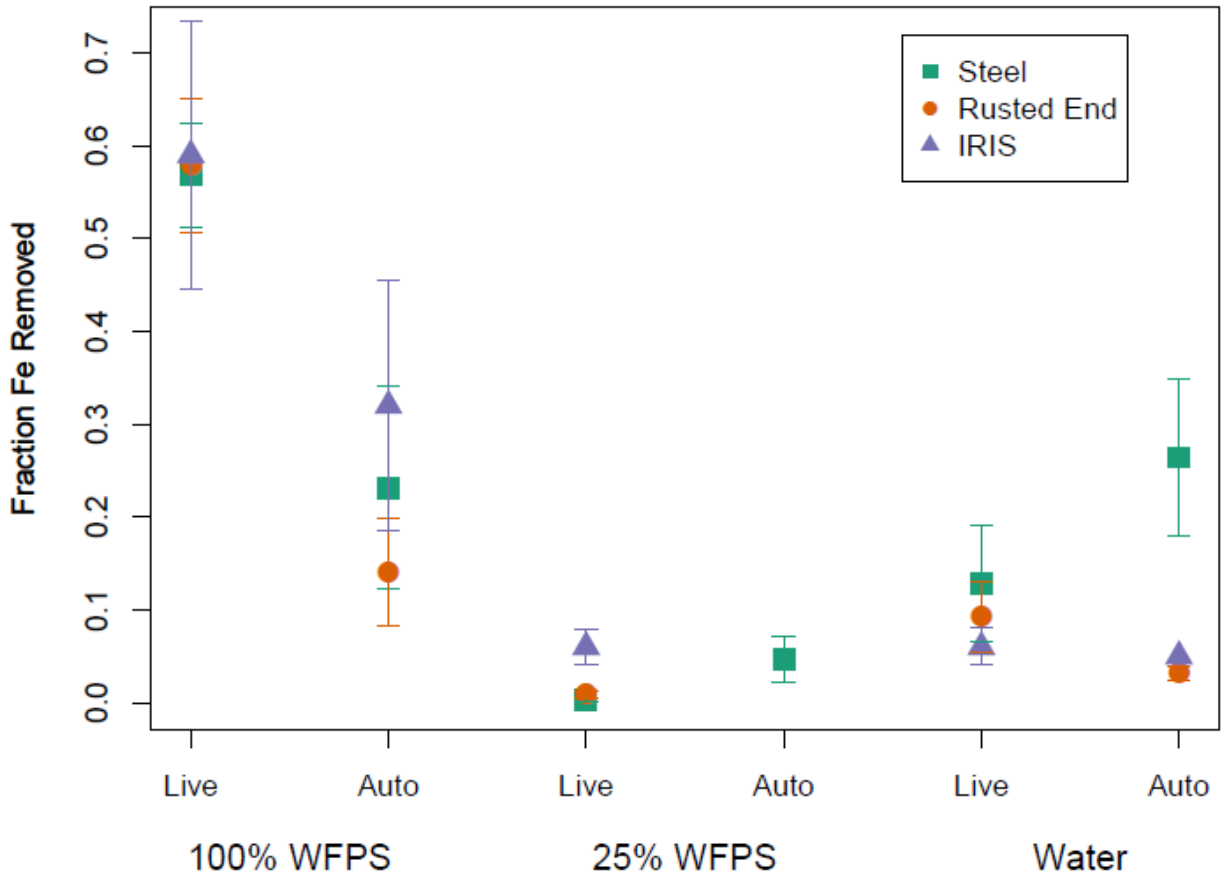

Figure 2.5: Fraction of Fe removed from the treatments of experiment 4 comparing Fe removal from Steel Iris Probes (square), Steel IRIS Probes with rusted ends (circle), and modified IRIS Tubes (triangle), in live and autoclaved (auto) soil with 100%, 25% WFPS, and in water. Points represent the mean of the measurements made in triplicate. Error bars represent one standard error from the mean. The different passive probes are not significantly different, except for in the autoclaved water treatment in which the steel IRIS without rusted ends is significantly higher than the others. The IRIS Tube treatments in 100% WFPS have much more variability.

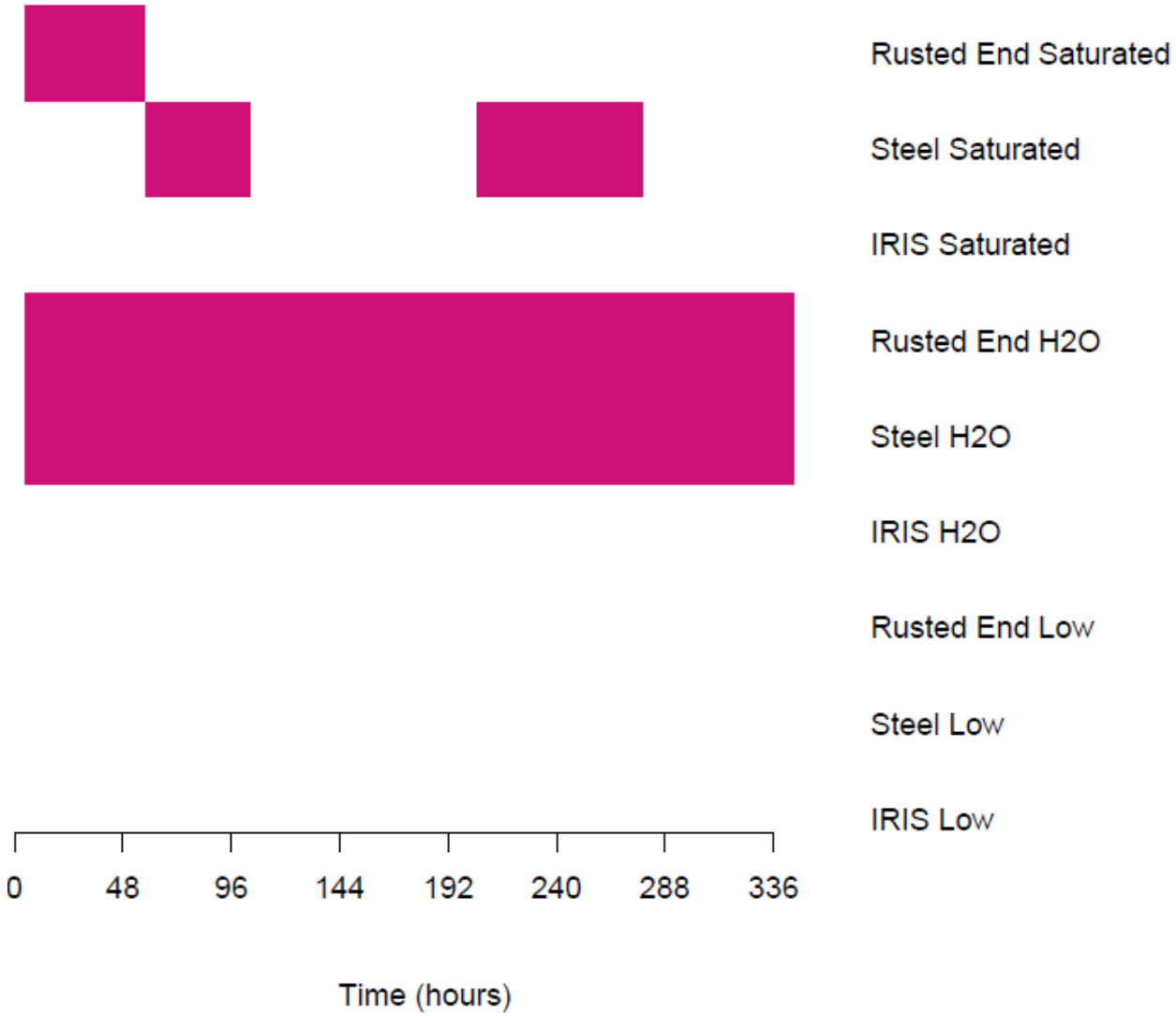

Figure 2.6: Presence of hydrogen peroxide in the solution of each live treatment over the two week sampling period. Pink indicates presence of Hydrogen peroxide. Measurements were taken at hour 0, 6, 18, 45, 72, 120, 168, 216, 288, and 336 (end point). Hydrogen peroxide persisted in the treatments with steel IRIS (rusted and unrusted ends) in water. This indicates that hydroxide free radicals were created that could facilitate the removal of Fe oxide from the steel surface.

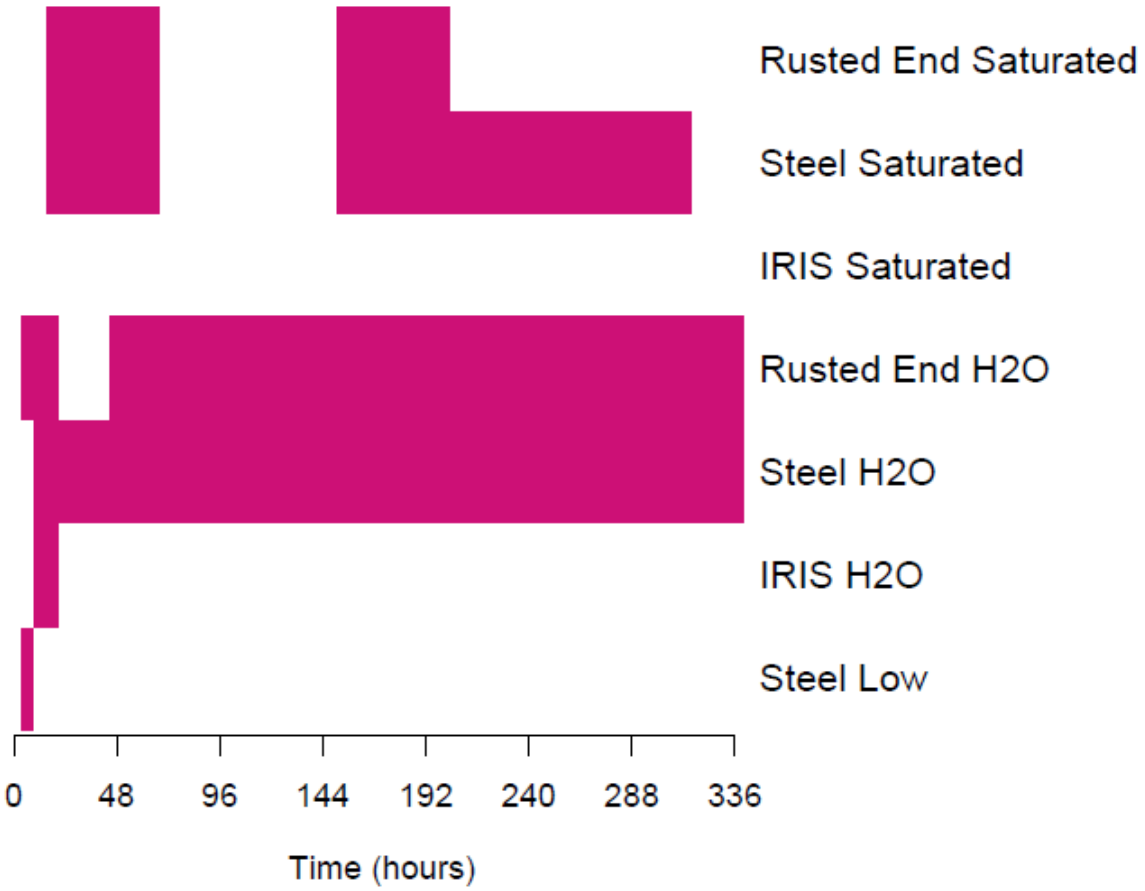

Figure 2.7: Presence of hydrogen peroxide in the solution of each autoclaved treatment over the two week sampling period. Pink indicates presence of Hydrogen peroxide. Measurements were taken at hour 0, 6, 18, 45, 72, 120, 168, 216, 288, and 336 (end point). Hydrogen peroxide persisted in the treatments with steel IRIS (rusted and unrusted ends) in water. This indicates that hydroxide free radicals were created that could facilitate the removal of Fe oxide from the steel surface.

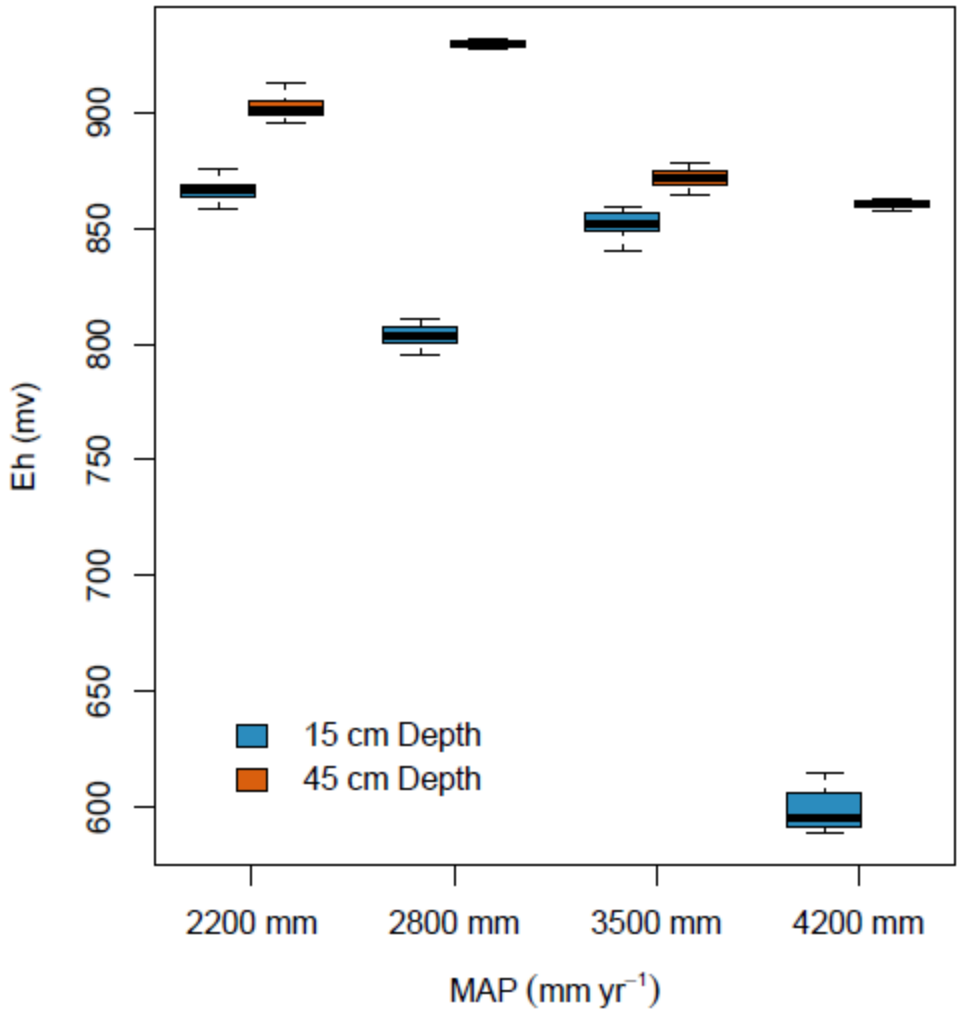

Fig. 2.8. Boxplots of the soil Eh_7 data collected across the MCG over five days from 15 and 45 cm depths.

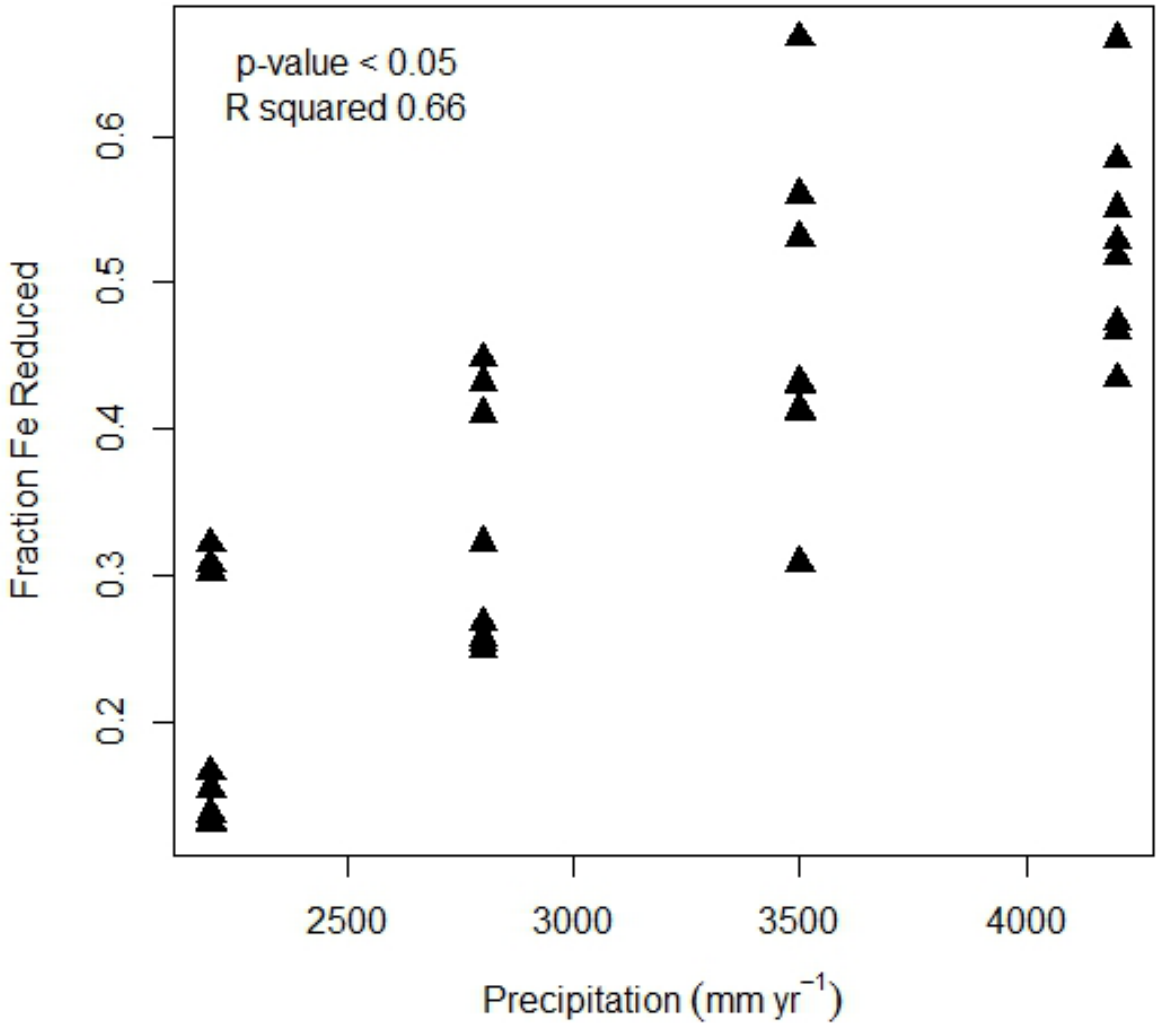

Fig. 2.9. Fraction of iron removed (i.e., m^2 m^{-2}) for the steel IRIS probes after 14 days at each site. Numbers signify the site number (Miller et al., 2001).($p= 0.016$; $r^2 = 0.66$).

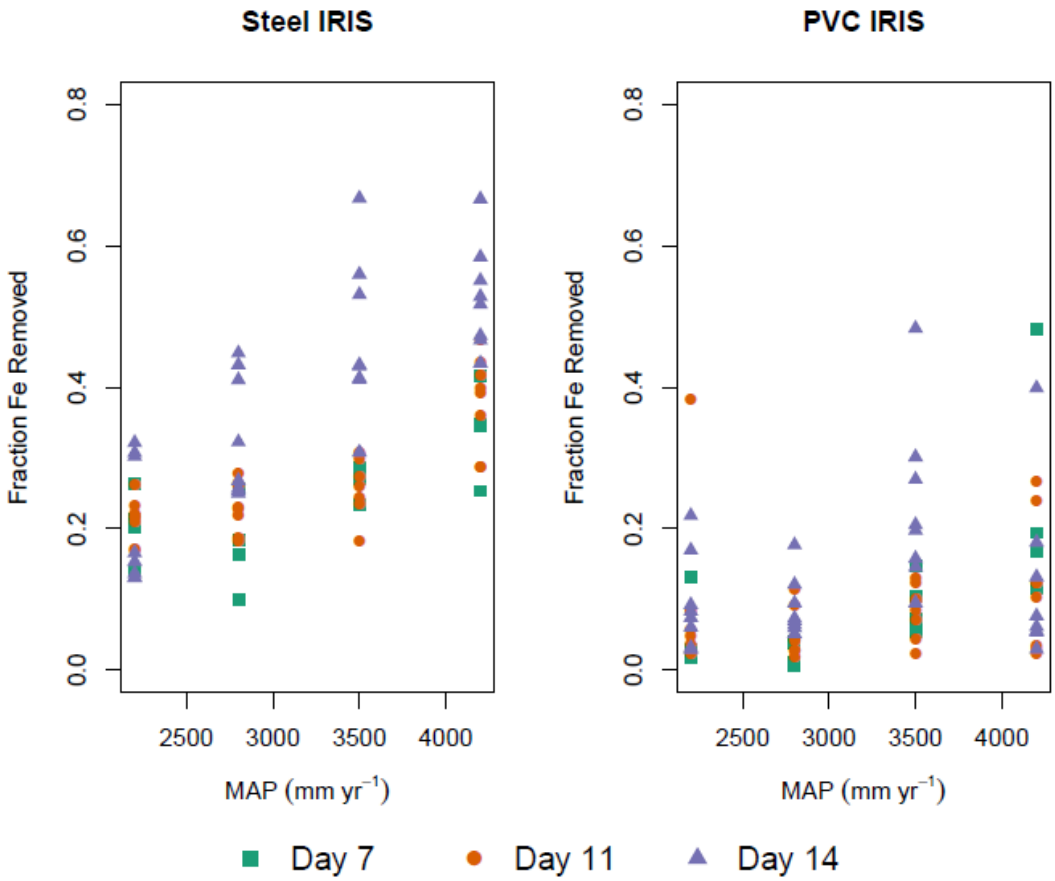

Fig. 2.10. Comparison of the fraction of Fe removed from the Steel and PVC IRIS probes at each sampling point and site.

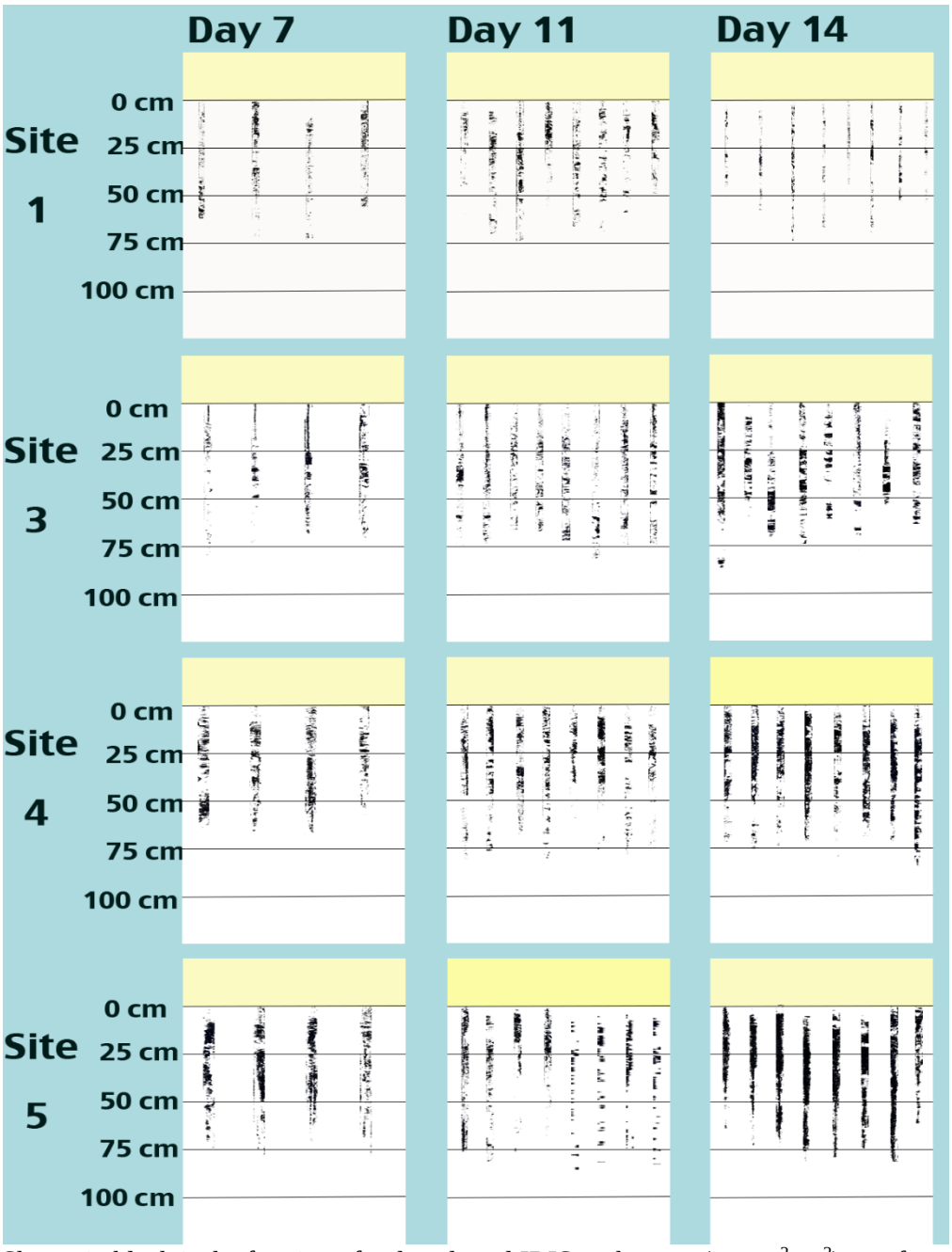

Fig. 2.11. Shown in black is the fraction of reduced steel IRIS probe area (i.e., m^2 m^{-2}) as a function of soil depth for one representative quarter of each replicate rod at 7, 11, and 14 d for each site.

CHAPTER 3

SEASONAL VARIATION IN THE POTENTIAL FOR IRON REDUCTION IN SOILS OF THE SOUTHEASTERN PIEDMONT[2]

[2] Hodges, C.A., J. Mallard, D. Markewitz, and A. Thompson. To be submitted to *Vadose Zone Journal*

ABSTRACT

Soil Iron reduction influences ecosystem form and function by altering the cycling of carbon, nutrients, and trace elements in both the aqueous and solid (or particulate) phases. Nearly all of our understanding of soil iron reduction comes from work on saturated soils (wetlands). However, recent work shows iron reduction can be a pivotal process in upland soils that experience dynamic redox conditions. We hypothesized that in upland soils, iron reduction intensity and prevalence would be affected by seasonal variations in soil moisture. We tested this by delineating the spatial and temporal distribution of the potential for iron reduction to 70 cm depth in upland sub-tropical forested watersheds using rusted steel "Indicators of Iron Reduction in Soil" (steel IRIS) probes, and non-invasive moisture sensing at three time-points over the course of a year: (a) after an extreme rainfall event in October 2015; (b) during the end-of-winter warming in March 2016; (c) and during a period of high evapotranspirational demand in June 2016. Our results indicate that the potential for iron reduction varied with depth and intensity over the year. Iron reduction was greatest at depth (40 – 60+ cm) following a rainfall event that generated prolonged subsurface soil saturation; whereas iron reduction was greatest near the surface (0 – 30 cm) in late winter/early spring when biological oxygen demand was likely high due to labile carbon and soil warming. In June 2016, the potential for Fe reduction was low across all depths. Our results indicate that soils of the Southeastern Piedmont likely experience strong seasonal trends in Fe reduction, as well as periodic spikes in response to large rain events. This work illustrates that otherwise oxic upland soils are likely to be shaped by Fe reduction processes at various points throughout the year.

INTRODUCTION

Iron (Fe) oxidation-reduction is well-studied in soils with frequent and predictable drops in soil oxygen concentration, but largely ignored in overall oxic upland soils until recently (Schuur et al., 2001; DeAngelis and Silver, 2010; Thompson et al., 2011; McNicol and Silver, 2014). When dissolved oxygen concentrations are suppressed, Fe(III) can compete as a terminal electron acceptor in microbial respiration. After soil flooding, which limits oxygen diffusion, this switch to Fe(III) occurs rapidly (Roden, 2012). For this reason, wetlands have been the focus of most soil iron reduction research. However, recent work documents iron reduction in upland soils, suggesting many ecosystems may be shaped by this key soil process (Fimmen et al., 2008; Borman et al., 2010; Fuss et al., 2010; Knorr, 2013; Yang and Liptzin, 2015; Ekström et al., 2016; Hall et al., 2016; Schulz et al., 2016). If soils from nearly any ecosystem are exposed to O_2-free conditions in the presence of labile carbon, iron reduction is likely to ensue (Lipson et al., 2010; De-Campos et al., 2012; Yang and Liptzin, 2015). Indeed, there is growing evidence that iron reduction (a low-oxygen transformation) may be an important process across a wide range of upland soils (Fimmen et al., 2008; Fuss et al., 2010; Keiluweit et al., 2016).

Upland soils of sub-tropical and temperate forests encompass a great range of spatial and temporal variability. Aseasonality of rainfall, transpiration, and temperature—key aspects of most temperate and sub-tropical forests—all affect soil water content and soil carbon stocks, which in turn determine the potential of a soil to foster Fe reducing conditions. This variability across space and time poses a difficult obstacle to characterizing Fe reduction across an upland landscape, as point measurements at one time in the year are inadequate to capture the full scope of the process. While most methods of characterizing Fe reduction in the field are expensive and time-consuming (Fiedler et al., 2007; Rabenhorst and Hively, 2009), passive indicator probes

used primarily to delineate wetlands (Bridgham and Faulkner, 1991; Castenson and Rabenhorst, 2006; Rabenhorst and Burch, 2006; Owens et al., 2008; Rabenhorst and Megonigal, 2010; Stiles et al., 2010; Dorau and Mansfeldt, 2016) may be applicable for landscape-scale questions regarding Fe reduction in upalnds.

Our goal was to characterize the spatial and temporal variation in the likelihood for Fe reduction to occur across three first order watersheds in the piedmont of the Southeastern United States. We hypothesized that the potential for Fe reduction would correlate with soil moisture status. We first characterized the variability in soil moisture conditions at the sites using electromagnetic induction (EMI) with bi-monthly surveys over the course of a year. Those surveys were then aggregated and used to select 100 sites of varying annual soil moisture status across the watersheds. At our distributed sites, we deployed Steel IRIS Probes (passive probes coated in easily-reducible Fe-minerals) at three ecologically significant times: after an extreme rainfall event, in late winter prior to leaf-out, and in late spring during a time of high evapotranspirational demand. We monitored soil moisture and water table level over the course of our deployments.

METHODS

Site Description

All experiments were conducted in first-order watersheds of the Calhoun Experimental Forest in Union, South Carolina (Figure 3.1). The experimental forest is located in the Southern Piedmont MLRA, and is underlain by granitic gneiss that has weathered mostly into Ultisols. The forested overstory consists of a mix of hardwood and pine. European settlement and subsequent clearcutting and agricultural use of the nineteenth and early twentieth centuries

disrupted the hydrologic cycle, which increased overland flow resulting in highly eroded surface soils. Mean annual temperature of the Calhoun Experimental Forest is 16˚ C, and mean annual precipitation is about 1170 mm (Richter et al., 1994).

Electromagnetic Induction Surveys

Surveys of the three watersheds were made every two months over the course of a year with a Dualem 2 electromagnetic induction (EMI) probe. EMI uses an electromagnetic field to measure soil specific conductance (Samouëlian et al., 2005), which has proven useful for characterizing variation in soil properties, especially soil texture and moisture (Doolittle et al., 1994; Corwin and Lesch, 2005; Harvey and Morgan, 2009; Francés and Lubczynski, 2011). Surveys of the Calhoun were conducted by walking along the contour of each of the three watersheds and collecting georeferenced point data. Soil specific conductance measurements collected to a soil depth of approximately 200 cm (horizontal co-planar, or HCP measurement), and 100 cm (perpendicular, or PRP). In ArcMap, point data were processed to remove anomalous values and then interpolated using an ordinary kriging routine in ArcMap's geostatistical analyst package.

Sites for the steel IRIS probe deployment were selected based on bi-monthly HCP measurements taken in the previous year, which were integrated into a single map that highlighted the areas in the three watersheds that maintained relatively high and low specific conductance over the course of the year. Using that map, sites for Steel IRIS deployment were distributed over relative soil moistures, so that Steel IRIS probes were installed in sites that experienced different conductance conditions. About 80 rods were deployed across the three watersheds at three different dates.

Steel IRIS Installation

Steel IRIS probes were prepared for installation following the methods detailed in Hodges et al. (2017). Briefly, 90 cm long, 0.6 cm diameter, low carbon steel rods were cleaned with a citrus degreaser, washed with water, sprayed with 0.1 M HCl, and then allowed to ripen in the sun for about a week. They were then installed on 9 October 2015, 1 March 2016, and 1 June 2016. The October 2015 date is five days after a 25 cm rainfall event. The March 2016 date falls within the spring "warmup" during which temperatures rise, and soil biological activity increases after the winter slow-down. Additionally, the March date occurred about 2 weeks prior to tree leaf-out so that evapotranspirational demand was still relatively low. The June installation date took place during a period of lower than average rainfall, and high transpirational demand. Specific conductance measurements of the three watershed were taken immediately prior to and after the installation of the March and June Steel IRIS probes.

Steel IRIS Removal and Processing

The steel IRIS probes were removed from the soil after two weeks. Within 2 h, the rods were cleaned with running water and gently rubbed with a sponge so that no soil remained on the probe, but the iron coatings remained intact and visible. The rods were labeled and pictures of each quarter of the diameter of the rod were taken. Combined, the quarters of the rods create a composite image of the entire rod surface area. Rod images were processed in Photoshop using the color range selection tool. With this tool, a range of colors that indicate a reduced color on the Steel IRIS probe was specified, and used to select pixels that were of a reduced color. This selection was then compared to the total number of pixels of the rod to denote the "fraction of Fe

removed from the rod." Also, the rod was split into 10 cm sections to describe potential Fe reduction with 10 cm depth increments to about 70 cm. Any black Fe coating—which is the formation of mixed valance phase, Magnetite (Hodges et al 2017)—was considered un-reduced so our summed "fraction of Fe removed" value is a conservative estimate.

Areas across the landscape at which all specific conductance estimates from the ordinary krig were made with less than 1.25 standard error were selected for more in-depth analysis. All Steel IRIS Probes deployed within this area of higher estimate confidence were used to compare interpolated specific conductance (HRP and PRP), slope aspect, elevation, plan slope curvature, and profile slope curvature to fraction of Fe removed in a multiple linear regression model.

Spatial relationships were examined in ArcMap using the geostatistical analyst package, and ANOVA and post hoc analyses were conducted in R to compare the results of the different sampling dates.

RESULTS

EMI Surveys

The EMI surveys indicated spatial and temporal variation of specific conductance in the soil over the course of the year (Figure 3.2 and 3.5). Generally, the soil had a higher specific conductance in late winter and lower specific conductance in late summer. To better visualize the variation throughout the year, we integrated each biomonthly specific conductance map into a single composite map indicating the mean conductance across the six EMI survey dates (Figure 3.2). While there was a large amount of variability, there were locations within the three watersheds that remained consistently wet or dry across all surveys (Figure 3.2, 3.5). While there was high variance across the measurements, the standard error of the interpolation within each

measurement was relatively low. When the mask of low standard error was created for the data extraction and multiple linear models, the mask encompassed the majority of the measured landscape (Fig 3.5).

Steel IRIS Probes

The integrated fraction of Fe removed from the steel IRIS rods was similar in October 2015 and March 2016 at an average of around 0.10 fraction of Fe removed, but significantly lower in June 2016 at an average of about 0.03 (Figure 2.3). Larger variations in the fraction of Fe removed occur with depth (Figure 2.4). The fraction of Fe removed was low (below 0.10) in all 10 cm segments in June save for the deepest depth (50 – 60 cm+ range), which was the same as the fraction of Fe removed in March 2016 and October 2015 at that depth. In October 2015, the majority of the removal of the Fe coatings occurred below 20 cm; whereas in March 2016, the majority of the removal of Fe coatings occurred above 30 cm (Figures 2.4 and 2.6).

There was no spatial correlation of fraction of Fe removed from the Steel IRIS Probes with landscape position (Figures 2.5 and 2.6)—for example, Fe removal was equally likely (or unlikely) to occur at a footslope position as at a summit across the sampling dates. Multiple linear models comparing fraction of Fe removed across the sampling dates and depths indicate no clear and consistent relationship of Fe removal with EMI measurements or topographic indices (Tables in Appendix B). Out of 28 initial models, the mean HCP measurement, which was used to distribute the Steel IRIS Probes across the landscape, was a significant predictor (p-value < 0.05) in about 30% of the initial models. Plan curvature also was a significant predictor in about 30% of the initial models. Profile curvature and aspect were significant predictors in about 25% of the initial models. However, even models with significant predictors did not

account for the majority of variation in Fe removal from the Steel IRIS probes (R^2 of 0.05 – 0.30). EMI surveys taken the same day of installation and retrieval were only significant predictors in 0-14% of the models (Tables in Appendix B).

DISCUSSION

Fe Reduction in Soils of the Calhoun CZO

The Steel IRIS Probe data from the three deployment dates indicate that Fe reduction is likely to occur in the first order watersheds of the Calhoun Forest. Specifically, the potential for Fe reduction is high both in response to an extreme rainfall event and in early spring. Early understanding of redox processes in soils indicated that reduction reactions would proceed based on decreasing thermodynamic favorability so that Fe reduction would occur only after oxygen, NO_3^-, and Mn^{IV} are depleted from the zone of microbial activity (Patrick and Jugsujinda, 1992; Peters and Conrad, 1996; De-Campos et al., 2012). However, closer studies of soil aggregates and *in situ* soil processes indicate that a wide range of redox processes occur simultaneously as pores of different sizes deliver oxygen at different rates. The least amount of oxygen is delivered to the interior of the ped as oxygen must follow a tortuous path through pores smaller than 30 microns (Sexstone and Parkin, 1985; Roy et al., 1997; Parry et al., 1999; Megonigal and Guenther, 2008). This means that the interior of soil aggregates, especially under high soil moisture conditions, foster greater reducing conditions than predicted from bulk soil oxygen and soil moisture status. Indeed, in an in-lab column study of the response of Steel IRIS Probes to soil moisture conditions, Hodges et al. (2017) found that significant amounts of Fe were removed when the soils were at field capacity, or 50% water filled pore space, significantly below saturation, which is generally assumed necessary for soil Fe reduction. Our results corroborate

this conclusion, as we observed significant Fe removal even under unsaturated conditions in March and in the base of the soil profile in June.

Variation in Fe Reduction with Depth and Time

The depth at which we observed the greatest fraction of Fe removed from the Steel IRIS Probes varied with installation date. We observed the greatest Fe removal from the subsurface (40-60+ cm) in October and June, and the greatest Fe removal from the surface soils in March (0-30 cm). These differences coincide with differences in soil moisture, carbon, and temperature that potentially have profound effects on microbial activity, and could better explain our results (Davidson et al., 1998; Scott-Denton et al., 2003; Davidson and Janssens, 2006; Megonigal and Guenther, 2008).

While both our and other's data indicate that water inputs are important in terms of limiting oxygen diffusion and stimulating the use of alternate electron acceptors, carbon input/availability is shown to be equally important in stimulating Fe reduction. Our March deployment data underlines this point, by indicating that Fe reduction was higher in the top ten centimeters at this time than at the other deployment dates. This depth interval, while moist, was not saturated, and therefore oxygen was most likely diffusing throughout the soil layer. However, high carbon availability at this time due to litter-fall, and higher temperatures than in the winter months, most likely stimulated microbial activity. This higher microbial activity generated an oxygen deficit as the rate of oxygen consumption outpaced the rate of diffusion (Hall et al., 2016). As this deficit grew, microbial populations likely shifted to alternate terminal electron acceptors, possibly burning quickly through any NO_3^- present, and shifting shortly thereafter to Fe^{III} reduction, as Mn concentrations in these soils are quite low due to the high degree of

weathering (Li et al., 2008; De-Campos et al., 2012). Our March data corroborate well with others' data on Fe reduction in upland soils, especially Hall et al. (2016) who have indicated that carbon availability is the greatest predictor of Fe reduction in warm, wet soils of Puerto Rico.

In October, the input of water, which saturated the top meter of the soil and limited oxygen diffusion, triggered the use of alternate electron acceptors (i.e. Fe^{III}) for microbial respiration. While this rainfall event was an extreme case, less extreme events have the potential to saturate the solum and stimulate alternate respiration pathways, pointing to the potential for many sites that experience pulses of water to foster Fe-reducing conditions (Bailey et al., 2014; Gannon et al., 2015). These pulses can range from extreme weather events, like a hurricane, to seasonal snowmelt, to more common-place rainfall events that deposit enough water to saturate all or part of the solum for enough time to affect microbial respiration (Knorr, 2013; Bourgault et al., 2015; Ekström et al., 2016). From in-lab studies, we know that Steel IRIS Probes indicate high potential for Fe reduction at soil moisture contents well below 100% WFPS, and that significant Fe reduction occurs at 50% WFPS (Hodges et al. 2017). From the field we know that the greatest fraction of Fe reduction removed from Steel IRIS Probes occurs in soils that receive high inputs of low-intensity rainfall that maintains soil saturation, but significant reduction also occurs in soils that are allowed to drain macropores between rainfall events (Hodges et al., 2017).

The depth-dependent data from October 2015 indicate that the greatest potential for Fe reduction was in the subsurface horizons. However, it is unclear whether this stimulation of Fe reduction at depth was in response to the immense amount of water delivered to the system ponding atop less structured soil horizons, and in turn limiting oxygen diffusion in the lower depths of the solum, or if the water transported labile carbon to the lower soil horizons, which

was then utilized by the microbial population at depth (Lohse et al., 2009). The use of that pulse of labile carbon at depth by soil microbes for respiration could have potentially outpaced the diffusion of oxygen, thereby necessitating the switch to alternate terminal electron acceptors, like Fe. Perhaps the most likely justification for high Fe removal at depth is a combination of the two previous explanations; water rich in labile carbon moved through the solum, and stagnated above the poorly-structured BC horizon. The carbon inputs provided an electron-rich substrate for the microbes, but the water prevented the diffusion of oxygen, forcing the soil bacteria to use an alternative terminal electron acceptor, like Fe, for respiration.

Specific Conductance and Fe Reduction

We found little to no correlation between specific conductance measurements and fraction of Fe removed (Fe reduction potential). While the EMI was a useful tool for understanding soil variability and distributing our Steel IRIS probes across that variability, it fell short in terms of its predictive power for this biogeochemical process. Others have had similar experiences when attempting to use EMI to explain soil biogeochemistry across a complex landscape. For example, Harvey and Morgan (2009), attempted to use EMI to characterize soil carbon stocks across a highly variable landscape in Southeastern Texas, but found that it mostly strongly correlated to soil clay content in the top meter. As this study indicates, EMI is helpful for prediction over uniform landforms and soil types, but is limited when there is a wide variation in clay and depth to clay-accumulating soil layers across a site, like in the first-order watersheds of the Calhoun Forest (Tabbagh et al., 2000; Corwin and Lesch, 2005; Samouëlian et al., 2005). Even though clay content greatly affects soil moisture, and therefore should play some role in determining the potential for Fe reduction, our results point to carbon inputs as being

more important, and consequently obscures the useful signal that the EMI may provide. Additionally, since EMI is an integrated measure of soil conductance over the depth of the electromagnetic signal (i.e. measures specific conductance), it does not pick up the depth-dependent hotspots that we identified in our study, which makes it less useful. For example, a site may have an average fraction of Fe removed of 0.08, but the fraction of Fe removed in the lowest 20 cm may be 0.20, while the top 40 cm the fraction Fe removed was only 0.02. Those depth-dependent data are important, but are overlooked with an integrated measure, as a fraction of Fe removed of 0.20 is quite high and indicative of reducing conditions. In summary, EMI is useful in characterizing site variability, but falls short in its predictive power of the fraction of Fe removed because it is greatly affected by the clay signal and only records an integrated measurement.

Implications

Evidence for widespread Fe reduction in upland soils of the Calhoun Forest hints at greater mobility of phosphorus and other elements that are often associated with Fe minerals. When Fe minerals are reduced, their constituents are released to the pedosphere to be scavenged by trees and other soil organisms, redistributed to lower soil horizons to re-associate with soil minerals, or lost from the regolith through leaching to groundwater (Chacon et al., 2006; Borch et al., 2009; Henderson et al., 2012; Buettner et al., 2014; Prem et al., 2014). Under the conditions that we observed in both October and March, reductive dissolution likely occurred in the soil resulting in greater phosphorus and trace metal mobility. Our findings necessitate greater study of element mobility under reduction events like those that we observed in an upland, sub-tropical forest, as Fe reduction events in upland soils could be a significant source of nutrients to

soil organisms. Potential avenues of future inquiry lie in determining the availability of mobilized constituents to soil organisms; are the processes too isolated at the interior of soil aggregates to make a difference, are these species simply re-sorbed or otherwise immobilized when transported to more oxygen-rich sites, or do they remain active in the soil environment after the release via reductive dissolution?

Carbon and iron share an intimate relationship in subsurface environments. Organic carbon is the most common electron donor in Fe respiration, so that Fe reduction results in carbon oxidation and soil CO_2 emissions under low oxygen conditions (Nealson and Saffarini, 1994; Weber et al., 2006). That said, the importance of this Fe respiration to overall soil CO_2 emissions is highly variable across ecosystems. While some have found that Fe reduction can account for nearly half of total soil CO_2 emissions, other have found that the Fe respiration signal is negligible under most conditions (Lipson et al., 2010; Hall et al., 2013). Of additional importance is the linkage of Fe and C in the pedosphere as mineral-organic carbon associations. When the Fe in these associations is reduced, the carbon is mobilized to either re-precipitate lower in the solum or leach to groundwater and eventually enter surface waters (Buurman and Jongmans, 2005; Mikutta et al., 2009; Colombo et al., 2014; Ferro-Vázquez et al., 2014). Others have presented evidence that Fe reduction in upland watersheds can be a significant source of DOC in surface water, and indicate the important role of Fe minerals in retaining carbon in terrestrial systems (Knorr, 2013; Gannon et al., 2015; Ekström et al., 2016; Linkhorst et al., 2016). Under the reduction events that we observed, we would predict a concurrent pulse of DOC into ground and surface waters, with specific implications for microbial activity in surface waters in response to rainfall and at the end of winter. While the importance of Fe reduction to soil carbon seems to be highly nuanced and ecosystem, site, and process dependent, our results

point to an episodic/seasonal importance of this pathway of potential carbon release from the solum.

CONCLUSIONS

We found that Fe reduction occurs both in response to extreme rainfall events, and at the end of winter prior to leaf-out in the Southeastern Piedmont. At these two sampling dates, we recorded similar amounts of total potential for Fe reduction, but also found that Fe reduction occurred at different depths in the solum. Water stagnating at the base of the structured Bt horizon in response to an extreme rainfall event in October, and carbon inputs to the soil surface encouraging microbial activity in March, both hindered oxygen diffusion, which stimulated the use of Fe as a terminal electron acceptor. Additionally, we found that Fe reduction is low in the late spring and summer months when evapotranspirational demand is high and exogenous carbon inputs are low. Our hypothesis focused on the role of soil moisture in limiting oxygen diffusion into the soil matrix, and in turn promoting alternate respiration processes, and while our results support this hypothesis, it also ignored the role of carbon in Fe reduction. The depth of the most intense reducing conditions in October and March point to carbon as a key component in stimulating Fe reduction in upland soils. We conclude that the potential for Fe reduction is episodically and seasonally high in upland soils of the Southeastern piedmont, and likely high in other humid climate regimes with periods of low evapotranspirational demand, pulsed soil moisture events, or periods of time with high inputs of electron donors.

REFERENCES

Bailey, S., P. Brousseau, K. McGuire, and D. Ross. 2014. Influence of landscape position and transient water table on soil development and carbon distribution in a steep, headwater catchment. Geoderma 226: 279–289.

Borch, T., R. Kretzschmar, and A. Kappler. 2009. Biogeochemical redox processes and their impact on contaminant dynamics. Environmental Science & Technology 44: 15–23.

Borman, C.J., P.B. Sullivan, C.M. Eggleston, and P.J. Colberg. 2010. Is iron redox cycling in a high altitude watershed photochemically or thermally driven? Chemical Geology 269(1): 33–39.

Bourgault, R., D. Ross, and S. Bailey. 2015. Chemical and Morphological Distinctions between Vertical and Lateral Podzolization at Hubbard Brook. Soil Science Society of America Journal 79(2): 428.

Bridgham, SD, and SP Faulkner. 1991. Steel rod oxidation as a hydrologic indicator in wetland soils. Soil Sci. Soc. Am. J. (55): 856–862.

Buettner, S., M. Kramer, O. Chadwick, and A. Thompson. 2014. Mobilization of colloidal carbon during iron reduction in basaltic soils. Geoderma (221-222): 139–145.

Buurman, and A.G. Jongmans. 2005. Podzolisation and soil organic matter dynamics. Geoderma 125(1-2): 71–83.

De-Campos, A., C. Huang, and C. Johnston. 2012. Biogeochemistry of terrestrial soils as influenced by short-term flooding. Biogeochemistry (111): 239–252.

Castenson, K., and M. Rabenhorst. 2006. Indicator of Reduction in Soil (IRIS): Evaluation of a New Approach for Asessing Reduced Conditions in Soil. Soil Science Society of America (70): 1222–1226.

Chacon, N., W. Silver, E. Dubinsky, and D. Cusack. 2006. Iron reduction and soil phosphorus solubilization in humid tropical forests soils: the roles of labile carbon pools and an electron shuttle compound. Biogeochemistry 78: 67–84.

Colombo, C., G. Palumbo, J. He, and R. Pinton. 2014. Review on iron availability in soil: interaction of Fe minerals, plants, and microbes. Journal of Soils and Sediments 14(3): 538-548.

Corwin, D., and Lesch. 2005. Characterizing soil spatial variability with apparent soil electrical conductivity: I. Survey protocols. Computers and Electronics in Agriculture (46): 103–133.

Davidson, E., E. Belk, and R.D. Boone. 1998. Soil water content and temperature as independent or confounded factors controlling soil respiration in a temperate mixed hardwood forest. Global change biology 4(2): 217–227.

Davidson, E., and I. Janssens. 2006. Temperature sensitivity of soil carbon decomposition and feedbacks to climate change. Nature 440: 165–173.

DeAngelis, K., W. Silver, A.W. Thompson, and M.K. Firestone. 2010. Microbial communities acclimate to recurring changes in soil redox potential status. Environmental Microbiology 12(12): 3137–3149.

Doolittle, J., K. Sudduth, and N. Kitchen. 1994. Estimating depths to claypans using electromagnetic induction methods . J. Soil and Water Conservation 49(6): 572–575.

Dorau, K., and T. Mansfeldt. 2016. Manganese and iron oxide-coated redox bars as a tool to in situ study the element sorption in wet soils. Journal of Soils and Sediments 16(3): 976–986.

Ekström, S., O. Regnell, H. Reader, A. Nilsson, S. Löfgren, and E. Kritzberg. 2016. Increasing concentrations of iron in surface waters as a consequence of reducing conditions in the catchment area. J Geophys Res Biogeosciences 121(2): 479–493.

Ferro-Vázquez, Nóvoa-Muñoz, Costa-Casais, Klaminder, and Martínez-Cortizas. 2014. Metal and organic matter immobilization in temperate podzols: A high resolution study. Geoderma 217-218: 225-234.

Fiedler, S., M. Vepraskas, and J. Richardson. 2007. Soil redox potential: importance, field measurements, and observations. Advances in Agronomy 94: 1–54.

Fimmen, R., D. RichterJr., D. Vasudevan, M. Williams, and L. West. 2008. Rhizogenic Fe–C redox cycling: a hypothetical biogeochemical mechanism that drives crustal weathering in upland soils. Biogeochemistry 87(2): 127–141.

Francés, A., and M. Lubczynski. 2011. Topsoil thickness prediction at the catchment scale by integration of invasive sampling, surface geophysics, remote sensing and statistical modeling. Journal of Hydrology 405(1-2): 3147.

Fuss, C., C. Driscoll, C. Johnson, R. Petras, and T. Fahey. 2010. Dynamics of oxidized and reduced iron in a northern hardwood forest. Biogeochemistry 104(1-3): 103–119.

Gannon, J.P., S.W. Bailey, K.J. McGuire, and J.B. Shanley. 2015. Flushing of distal hillslopes as an alternative source of stream dissolved organic carbon in a headwater catchment. Water Resources Research (51): 8114–8128.

Hall, S., D. Liptzin, H. Buss, K. DeAngelis, and W. Silver. 2016. Drivers and patterns of iron redox cycling from surface to bedrock in a deep tropical forest soil: a new conceptual model. Biogeochemistry 130(1-2): 177–190.

Hall, S., W. McDowell, and W. Silver. 2013. When wet gets wetter: decoupling of moisture, redox biogeochemistry, and greenhouse gas fluxes in a humid tropical forest soil. Ecosystems (16): 576–589.

Harvey, O., and C. Morgan. 2009. Predicting regional-scale soil variability using a single calibrated apparent soil electrical conductivity model. Soil Science Society of America 73(1): 164-169.

Henderson, R., N. Kabengi, N. Mantripagada, M. Cabrera, S. Hassan, and A. Thompson. 2012. Anoxia-induced release of colloid-and nanoparticle-bound phosphorus in grassland soils. Environmental Science & Technology 46: 11727–11734.

Knorr, K.-H. 2013. DOC-dynamics in a small headwater catchment as driven by redox fluctuations and hydrological flow paths–are DOC exports mediated by iron reduction/oxidation cycles? Biogeosciences 10(2): 891–904.

Li, J., D. Richter, A. Mendoza, and P. Heine. 2008. Four-decade responses of soil trace elements to an aggrading old-field forest: B, Mn, Zn, Cu, and Fe. Ecology 891(10): 2911–2923.

Linkhorst, A., T. Dittmar, and H. Waska. 2016. Molecular fractionation of dissolved organic matter in a shallow subterranean estuary: the role of the iron curtain. Environ Sci Technology 51(3): 1312–1320.

Lipson, D., M. Jha, T. Raab, and W.C. Oechel. 2010. Reduction of iron (III) and humic substances plays a major role in anaerobic respiration in an Arctic peat soil. Journal of Geophysical Research 115: 1–13.

Lohse, K., P. Brooks, and J. McIntosh. 2009. Interactions between biogeochemistry and hydrologic systems. Annual Review of Environment and Resources 34: 65–96.

McNicol, G., and W. Silver. 2014. Separate effects of flooding and anaerobiosis on soil greenhouse gas emissions and redox sensitive biogeochemistry. Journal of Geophysical Research: Biogeosciences 119(4): 557–566.

Megonigal, J., and A. Guenther. 2008. Methane emissions from upland forest soils and vegetation. Tree Physiology 28: 491–498.

Mikutta, R., G. Schaumann, and D. Gildemeister. 2009. Biogeochemistry of mineral–organic associations across a long-term mineralogical soil gradient (0.3–4100kyr), Hawaiian Islands. Geochimica et Cosmochimica Acta 73: 2034–2060.

Nealson, K., and D. Saffarini. 1994. Iron and manganese in anaerobic respiration: environmental significance, physiology, and regulation. Annual Reviews in Microbiology 48: 311–343.

Owens, P., L. Wilding, W. Miller, and R. Griffin. 2008. Using iron metal rods to infer oxygen status in seasonally saturated soils. Catena 73: 197–203.

Parry, S., P. Renault, C. Chenu, and R. Lensi. 1999. Denitrification in pasture and cropped soil clods as affected by pore space structure. Soil Biol. Biochem.: 493–501.

Patrick, W., and A. Jugsujinda. 1992. Sequential reduction and oxidation of inorganic nitrogen, manganese, and iron in flooded soil. Soil Science Society of America 56: 1071–1073.

Peters, V., and R. Conrad. 1996. Sequential reduction processes and initiation of CH 4 production upon flooding of oxic upland soils. Soil Biology and Biochemistry 28(3): 371–382.

Prem, M., H. Hansen, W. Wenzel, L. Heiberg, H. Sørensen, and O. Borggaard. 2014. High Spatial and Fast Changes of Iron Redox State and Phosphorus Solubility in a Seasonally Flooded Temperate Wetland Soil. Wetlands 35(2): 237–246.

Rabenhorst, M., and S. Burch. 2006. Synthetic iron oxides as an indicator of reduction in soils (IRIS). Soil Science Society of America 70: 1227–1236.

Rabenhorst, M., and W. Hively. 2009. Measurements of soil redox potential. Soil Science Society of America Journal 73: 668–674.

Rabenhorst, M., and J. Megonigal. 2010. Synthetic iron oxides for documenting sulfide in marsh pore water. Soil Science Society of America 74: 1383–1388.

Richter, D.D., D. Markewitz, C. Wells, H. Allen, R. April, P. Heine, and B. Urrego. 1994. Soil chemical change during three decades in an old-field loblolly pine (Pinus taeda L.) ecosystem. Ecology 75(5): 1463–1473.

Roden, E. 2012. Microbial iron-redox cycling in subsurface environments. Biochemistry Society Transaction 40: 1249–1256.

Roy, R., H. Klüber, and R. Conrad. 1997. Early initiation of methane production in anoxic rice soil despite the presence of oxidants. FEMS Microbiology Ecology 24: 311–320.

Samouëlian, A., I. Cousin, A. Tabbagh, and A. Bruand. 2005. Electrical resistivity survey in soil science: a review. Soil and Tillage Research 83: 173–193.

Schulz, M., D. Stonestrom, and C. Lawrence. 2016. Structured heterogeneity in a marine terrace chronosequence: Upland mottling. Vadose Zone Journal 15: 11–14.

Schuur, E., O. Chadwick, and P. Matson. 2001. Carbon cycling and soil carbon storage in mesic to wet Hawaiian montane forests. Ecology 82(11): 3182–3196.

Scott-Denton, L.E., K.L. Sparks, and R.K. Monson. 2003. Spatial and temporal controls of soil respiration rate in a high-elevation, subalpine forest. Soil Biology and Biochemistry 35(4): 525–534.

Sexstone, A., and T. Parkin. 1985. Temporal response of soil denitrification rates to rainfall and irrigation. Soil Science Society of America Journal 49: 99–103.

Stiles, C., E. Dunkinson, C. Ping, and J. Kidd. 2010. Initial field installation of manganese indicators of reduction in soils, Brooks Range, Alaska. Soil Horizons 51: 102–107.

Tabbagh, A., M. Dabas, A. Hesse, and C. Panissod. 2000. Soil resistivity: a non-invasive tool to map soil structure horizonation. Geoderma 97: 393–404.

Thompson, A., D. Rancourt, and O. Chadwick. 2011. Iron solid-phase differentiation along a redox gradient in basaltic soils. Geochimica et Cosmochimica Acta 75: 119–133.

Weber, K., L. Achenbach, and J. Coates. 2006. Microorganisms pumping iron: anaerobic microbial iron oxidation and reduction. Nature Reviews Microbiology 4(10): 752–764.

Yang, W., and D. Liptzin. 2015. High potential for iron reduction in upland soils. Ecology 96(7).

FIGURES

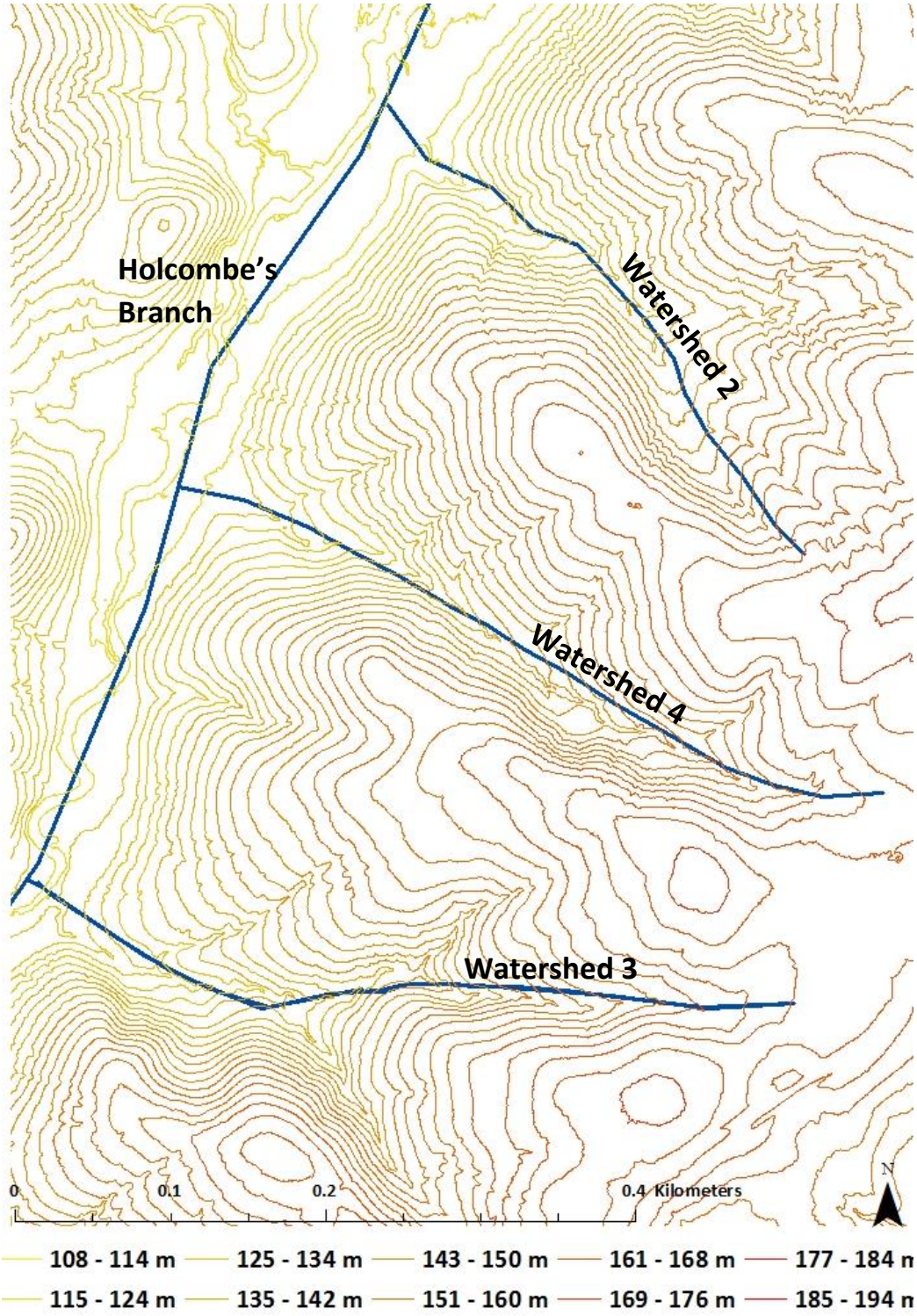

Figure 3.1: Contour map of the first order, experimental watersheds at the Calhoun CZO in which the steel IRIS rods were deployed. Contours are on a 2 m interval, and the blue lines represent drainages.

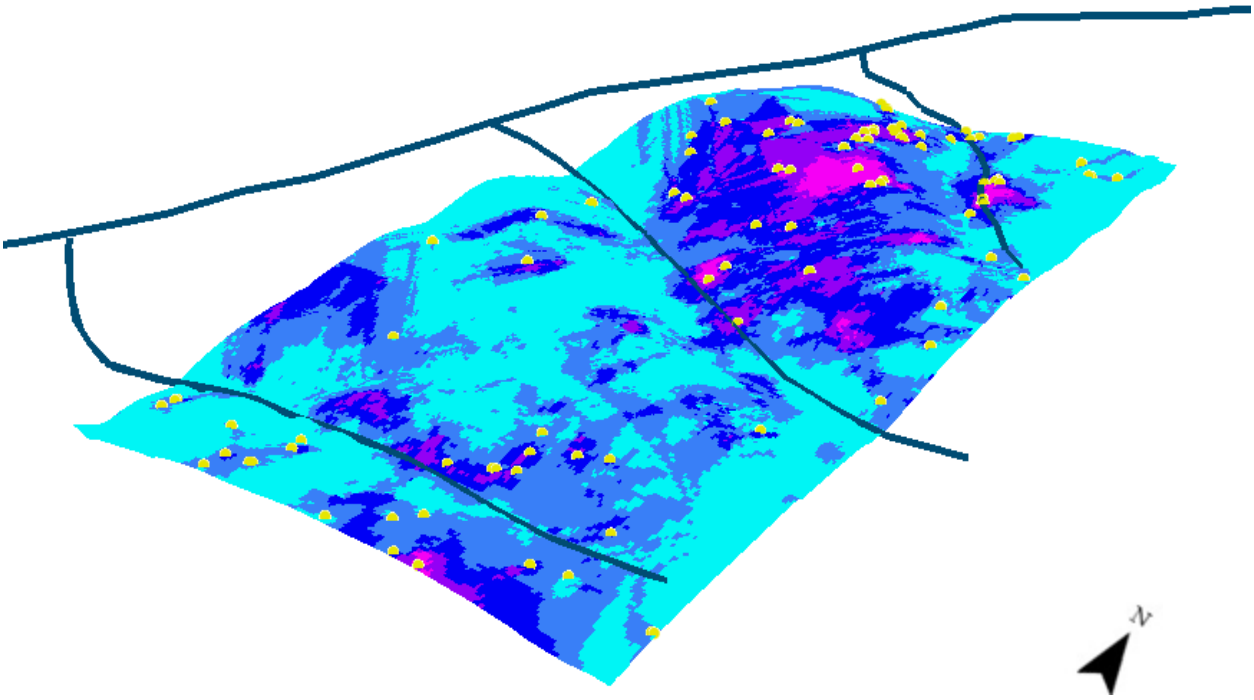

Figure 3.2: Integrated map of soil specific conductance from the bi-monthly electromagnetic induction surveys. Purple colors represent the locations that have the highest relative specific conductance over the course of the year, light blue colors represent the locations with the lowest relative specific conductance over the course of the year. Yellow dots represent the 100 sampling points distributed across the annual relative specific conductance.

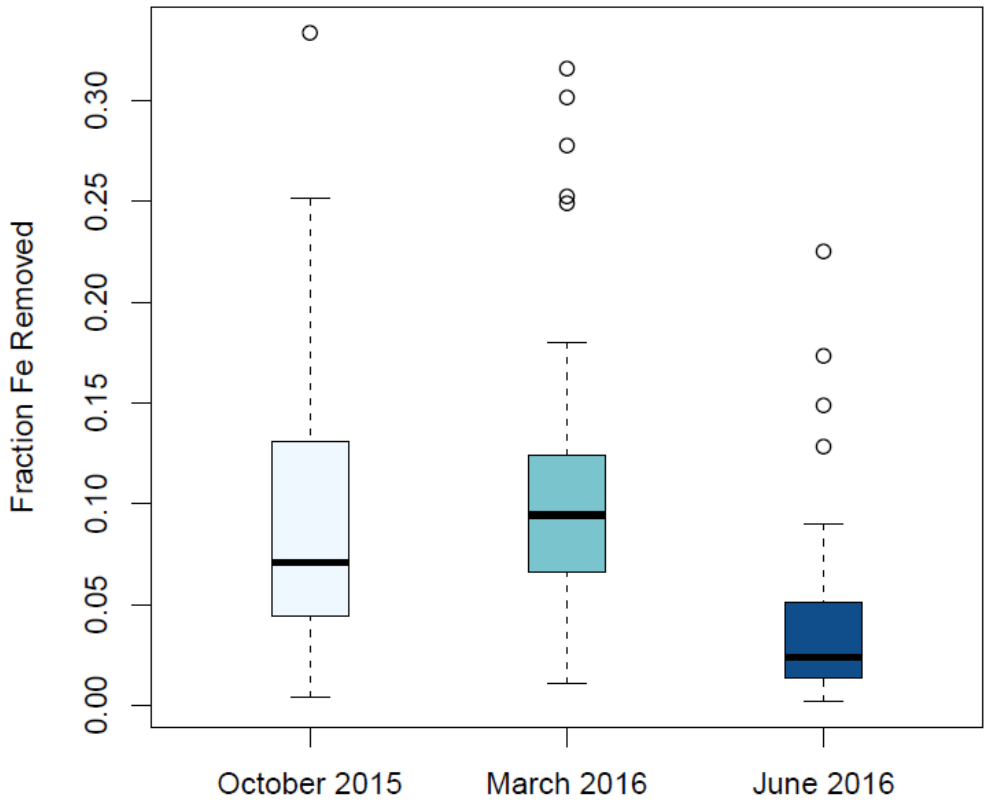

Figure 3.3: Boxplots of potential for upland Fe reduction (represented by fraction of Fe removed) during October 2015, March 2016, and June 2016 at the Calhoun CZO. October 2015 and March 2016 are significantly higher than June 2016, and there is no statistical difference between October 2015 and March 2016.

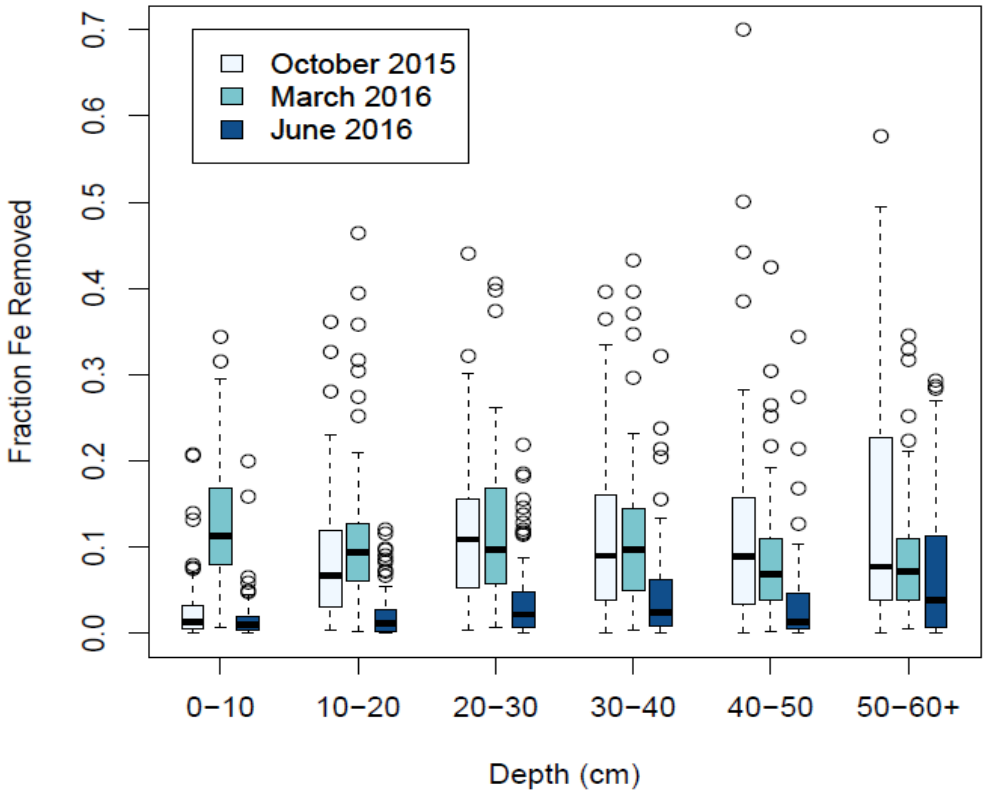

Figure 3.4: Potential for Fe reduction at ten cm depth intervals represented by fraction of Fe removed from steel IRIS rods.

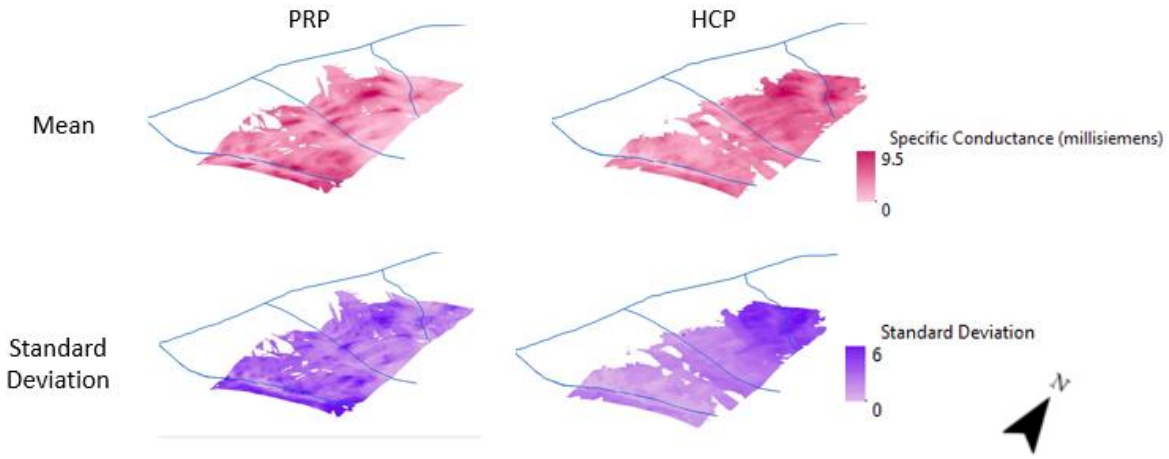

Fig. 3.5: Low variance mask (variance less than 1.25) of the HCP and PRP mean (in magenta) and standard deviation (in purple) from the 6 bimonthly measurements.

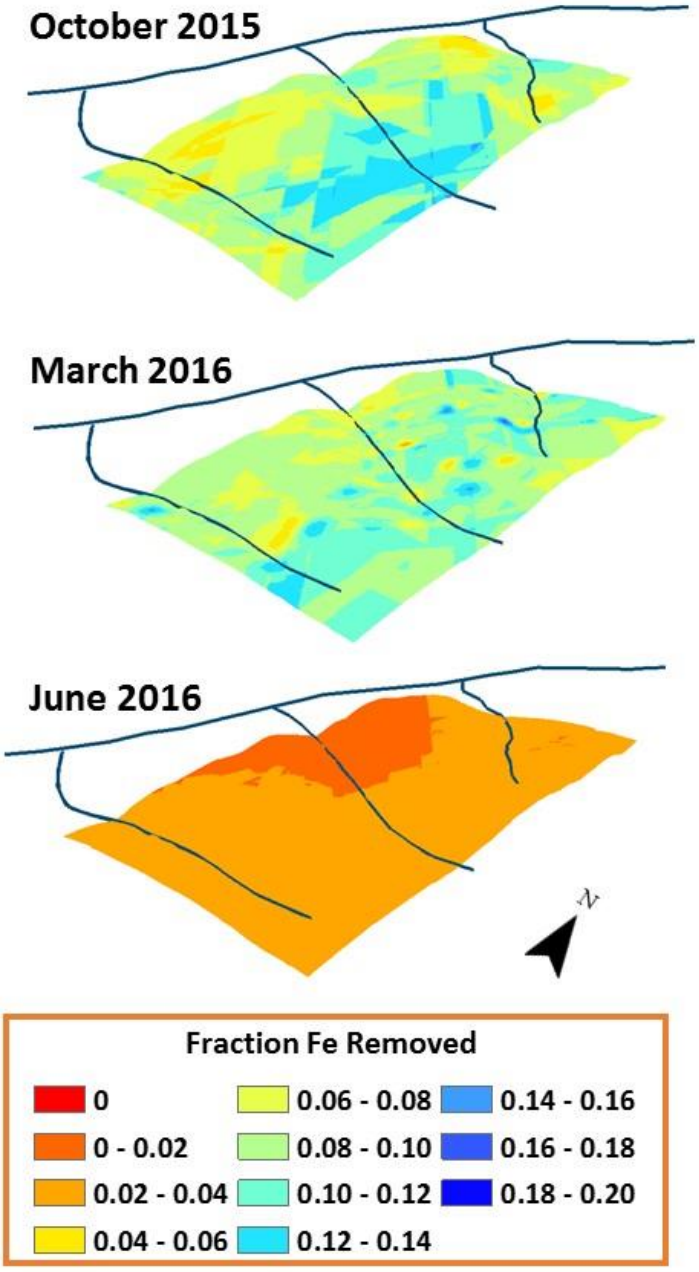

Figure 3.6: Ordinary Krig of fraction of Fe removed from steel IRIS rods in October 2015, March 2016, and June 2016. Warm colors represent lower potential for Fe reduction, and cool colors represent higher potential for Fe reduction.

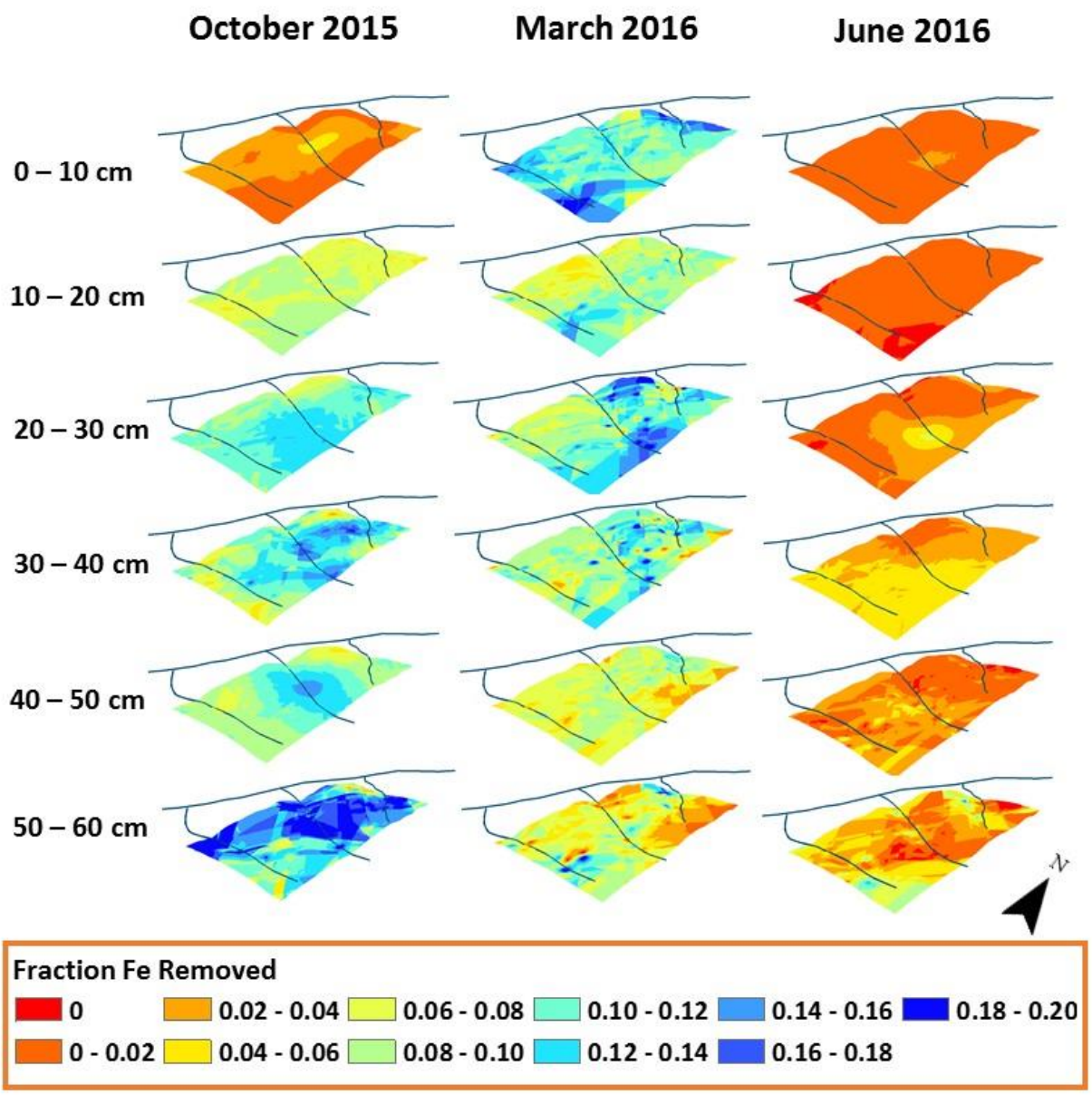

Figure 2.7: Ordinary Krig of fraction of Fe removed at ten cm depth intervals from steel IRIS rods during October 2015, March 2016, and June 2016. Warm colors represent lower potential for Fe reduction, and cool colors represent higher potential for Fe reduction.

CHAPTER 4

PEDOGENIC THRESHOLDS OF CLIMATE AND PARENT MATERIAL IMPACT SOIL IRON REDUCTION[3]

[3] Hodges, C.A., O. Chadwick, A. Thompson. To be submitted to *Geoderma*

ABSTRACT

Iron minerals, and their capacity to undergo reductive dissolution, control the fate and mobility of nutrients and carbon in soils, and can shape the course of pedogenesis. We know that soil moisture and Fe mineral speciation exert controls on the thermodynamic favorability of Fe reduction in soils, but the interplay of soil moisture, mineralogy, and Fe reduction still remains unclear. To better tease apart this interplay, we installed passive redox probes (Steel IRIS Probes), which quantify the potential for Fe reduction, across three precipitation gradients of ages 0.3, 120, and 4100 ky. We hypothesized that the potential Fe reduction would increase with mean annual precipitation, a proxy for soil moisture, and would be highest at the intermediate, 120 ky, site, at which the majority of the Fe remains in the solum as poorly-crystalline secondary minerals. We found that the potential for Fe reduction increased linearly with mean annual precipitation across all sites ($p<0.001$), with no effect of soil age ($p=0.73$). However, when taking into account the native Fe pools across the gradients, we predict that Fe reduction is an active force driving soil processes of an increasingly smaller range of soil precipitations as soil age increases (from 2000-4000+ mm MAP at 0.3 ky, to 2000-2500 mm MAP at 4100 ky). The active Fe reduction precipitation and mineralogy range that we delineate demarcates soil conditions at which Fe minerals play a pivotal role in the nutrient and carbon cycles of these Hawaiian soils.

INTRODUCTION

Iron redox is an important soil process for nutrient cycling and trace metal activity across a range of ecosystems (Hutchison and Hesterberg, 2004; Borch et al., 2009; Henderson et al., 2012; Colombo et al., 2014). Under low oxygen conditions, Fe^{III} becomes a favorable electron acceptor for microbial respiration, stimulating reductive dissolution of Fe minerals, and the release of any constituents associated with the high surface-area Fe^{III} minerals (Polizzotto et al., 2008; Henderson et al., 2012; Paul et al., 2015; Pan et al., 2016). Since low oxygen conditions stimulate Fe reduction, the main focus of Fe reduction studies have been on continuously or temporarily inundated soils, but recent works indicate that Fe reduction is periodically important across a range of humid soils (Mansfeldt, 2003; Fimmen et al., 2008; Polizzotto et al., 2008; Fuss et al., 2010; Hong et al., 2010; Roden, 2012; Knorr, 2013; Bourgault et al., 2015; Hall and Silver, 2015; Yang and Liptzin, 2015; Ekström et al., 2016; Hall et al., 2016; Schulz et al., 2016).

In upland soils, conditions that preclude oxygen from the interior of soil aggregates—such as pulses of water and organic carbon—stimulate microbial activity and foster Fe-reducing conditions (Sexstone and Parkin, 1985; van der Lee et al., 1999; Parry et al., 1999; Hall et al., 2016; Keiluweit et al., 2016). These pulses limit the diffusion of oxygen to soil microsites, either through a slowing of diffusion through water, or an outpacing of oxygen consumption vs. diffusion (Zausig et al., 1993; Horn and Smucker, 2005; Keiluweit et al., 2016). There has been much work documenting the effect of these pulsed events on denitrification and methane production, between which Fe reduction is thermodynamically intermediate (Roy et al., 1997; Priemé and Christensen, 2001; Khalil and Baggs, 2005; Knorr and Blodau, 2009; Angel et al., 2011; Lawrence et al., 2015). Under conditions that foster both denitrification and methane production, microbial populations are also most likely using Fe for respiration. Indeed, we know

that the potential for Fe reduction increases with mean annual precipitation in intermediate-aged volcanic soils (Hodges et al., 2017). It is clear that pulses of water stimulates Fe reduction, but we are less certain of the range of soil and environmental conditions that foster Fe redox cycling on a regular or periodic basis.

Of additional importance to the extent of Fe redox in soils is mineral crystallinity. Poorly crystalline minerals more readily undergo reduction than their crystalline counterparts, with clear repercussions on the mobility of Fe mineral-associated materials (Miller et al., 2001; Schuur et al., 2001; Masiello et al., 2004; Thompson et al., 2011; Buettner et al., 2014). The state factors of formation, especially climate and soil age, are main factors in the manifestation of this crystallinity and speciation of minerals in soils over time in basalt-based systems (Chadwick et al., 2003; Chorover et al., 2004; Mikutta et al., 2009; Vitousek and Chadwick, 2013). As soils form through the weathering of primary minerals, initial secondary products are poorly crystalline, and become more crystalline as they age. Wetter, warmer climates initially accelerate this secondary mineral formation and subsequent crystallization. However, excess water in the soil system eventually leads to reductive dissolution that results in a loss of Fe from the system altogether as the Fe mobilized from the reducing conditions is leached through the solum (Chadwick et al., 2003; Chorover et al., 2004; Mikutta et al., 2009; Vitousek and Chadwick, 2013). In general, older soils are more crystalline than younger soils, and soil moisture increases Fe mineral development to a point, after which it causes a general loss of Fe from the soil system through reductive dissolution. Poorly crystalline Fe minerals, with the highest surface area, have the greatest capacity to associate with other soil constituents (like P, micronutrients, and other trace metals). In other words, intermediate weathering environments generate Fe minerals that are most important in terms of their ability to exert control over biogeochemical cycling.

Studies across the Hawaiian climate and age gradients have provided us with a characterization of the results of biogeochemical processes on soil Fe over time. For example, we have detailed elemental enrichment values and mineralogy. From this information we have a relatively static view of how soil Fe interacts with other constituents in the pedosphere. We do not know the extent to which Fe minerals are actively taking part in the mobility of other elements in the soil-system on a day-to-day timescale through chemical reactions like reduction, and we lack clarity on the short-term processes that cumulatively work to expose the "static" pedogenic realities that we see across the Hawaiian Islands today. To address this knowledge gap we sought to link short-term Fe reduction dynamics based on MAP to previously collected pedogenic information, with a main goal of explaining how Fe, and its associated constituents, cycle in tropical basalt systems. We measured the potential for Fe reduction with passive Fe redox probes (Steel IRIS Probes), installed across three Hawaiian climate gradients of 0.3, 120, and 4100 ky. We hypothesized that potential for Fe reduction would increase with MAP across all gradients, and would be highest at the intermediate-age site, according to Fe mineralogy.

METHODS

Site Description

The Hawaiian Islands encompass a wide range of soil forming processes that manifest systematically over a relatively small area. This is due to the nature of the formation of the Hawaiian archipelago, which is a chain of shield volcanoes originating from one hot spot in the earth's crust. This resulted in mountainous, volcanic islands of uniform parent material that vary in age over a short distance (Macdonald et al., 1983). The combination of the trade winds carrying humid air and the mountainous islands results in strong orographic effects that produce

extreme ranges in precipitation. This variation in pedogenic processes—especially climate and parent material age—lends the islands to studies focused on changes in soil chemical and physical processes with respect to the state factors of formation. For our study on Fe redox dynamics we chose three climate gradients formed on similar basalt flows with ages ranging from 4100 ky to 0.3 ky (Figure 4.1).

The Kauai precipitation gradient is the oldest in our set at 4100 ky. The soils along this gradient are mainly oxisols, and are comprised of well-ordered, crystalline minerals, that have weathered to the point where they are devoid of most of the base cations that are present in the parent basalt. Along this gradient we chose sites of MAP at 1000, 1500, 2500, and 4000 mm. The next site (not including the Maui Climate Gradient), is the Kohala gradient located on the Hawi flow of the big island of Hawaii. The age of the flow is about 140 ky. All soils along this gradient are andisols. This gradient is described in depth by Chadwick et al. (2003). Along the Kohala gradient we chose sites of 300, 1000, 1800, 2500, 3000, and 4000 mm of MAP. The youngest of our gradients is also located on the big island of Hawaii on a flow that was active 300 years ago. These soils are gravelly inceptisols. We sampled sites of 2500 and 4000 mm MAP at this soil age.

Steel IRIS Probe Installation

Steel IRIS probes were prepared as outlined in Hodges et al. (2017). Briefly, 90 cm long, low-carbon steel rods were degreased, washed, sprayed with low molarity HCL, and allowed to dry. After two spray/dry cycles a thin, uniform coating of SRO $Fe^{(II)}$ oxides form, and at that point the Steel IRIS probes are ready to be used. We installed 10 of the steel IRIS probes on geomorphically stable landforms at each of the sites along the chosen precipitation gradients.

After two weeks, the rods were taken out of the ground, gently washed of all soil in running water with a sponge, and then imaged in quarters of diameter so that 4 pictures would represent the total surface area of the rod.

The images of the rod were analyzed in Photoshop for Fe^{III} removal (an indication of Fe^{III} reduction). Using the select color tool, a range of RGB values were specified as the gray color of the "parent rod." When present, the color indicates removal of the Fe oxide coating from the Steel IRIS probe, and Fe reduction. The tool selected the total gray area on each rod, and reported the total number of pixels in that color range. Visual analysis of the selection was performed to ensure that all selections were indicating Fe removal from biogeochemical, and not physical processes (e.g. all long vertical gray lines were ignored as they were due to physical abrasion, and not Fe reduction). Comparing the pixel value of the gray areas to the number of pixels of the total rod provides a measure of "fraction of Fe removed" for each rod, which we have used to quantify the intensity of Fe reducing potential at the sites.

Data Analysis

All image data were initially analyzed in Photoshop to produce the fraction of Fe removed quantification. Afterwards, regressions were performed to evaluate the relationship of the fraction of Fe removed with MAP and substrate age. Additionally, ANOVA were performed to determine differences, and post hoc Tukey's HSD were used to evaluate the ANOVA results. The regressions, ANOVA, and Tukey's HSD tests were performed in R.

RESULTS

Fe reduction increased with MAP across all sites along all rainfall gradients. At both the Kokee and Kohala gradients, the fraction of Fe removed significantly varied with MAP (p-value< 0.001). At the Volcano gradient sites, the fraction of Fe removed at 4000 mm MAP was significantly greater than the fraction of Fe removed at 2500 mm MAP, but too few MAP sites were used to conduct a linear regression.

We modeled the Fraction of Fe Removed from the Steel IRIS Probes with respect to both MAP and parent material age using a logistic regression (Table 4.1, Figure 4.2). From this model, we found that parent material age (p-value = 0.897) is not a significant variable in describing Fraction of Fe Removed, but MAP is significant (p-value = 0.00864) (Table 4.1). The logistic model with both age and MAP accounted for about 67% of variability in Fe Removal from the Steel IRIS Probes (R^2 of 0.668 vs. 0.667) (Table 4.1). From the logistic regression with only MAP as a predictor variable, we determined a threshold of 1800 mm MAP at which the variance and Fraction of Fe removed indicates that the Potential for Fe reduction is high at all points afterwards (Figure 4.2). Fe reduction is low at all MAP levels less than this threshold (Figure 4.2).

DISCUSSION

Potential Fe Reduction Increases with Mean Annual Precipitation

The potential for Fe reduction increased with MAP across all gradients. At 2000 mm MAP, the potential for Fe reduction becomes significantly higher than 0. Although MAP does not act as a proxy for soil oxygen concentration, we assume that higher precipitation results in more water in the solum, which limits oxygen diffusion. While this is not a perfect replacement

for direct soil oxygen or Eh measurements, others have shown that pulses of water into soil systems stimulates redox reactions, like denitrification and methane production, that normally take place under anoxic conditions (Knorr and Blodau, 2009; Parry et al., 1999; Smith and Tiedje, 1979). Less oxygen diffusion drives soil bacteria to utilize alternate terminal electron acceptors, like Fe^{III}. These studies, and our results, follow well with others that have found increases in moisture of upland soils induces reducing events (Knorr and Blodau, 2009; Knorr, 2013; Ekström et al., 2016).

Others have observed threshold effects of MAP on certain soil properties (Chadwick and Chorover, 2001; Vitousek and Chadwick, 2013). Likewise, we observe that 1800 mm MAP is a threshold in potential for Fe reduction across the Hawaiian Islands. The threshold acts as a sort of most limiting factor in soil Fe reduction across the sites, as variance in fraction of Fe removed from the Steel IRIS Probes increases with precipitation after 1800 mm MAP. Once the necessary soil moisture is achieved to preclude oxygen from soil aggregates and reducing conditions to develop, meso-scale variation in factors influencing Fe reduction become important. The most key of these in-site variations would be labile carbon availability, soil structure providing for drainage (and therefore greater soil aeration), and presence of microbial populations capable of reducing Fe (Colombo et al., 2014).

.

Parent Material Age Does Not Affect Potential for Fe Reduction

We observed that substrates of all ages at the same MAP demonstrated the same potential for Fe reduction. This was a somewhat unexpected result, as Fe mineral crystallinity, soil organic matter, and nutrient levels change drastically over the age gradient encapsulated by our study sites (Torn et al., 1997; Chadwick et al., 1999; Masiello et al., 2004; Porder et al., 2007;

Vitousek et al., 2010). We anticipated that potential for Fe reduction would be highest in soils with high carbon contents and greater proportions of poorly crystalline minerals, but we saw no effect of these factors on Fe removal from the Steel IRIS Probes. Our results can be attributed to the nature of our measurements; we were observing the potential for Fe reduction to proceed in the soils when Fe^{III} concentration and Fe-mineral composition were not limiting. By most measures, all of the soils along the Hawaiian gradients are high in C (Torn et al., 1997; Chadwick et al., 2003), so that the only limiting variables to Fe reduction when using Steel IRIS Probes are presence of Fe-reducing microbial populations and anoxic microsites. Other have shown that in tropical soils, like our study sites, microbial populations quickly shift from one terminal electron acceptor to the next dependent upon availability and thermodynamic favorability (Pett-Ridge et al., 2006; DeAngelis et al., 2010). For this reason, across the Hawaiian ecosystems, Fe removal from the Steel IRIS probes is only limited by the frequency and magnitude of precipitation events that generate low-oxygen conditions which necessitate the use of Fe as a terminal electron acceptor.

Potential vs. Actual Fe Reduction

Again, while these sites are noted to have high *potential* for Fe reduction, it does not mean that there is *actual* Fe reduction taking place. We provided an easily reducible source of Fe to soils that may be depleted of Fe, or have Fe predominately bound in primary, or more crystalline secondary minerals. This is especially important to note for the wettest sites, as persistently low oxygen conditions over tens to hundreds of thousands of years have depleted these soils of Fe^{III} (Vitousek and Chadwick, 2013). There is very little Fe^{III} to reduce in the first place, and therefore microbial populations have most likely turned to other forms of anaerobic

respiration with the terminal electron acceptors still available (most likely sulfate oxidation and methane production). Using total Fe data collected across the Hawaiian gradients, we have outlined key climate ranges at which we predict *actual* Fe reduction will be high and have the greatest effects on soil chemical processes (Figs 4.3 and 4.4). These sites of high *actual* Fe reduction are comprised of poorly crystalline, secondary, Fe minerals, have retained most Fe inherited from the parent basalt, and receive at least 2000 mm MAP. These are the sites that indicate high potential for Fe reduction (greater than 0.1 fraction of Fe removed), and also have native pools of Fe minerals that are easily reducible without the addition of the Steel IRIS Probes (Chorover et al., 2004; Mikutta et al., 2009).

At the youngest gradient, with high potential for Fe reduction at both study sites, we anticipate actual Fe reduction to be low, as the soil is dominated by primary minerals. We anticipate that soil Fe status will not inhibit Fe reduction along the Kohala climate gradient until 1about 3500 mm of MAP, as Fe concentrations are high, and the majority of the Fe minerals exists as poorly crystalline oxides until this precipitation amount (Fig 4.3). The Maui climate gradient, over which steel IRIS probes were deployed for a previous study (Hodges et al., 2017), also contains predominately poorly crystalline Fe oxides, but Fe concentration does begin to decline at the wettest end of the gradient. We anticipate that Fe reduction will be high along the Maui climate gradient at a range of 2000-3000 mm MAP. Along the Kokee gradient, the Fe minerals are mostly crystalline at the lower precipitation sites, and devoid of Fe at sites with precipitation above 2500 mm yr^{-1} (Fig 4.4). For these reasons, actual Fe reduction is likely low across the gradient. If Fe reduction is occurring along this gradient, it is probably only in a slim range of precipitation from 2000 – 2200 mm MAP.

Fe reduction is probably also a reality for soils that receive lower than 2000 mm MAP on an episodic basis in response to higher volume than average rainfall events. Other have shown that periodic or seasonal high soil moisture conditions, like extreme rainfall events, induces use of alternate terminal electron acceptors (Knorr and Blodau, 2009; Ekström et al., 2016). While the Hawaiian Island hydrologic cycle is generally aseasonal, with evenly distributed evapotranspiration and precipitation across the year, there are still extreme rainfall events that deliver higher than average amounts of water to the soil system. Based on our observations, and those of others, we anticipate that there is actual Fe reduction episodically at MAP ranges from ~1000-2000 MAP. We choose 1000 as the lower bound, because there is the lowest range of MAP for which there is evidence in ecosystems of periodic reducing conditions in response to pulsed water inputs.

Implications

This distinction between *actual* and *potential* Fe reduction is not arbitrary, and has implications for the soil environment that span from nutrient availability, pedogenic development, and the carbon cycle (Borch et al., 2009; Henderson et al., 2012; Li et al., 2012; Colombo et al., 2014). The redox environment of the soil influences soil development; Fe reduction and then re-precipitation of Fe minerals develops Fe minerals, and reductive dissolution, mobilization, and eventual leaching of soil Fe translates into a loss of soil mineral structure and an important element in controlling the rentention of key soil nutrients, like phosphorus (Peretyazhko and Sposito, 2005; Thompson et al., 2006).

Under acidic conditions, Fe oxides control the mobility of P in soil (Peretyazhko and Sposito, 2005; Chacon et al., 2006). P sorbed onto Fe oxides is immobile and relatively

inaccessible to plants and other organisms (Miller et al., 2001; Henderson et al., 2012). When Fe oxides onto which P is sorbed undergo reductive dissolution, the sorbed P is released into the pedosphere to either be scavenged by organisms or to be leached lower into the solum. This means that with persistent or recurring reducing conditions, P not held in biomass is lost from the soil. The wettest sites of our climate gradients are at this point of phosphorus depletion, as others have shown along the Maui Climate Gradient (Miller et al., 2001). This P deficiency translates into stunted forest productivity with key implications for forest carbon accumulation. Combining our results with those of Schuur et al. (2001), we can predict that all sites on the Hawaiian Islands that we have indicated as too depleted in soil Fe to foster Fe reduction, are subject to persistent reducing conditions resulting in P depletion and a decrease in forest productivity.

The relationship of soil Fe with carbon is complex. In terms of chemical relationships, carbon can sorb onto Fe oxides, and coprecipitate with Fe as Fe oxides form in the solum (Colombo et al., 2014). Additionally, organic carbon is used as an electron source by soil microorganisms for both aerobic and anaerobic respiration. Without adequate levels of organic carbon, Fe respiration cannot take place. Moreover, inputs of carbon have been shown to stimulate Fe reduction in upland soils (Yang and Liptzin, 2015; Hall et al., 2016). This, along with our findings on the relationship of Fe redox dynamics with MAP, would lead one to believe that more mean annual precipitation leads to an observed loss in organic carbon from the solum due to release of absorbed and coprecipitated Fe, and organic matter oxidation through Fe respiration. Indeed, others have found a decrease in soil organic matter with age and precipitation across the Hawaiian Climate Gradients (Torn et al., 1997). However, this is not necessarily what has been observed by many, as others have shown that wetter soils that foster greater reducing conditions have higher soil organic matter concentrations due to a slow in the more efficient

aerobic respiration. The reason for these varied findings is that soil carbon is controlled by many factors including, but not limited to, climate, soil mineral composition, soil structure, soil microbial community, soil moisture, forest litter type, availability of other nutrients to sustain microbial activity, etc. That the majority of these factors also vary with age and precipitation across the Hawaiian basalt flows, confounds our ability to tease apart the true drivers of soil organic matter's relationship with Fe redox. At least in this system, there is no clear conclusion to make about the relationship of soil carbon content and the potential to reduce Fe, probably because even the most carbon-poor site still contains quite high amounts of carbon.

In terms of pedogenesis, we observe mostly poorly crystalline Fe oxides at the precipitation ranges that foster Fe reducing conditions (Figure 4.5). Our results indicate that Fe redox cycling in these soils is a force of soil development, moving the soils from primary minerals, to poorly crystalline secondary minerals, to crystalline secondary minerals, and finally to Fe depletion as active reducing conditions persist over time. These final two steps lead to the eventual decrease in active Fe reduction, as Fe no longer is present in the pedosphere.

CONCLUSIONS

In summary, we found that the potential for Fe reduction increased with MAP across all Hawaiian precipitation gradients, but we did not observe a parent material effect on the fraction of Fe removed from the Steel IRIS Probes. Additionally, we found 2000 mm MAP to be an important point along the climate gradients in determining the potential for Fe reduction, supporting work done by others performed across the same sites. Below 2000 mm MAP we did not observe a high potential for Fe reduction, while above 2000 mm MAP we did. While the potential for Fe reduction is not affected by the soil age, we reason that actual Fe reduction is,

because different Fe minerals that are more or less amenable to Fe reduction are present in different proportions along an age gradient. In other words, while Fe reduction is possible, it is probably not occurring at sites with low Fe concentrations and more-crystalline Fe minerals. Using data on soil Fe concentration and crystallinity collected by others, along with our Steel IRIS probe data, we have delineated key soil age/precipitation ranges at which actual Fe reduction is a key driver of the soil biogeochemistry. This exploration of the Fe redox dynamics of the Hawaiian Islands provides a framework for others to predict soil environments in which Fe reduction is a significant driver of biogeochemistry, offering insights into the mobility and cycling of key soil constituents.

REFERENCES

Ambus, P., and S. Christensen. Spatial and Seasonal Nitrous Oxide and Methane Fluxes in Danish Forest-, Grassland-, and Agroecosystems. J. Environ. Qual. 24(5): 993–1001.

Angel, R., D. Matthies, and R. Conrad. 2011. Activation of Methanogenesis in Arid Biological Soil Crusts Despite the Presence of Oxygen. PLoS ONE 6(5): e20453.

Borch, T., R. Kretzschmar, and A. Kappler. 2009. Biogeochemical redox processes and their impact on contaminant dynamics. Environmental Science & Technology 44: 15–23.

Bourgault, R., D. Ross, and S. Bailey. 2015. Chemical and Morphological Distinctions between Vertical and Lateral Podzolization at Hubbard Brook. Soil Science Society of America Journal 79(2): 428.

Buettner, S., M. Kramer, O. Chadwick, and A. Thompson. 2014. Mobilization of colloidal carbon during iron reduction in basaltic soils. Geoderma (221-222): 139–145.

Chacon, N., W. Silver, E. Dubinsky, and D. Cusack. 2006. Iron reduction and soil phosphorus solubilization in humid tropical forests soils: the roles of labile carbon pools and an electron shuttle compound. Biogeochemistry 78: 67–84.

Chadwick, O., and J. Chorover. 2001. The chemistry of pedogenic thresholds. Geoderma (100): 321–353.

Chadwick, O.A., L.A. Derry, P.M. Vitousek, B.T. Huebert, and L.O. Hedin. 1999. Changing sources of nutrients during four million years of ecosystem development. Nature 397(6719): 491–497.

Chadwick, O., R. Gavenda, E. Kelly, K. Ziegler, C. Olson, C. Elliott, and D. Hendricks. 2003. The impact of climate on the biogeochemical functioning of volcanic soils. Chemical Geology 202(3): 195–223.

Chorover, J., M. Amistadi, and O. Chadwick. 2004. Surface charge evolution of mineral-organic complexes during pedogenesis in Hawaiian basalt. Geochimica et Cosmochimica Acta 68(23): 4859–4876.

Colombo, C., G. Palumbo, J. He, and R. Pinton. 2014. Review on iron availability in soil: interaction of Fe minerals, plants, and microbes. Journal of Soils and Sediments 14(3): 538-548.

DeAngelis, K., W. Silver, A.W. Thompson, and M.K. Firestone. 2010. Microbial communities acclimate to recurring changes in soil redox potential status. Environmental Microbiology 12(12): 3137–3149.

Ekström, S., O. Regnell, H. Reader, A. Nilsson, S. Löfgren, and E. Kritzberg. 2016. Increasing concentrations of iron in surface waters as a consequence of reducing conditions in the catchment area. J Geophys Res Biogeosciences 121(2): 479–493.

Fimmen, R., D. RichterJr., D. Vasudevan, M. Williams, and L. West. 2008. Rhizogenic Fe–C redox cycling: a hypothetical biogeochemical mechanism that drives crustal weathering in upland soils. Biogeochemistry 87(2): 127–141.

Fuss, C., C. Driscoll, C. Johnson, R. Petras, and T. Fahey. 2010. Dynamics of oxidized and reduced iron in a northern hardwood forest. Biogeochemistry 104(1-3): 103–119.

Hall, S., D. Liptzin, H. Buss, K. DeAngelis, and W. Silver. 2016. Drivers and patterns of iron redox cycling from surface to bedrock in a deep tropical forest soil: a new conceptual model. Biogeochemistry 130(1-2): 177–190.

Hall, S., and W. Silver. 2015. Reducing conditions, reactive metals, and their interactions can explain spatial patterns of surface soil carbon in a humid tropical forest. Biogeochemistry 125: 149–165.

Henderson, R., N. Kabengi, N. Mantripagada, M. Cabrera, S. Hassan, and A. Thompson. 2012. Anoxia-induced release of colloid-and nanoparticle-bound phosphorus in grassland soils. Environmental Science & Technology 46: 11727–11734.

Hong, H., Y. Gu, K. Yin, K. Zhang, and Z. Li. 2010. Red soils with white net-like veins and their climate significance in south China. Geoderma 160(2): 197–207.

Horn, R, and A Smucker. 2005. Structure formation and its consequences for gas and water transport in unsaturated arable and forest soils. Soil and Tillage Research 82(1): 5–14.

Hutchison, K., and D. Hesterberg. 2004. Dissolution of Phosphate in a Phosphorus-Enriched Ultisol as Affected by Microbial Reduction. J Environ Qual 33(5): 1793.

Keiluweit, M., P. Nico, M. Kleber, and S. Fendorf. 2016. Are oxygen limitations under recognized regulators of organic carbon turnover in upland soils? Biogeochemistry.

Khalil, M., and E. Baggs. 2005. CH_4 oxidation and N_2O emissions at varied soil water-filled pore spaces and headspace CH_4 concentrations.Soil Biology and Biochemistry 37(10): 1785-1794.

Knorr, K.-H. 2013. DOC-dynamics in a small headwater catchment as driven by redox fluctuations and hydrological flow paths–are DOC exports mediated by iron reduction/oxidation cycles? Biogeosciences 10(2): 891–904.

Knorr, K.-H., and C. Blodau. 2009. Impact of experimental drought and rewetting on redox transformations and methanogenesis in mesocosms of a northern fen soil. Soil Biology and Biochemistry 41(6): 1187–1198.

Lawrence, B.M., C.D. Koven, S.C. Swenson, W.J. Riley, and A.G. Slater. 2015. Permafrost thaw and resulting soil moisture changes regulate projected high-latitude CO2 and CH4 emissions. Environ Res Lett 10(9): 094011.

Lee, G. van der, B. de Winder, W. Bouten, and A. Tietama. 1999. Anoxic microsites in Douglas fir litter.Applied and Environmental Microbiology 54(6) 1472-1480.

Li, Y., S. Yu, J. Strong, and H. Wang. 2012. Are the biogeochemical cycles of carbon, nitrogen, sulfur, and phosphorus driven by the “FeIII–FeII redox wheel” in dynamic redox environments? J Soils Sediments 12(5): 683–693.

Mansfeldt, T. 2003. In situ long-term redox potential measurements in a dyked marsh soil. Journal of Plant Nutrition and Soil Science 166: 210–219.

Masiello, C., O. Chadwick, and J. Southon. 2004. Weathering controls on mechanisms of carbon storage in grassland soils. Global Biogeochemical Cycles 18: 1–9.

Mikutta, R., G. Schaumann, and D. Gildemeister. 2009. Biogeochemistry of mineral–organic associations across a long-term mineralogical soil gradient (0.3–4100kyr), Hawaiian Islands. Geochimica et Cosmochimica Acta 73: 2034–2060.

Miller, A., E. Schuur, and O. Chadwick. 2001. Redox control of phosphorus pools in Hawaiian montane forest soils. Geoderma 102: 219–237.

Pan, W., J. Kan, S. Inamdar, C. Chen, and D. Sparks. 2016. Dissimilatory microbial iron reduction release DOC (dissolved organic carbon) from carbon-ferrihydrite association. Soil Biology and Biochemistry: 232–240.

Parry, S., P. Renault, C. Chenu, and R. Lensi. 1999. Denitrification in pasture and cropped soil clods as affected by pore space structure. Soil Biol. Biochem.: 493–501.

Paul, D., S.K. Kazy, T. Banerjee, A.K. Gupta, T. Pal, and P. Sar. 2015. Arsenic biotransformation and release by bacteria indigenous to arsenic contaminated groundwater. Bioresource technology 188: 14–23.

Peretyazhko, T., and G. Sposito. 2005. Iron (III) reduction and phosphorous solubilization in humid tropical forest soils. Geochimica et Cosmochimica Acta 69(14): 3643–3652.

Pett-Ridge, J., W. Silver, and M. Firestone. 2006. Redox Fluctuations Frame Microbial Community Impacts on N-cycling Rates in a Humid Tropical Forest Soil. Biogeochemistry 81(1): 95–110.

Polizzotto, M., B. Kocar, S. Benner, and M. Sampson. 2008. Near-surface wetland sediments as a source of arsenic release to ground water in Asia. Nature 454: 505–509.

Porder, S., P. Vitousek, O. Chadwick, and C. Chamberlain. 2007. Uplift, erosion, and phosphorus limitation in terrestrial ecosystems. Ecosystems 10: 158–170.

Priemé, A, and S Christensen. 2001. Natural perturbations, drying–wetting and freezing–thawing cycles, and the emission of nitrous oxide, carbon dioxide and methane from farmed organic soils. Soil Biology and Biochemistry 33(15): 2083.

Roden, E. 2012. Microbial iron-redox cycling in subsurface environments. Biochemistry Society Transaction 40: 1249–1256.

Roy, R., H. Klüber, and R. Conrad. 1997. Early initiation of methane production in anoxic rice soil despite the presence of oxidants. FEMS Microbiology Ecology 24: 311–320.

Schulz, M., D. Stonestrom, and C. Lawrence. 2016. Structured heterogeneity in a marine terrace chronosequence: Upland mottling. Vadose Zone Journal 15: 11–14.

Schuur, E., O. Chadwick, and P. Matson. 2001. Carbon cycling and soil carbon storage in mesic to wet Hawaiian montane forests. Ecology 82(1): 3182-3196.

Sexstone, A., and T. Parkin. 1985. Temporal response of soil denitrification rates to rainfall and irrigation. Soil Science Society of America Journal 49: 99–103.

Smith, M., and J. Tiedje. 1979. Phases of denitrification following oxygen depletion in soil. Soil Biology and Biochemistry 11: 261–267.

Thompson, A., O. Chadwick, D. Rancourt, and J. Chorover. 2006. Iron-oxide crystallinity increases during soil redox oscillations.Geochimica et Cosmochimica Acta 70(7) 1710-1727.

Thompson, A., D. Rancourt, O. Chadwick, and J. Chorover. 2011. Iron solid-phase differentiation along a redox gradient in basaltic soils. Geochimica et Cosmochimica Acta 75: 119–133.

Torn, M., S. Trumbore, O. Chadwick, and P. Vitousek. 1997. Mineral control of soil organic carbon storage and turnover. Nature 389: 170–173.

Vitousek, P., and O. Chadwick. 2013. Pedogenic thresholds and soil process domains in basalt-derived soils. Ecosystems 16(8): 1379–1395.

Vitousek, P., S. Porder, and B. Houlton. 2010. Terrestrial phosphorus limitation: mechanisms, implications, and nitrogen–phosphorus interactions. Ecological Applications 20(1): 5–15.

Yang, W., and D. Liptzin. 2015. High potential for iron reduction in upland soils. Ecology 96(7).

Zausig, J., W. Stepniewski, and R. Horn. 1993. Oxygen Concentration and Redox Potential Gradients in Unsaturated Model Soil Aggregates. S. Sci. Soc. Am. J. 57: 908–916.

FIGURES and TABLES

Table 4.1 Logistic Regressions Modelling Fraction Fe Removed

	Model A		**Model B**	
	Coefficient	**Probability Statistic**	**Coefficient**	**Probability Statistic**
Intercept	-3.63 (0.892)	$4.68 * 10^{-5}$	-3.67 (0.849)	$1.59 * 10^{-5}$
MAP	$6.92 * 10^{-4}$ ($2.65 *10^{-4}$)	0.00916	$6.94 * 10^{-4}$ ($2.65*10^{-4}$)	0.00864
Age	$-1.92 *10^{-8}$ ($1.49 *10^{-7}$)	0.89733	--	--
Pseudo - R Squared		0.668		0.667

*Standard error in parentheses

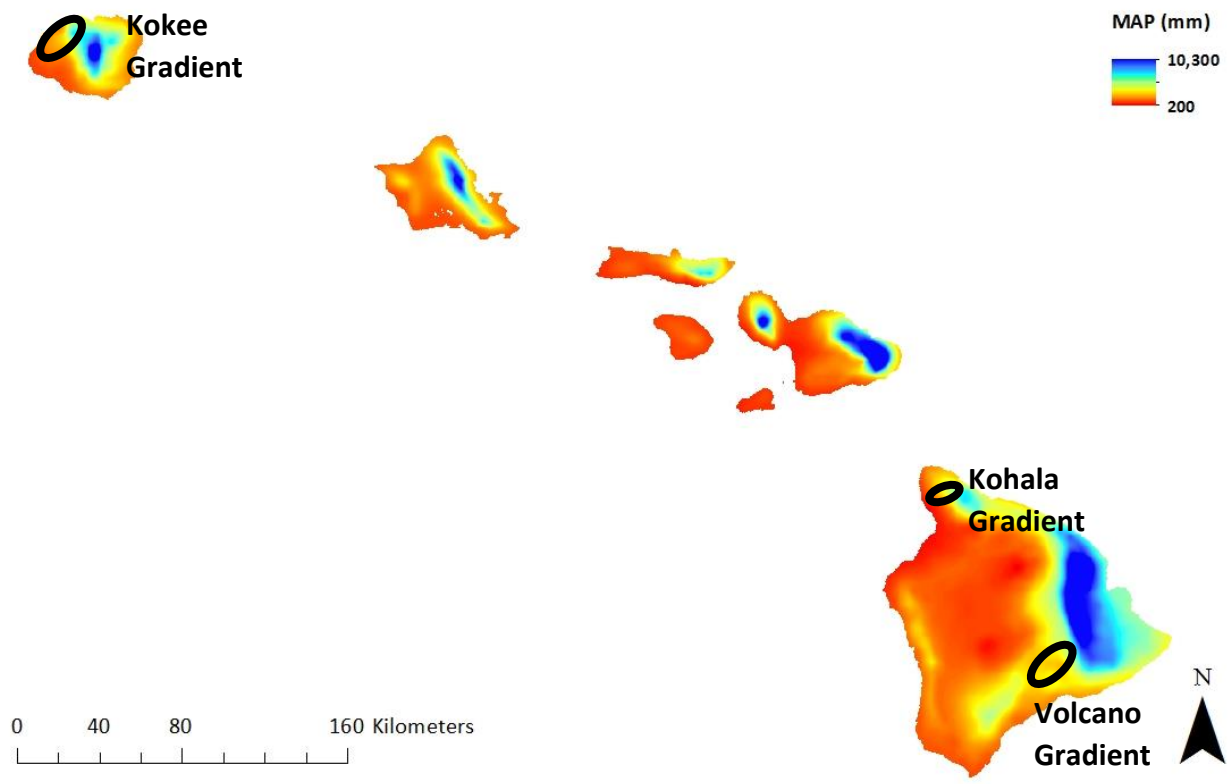

Figure 4.1: Map of MAP (mm) of the Hawaiian Islands adapted from Giambelluca et al. (2013). Black circles represent the general location of the precipitation gradients used for this study.

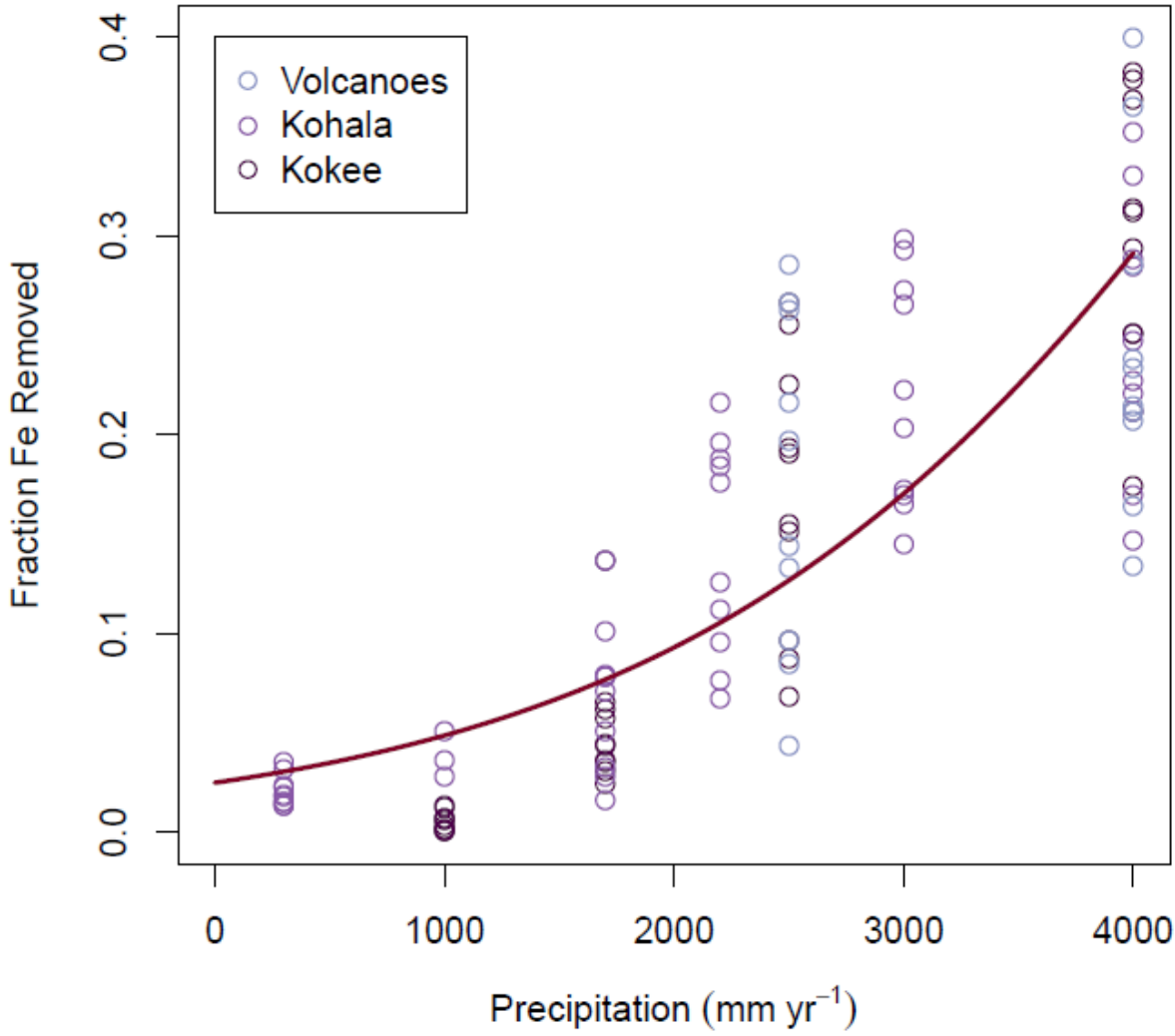

Figure 4.2: Logistic regression modelling response of Fraction of Fe Removed from the Steel IRIS Probes with changes in mean annual precipitation. Age was found to not be a significant variable in describing this relationship.

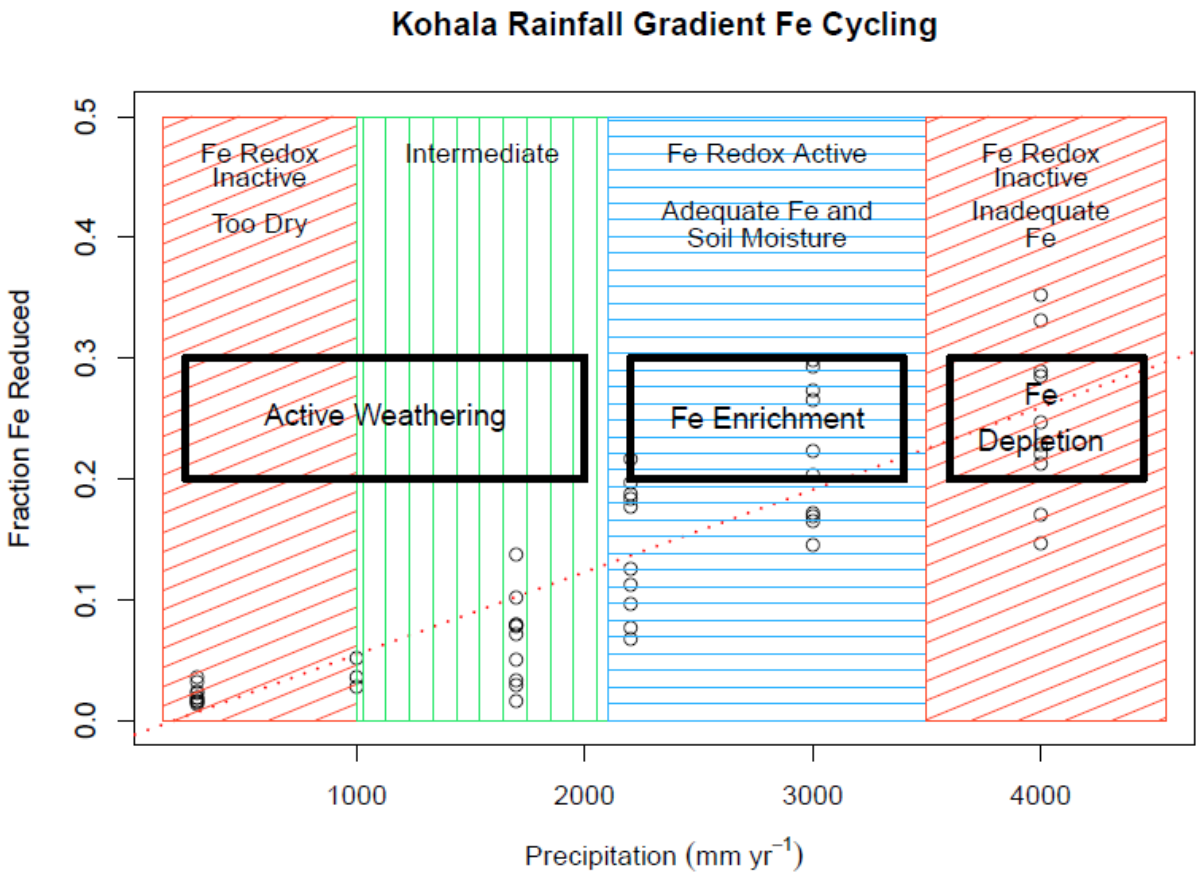

Figure 4.3: Different precipitation ranges of the soil Fe life-cycle are outlined in blue. The points in the background denote fraction of Fe removed from the rusted steel reduction indicators (steel IRIS). Red dotted line represents the regression of those points. Shaded boxes propose the role that Fe redox plays across the ecosystem within the rainfall range encompassed, taking into account the fraction of Fe removed and the stage of the Fe life-cycle.

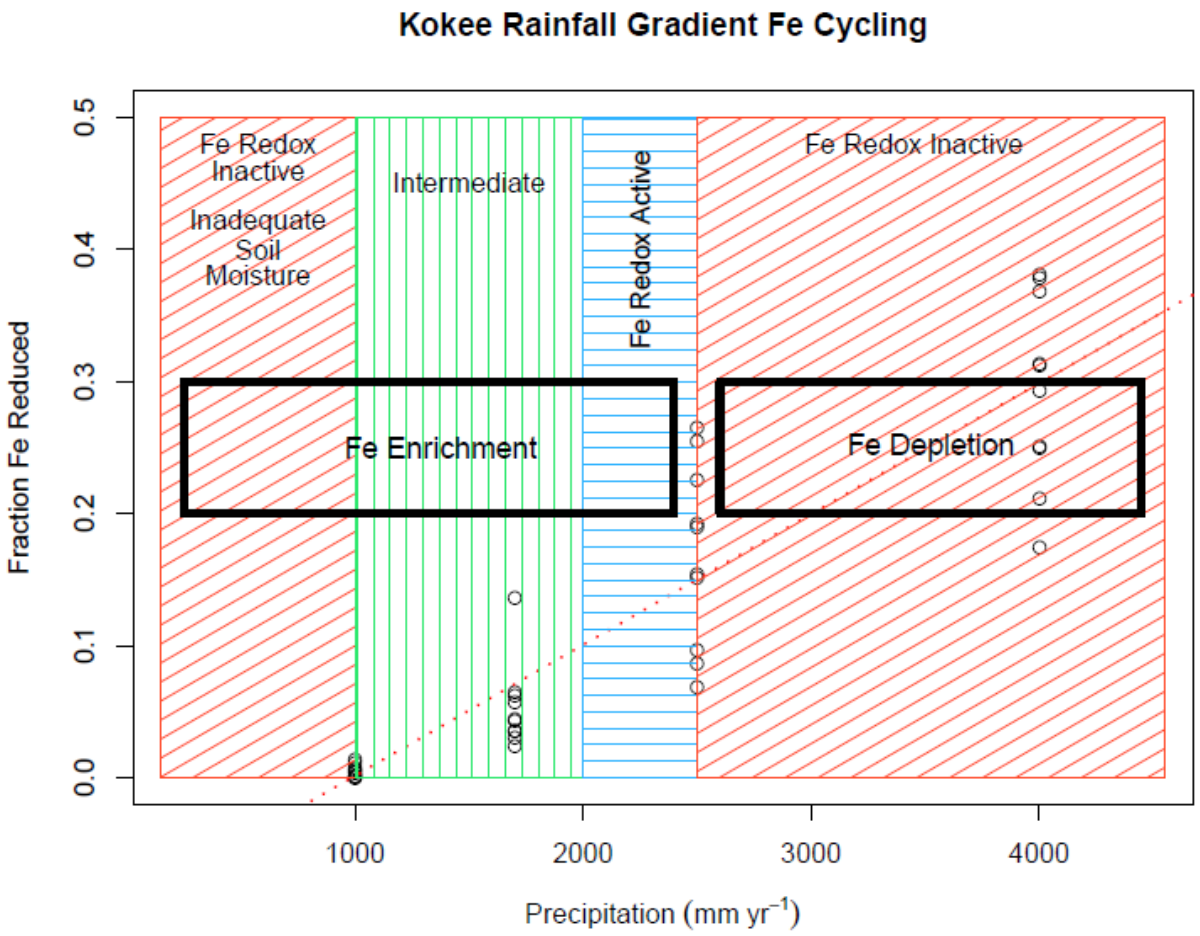

Figure 4.4: Different precipitation ranges of the soil Fe life-cycle are outlined in blue. The points in the background denote fraction of Fe removed from the rusted steel reduction indicators (steel IRIS). Red dotted line represents the regression of those points. Shaded boxes propose the role that Fe redox plays across the ecosystem within the rainfall range encompassed, taking into account the fraction of Fe removed and the stage of the Fe life-cycle.

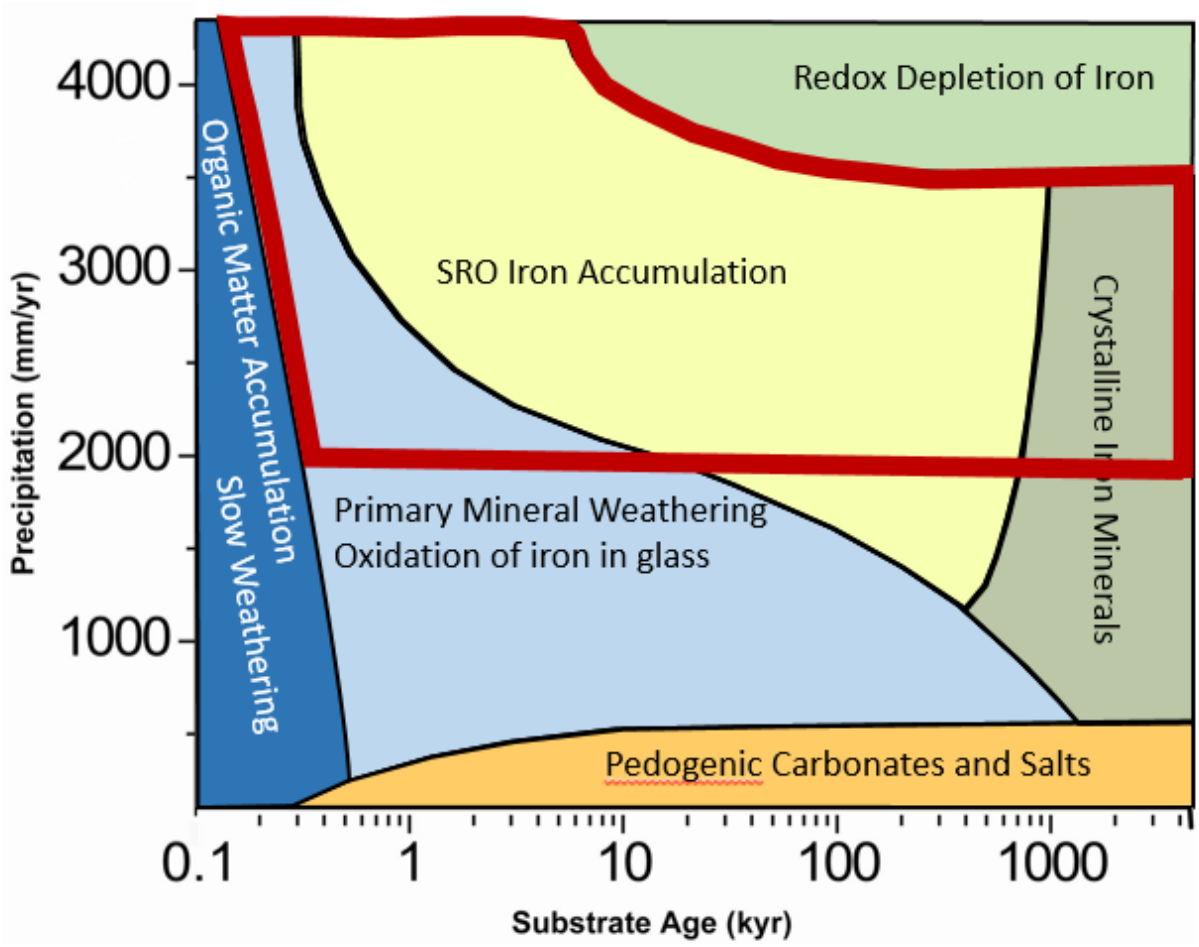

Figure 4.5: The range of substrate age and MAP at which Fe redox exerts significant controls on soil biogeochemistry outlined in red.

CHAPTER 5

CONCLUSIONS

These experiments display clearly that the potential for Fe reduction in humid upland soils, at least episodically, is high, and is affected by exogenous inputs (water and carbon), and Fe mineralogy and crystallinity.

We found that in the piedmont of the Southeastern United States there are strong seasonal and environmental effects on the intensity, depth, and location of Fe reduction. The potential for Fe reduction is high at depth in response to periodic rainfall events that increase soil moisture and raise the water table. Additionally, the potential for Fe reduction is high in the soil surface seasonally in early spring when soil moisture is high and labile carbon is more readily available to microbial populations. Conversely, the potential for Fe reduction is low when evapostranspirational demand is high, and in effect, soil moisture is low. That soil moisture played a large role in determining the potential for Fe reduction is important, but somewhat expected based on prior works. More impactful is the finding that labile carbon availability stimulated Fe reduction in the surface soil. There has been less emphasis on the role of high microbial activity, stimulated by labile carbon availability, on reduction processes in upland soils. Our results indicate that Fe redox cycling, especially at the soil surface, could be controlled largely by soil carbon availability, and thereby acting as a potential means of nutrient mineralization or release.

Across the Hawaiian Islands, we found that the potential for soil Fe reduction increases with mean annual precipitation, but is not affected by parent material age. However, upon closer

investigation, we determined that while the *potential* for Fe reduction was high, *actual* Fe reduction was not necessarily high, and is controlled by a combination of mean annual precipitation, soil Fe depletion/enrichment, and Fe mineralogy. The greatest range of actual Fe reduction exists in intermediate-aged lava flows, between 2000-3500 mm MAP, as soil minerals are poorly crystalline and soil Fe concentrations are high. As soils age, Fe minerals become more crystalline and Fe is eventually lost from the system, the range of Fe reduction's influence becomes much smaller; it is only prevalent between 2000-2500 mm MAP. These findings provide a more complete view of how the influence of Fe redox on soil biogeochemistry changes with respect to climate and parent material age in tropical, volcanic soils. We can apply our findings to those of others across the Hawaii climate gradients to better describe and understand the role of Fe reduction on previously determined relationships of pedogenesis, soil carbon, phosphorus, and other soil constituents with climate and age.

By better constraining the extent of Fe reduction *in situ* across two ecosystems, our findings build upon those of others who have investigated the mechanisms and potential impacts of Fe reduction in upland soils. We now know potential climates, weathering environments, and soil moisture and carbon conditions that foster Fe reduction in fine-textured, humid soils. With our results, the biogeochemical impacts of Fe reduction, including carbon mineralization, and DOC, phosphorus, and trace element mobilization, can be more accurately scaled-out across a landscape or ecosystem to better hone our understanding of elemental fluxes through terrestrial systems.

APPENDICES

APPENDIX A

MECHANISMS OF FE REMOVAL FROM STEEL IRIS PROBES

INTRODUCTION

Fe redox reactions exert strong controls on soil biogeochemistry. High surface area Fe oxides retain nutrients and other trace metals within the pedosphere. Under low oxygen conditions, those Fe oxides can undergo reductive dissolution and release sorbed constituents, inducing far-reaching effects on the nutrient status of the soil environment. Like-wise, reducing conditions in soils in general (not just conditions at which Fe is reduced), affect microbial respiration pathways, root function, and soil carbon turnover.

There are many methods that have been developed to measure and quantify Fe-reducing conditions in the soil. Platinum electrodes, the most widely used method for tracking redox conditions *in situ*, present certain problems when used in the field; they are strongly affected by the immediate surrounding soil and solution chemistry, are sensitive to minute changes in the environment, and only make point observations that rarely represent the overall condition of the soil. They are, however, useful for repeated measurements tracking cumulative changes over days to months. However, platinum Eh electrodes are expensive, time consuming, and require some technical knowledge. To avoid the inherent difficulties with platinum electrodes, others have adopted "passive" methods. These include the use of dyes and measurement of the concentration of reduced species in soil solution. Recently, passive redox probes have come into popularity as a passive means of quantifying redox conditions in soil. While the execution is somewhat different, all affix a redox-active mineral that becomes water-soluble under reducing conditions to an inert material (such as a PVC tube). It is then inserted into the ground for a prescribed amount of time. The amount of mineral removed after that period of time is quantified using image analysis, which is then related to the relative reducing conditions of the soil. The more of the mineral that is removed from the probe, the greater the inferred reducing conditions.

The benefits of this type of approach are many: ease of construction, no chance of data not collected after inserted, and simple data analysis and interpretation. On the other hand, the mineral painted onto the PVC can be sensitive to scratching from sand grains, rocks, roots, and other soil constituents. These scratches can confound analysis as removal due to abrasion could potentially be ascribed to removal by redox processes. Physical abrasion is of a greater concern when examining upland soils, which remain drier and contain more rock fragments than wetlands and floodplains. To address this potential problem, we developed a passive redox probe of rusted steel (Steel IRIS Probe). The underlying steel, Fe^{0}, is coated is coated in rust, which is comprised of readily reducible Fe^{III} oxides. The rust is less susceptible to removal via abrasion, and is therefore better suited to upland soil characterization.

However, there have been several questions as to how the Fe^{III} oxides of the Steel IRIS Probe interacts with the soil environment. In soils with high organic carbon, there have been concerns that DOC could chelate the Fe^{III} affixed to the Steel IRIS Probe, removing Fe without reduction to Fe^{+2}. Also, there are questions as to whether this redox probe targets Fe respiration by soil microorganisms, or all Fe reduction, microbially-mediated or otherwise. Finally, Fenton chemistry could potentially work towards removal of Fe without interaction with soil constituents. In order to address these questions, we designed a suite of in-lab experiments with Steel IRIS Probes to examine the mechanisms of Fe removal under different conditions. We hypothesized that microbially-mediated Fe reduction is the main means of Fe^{III} removal from the Steel IRIS Probe, but that there may be some abiotic reduction contributing to this process.

METHODS

Experiment 1 – Potential effects of DOM on Fe removal compared to removal in soil

We designed our first experiment to probe the potential effect of DOM on Fe-oxide removal from the Steel IRIS Probes. We cut Steel IRIS probes into 5 cm long pieces, and subjected each piece to one of 6 treatments: a 1:10 O horizon water extract, saturated soil, or a 1:8 A horizon soil slurry kept under ambient conditions or in an anoxic glovebox for two weeks. Each treatment was replicated six times. Individual Steel IRIS Probe pieces were subjected to the treatments in 15 mL test tubes.

After two weeks the rods were removed from the test-tubes, gently cleaned under running water, dried, and then imaged in quarter diameter segments. In this way four images of the rod would cumulatively represent the whole surface area subjected to the treatment. In Photoshop, the rods were analyzed for Fe-Oxide removal using colors. Comparing area with Fe-Oxides removed to total Surface area produces the metric "fraction of Fe removed."

Experiment 2 – Microbially-mediated Fe reduction vs. chemical Fe reduction

After experiment 1 we noted that there was the same amount of Fe removed from the Steel IRIS under saturated and slurried soil conditions under oxic and anoxic ambient conditions. In order to better understand these results, we created an experiment in which we varied soil water contents at 100%, 50%, and 15% water filled pore space (WFPS) with live or autoclaved soil, and under oxic or anoxic conditions. The Steel IRIS Probes were again cut into 5 cm pieces, and soil, water and Steel IRIS Probe piece were placed in 15 mL plastic test tubes. Treatments were done in 6 replicates again. After two weeks, the rods were taken out of the test tubes, gently

cleaned, and then imaged in the same way as in experiment 1. Image analysis was also done in the same way in Photoshop.

Experiment 3 – Effects of DOM concentration on Fe removal

Experiment 3 was done to better understand the removal of Fe by OM and the potential for chelation or reduction by the DOC. 5 cm long Steel IRIS Probes were placed in test tubes of water-extracted O horizon at 1:10, 1:100, 1:1000, and 1:10000 concentrations from live or autoclaved O horizon material. Rods were kept under oxic conditions. The tubes were uncapped, recapped, and agitated each day. After the two week period, a portion of the solution was removed and acidified for Fe concentration analysis, and then the rods were removed from the solution, cleaned and imaged as previously done. Acidified samples were analyzed for Fe^{+2} and total Fe using the ferrozine method.

Experiment 4 – Fenton reactions as a means of Fe removal from steel IRIS rods

Finally, to address potential concerns about Fenton chemistry stimulating Fe removal, we placed 5 cm segments of Steel IRIS Probes, Steel IRIS Probes with rusted ends, and IRIS Tubes (Fe-Oxides painted onto PVC) in live and autoclaved treatments at 100% WFPS, 25% WFPS, and water under ambient oxygen conditions. Each treatment was done in triplicate. Since IRIS Tubes are only Fe^{III} oxides, they should not have the potential to stimulate Fenton Chemistry free radicals that consume Fe^{III} like the steel IRIS Probes. The treatments were again left for two weeks, but at different time points the soil or water was tested for hydrogen peroxide presence (evidence of Fenton Chemistry). Hydrogen peroxide assays were performed at hour 0, 6, 18, 45, 72, 120, 168, 216, 288, and 336. All hydrogen peroxide assays were performed using Amplex

Ultrared Reagent. Soil treatments were extracted with water at 1:10 ratio, and water treatments were diluted 1:10 with phosphate buffer. Hydrogen peroxide assays were performed as specified by Amplex Ultrared guides. Reactions were allowed to proceed for 30 minutes and were then analyzed for absorbance at 560 nm.

After two weeks, the probes were removed from the treatments, cleaned, and then imaged in quarters. Photoshop analysis was performed as in the other experiments, resulting in a measure of fraction of Fe removed.

RESULTS and DISCUSSION

We designed each experiments in response to the results of the previous experiments so that they are meant to be interpreted cumulatively; the results of one build upon the results of the previous. For this reason, in addition to the main purpose of these experiments, it is easiest to report and discuss the results in terms of the main questions that drove our experimental process. For these reasons, we will discuss the pertinent results and relate them back to our guiding questions sequentially, instead of in order of experiment.

The Role of Chelation in Fe Oxide Removal from Steel IRIS Probes

Both experiments 1 and 3 address the potential role of DOM in removing Fe^{III} oxides from the Steel IRIS surface. In experiment 1 we found that fraction of Fe removed from the Steel IRIS probes was significantly lower in a 1:10 DOM extract than in a saturated soil and a soil slurry (Fig A.1). However, there was some Fe removed from the Steel IRIS Probes in the oxic DOM solution, suggesting not reduction or chelation, since there was not the same removal witnessed under anoxic conditions, but some oxygen-dependent process, like Fenton Chemistry.

The results of experiment 3 further point to reduction processes, and not chelation (Fig. A.3). Under oxic conditions, we found no effect of DOM concentration on fraction on Fe removed from the Steel IRIS Probes (Fig. A.3). Additionally, we observed after the experimental period that the majority of Fe in solution was of Fe^{+2} (reduced) redox state, and not the oxidized Fe^{III} (Fig. A.3). Since chelation occurs irrespective of redox state, there would be more Fe^{III} in solution than we observed, if chelation were a major force of Fe removal from the Steel IRIS Probes. However, we did observe some removal of Fe^{III} oxides that resulted in Fe^{+2} in solution across all treatments irrespective of microbial presence and DOM concentration. This suggests that an aerobic process, not related to reduction by bacteria or organic functional groups, is a source of some Fe removal from Steel IRIS Probes under the experimental condtions. These results led us to test whether Fenton Chemistry drives some of the Fe Removal under these conditions.

Fe Reduction – Biotic, Abiotic, or Both?

The results of experiment 2 (and experiment 4, to an extent) examine the role of soil bacteria in stimulating Fe reduction under different soil water conditions. We found that under saturated conditions (100% WFPS), with live soil that fraction of Fe removed was highest, indicating that Fe reducers play a large role in the signature of reducing conditions that the Steel IRIS Probes record (Fig. A.2). However, the 100% WFPS autoclaved soils also indicate a relatively high Fraction of Fe Removed. This suggests that the Steel IRIS Probes also record some abiotic Fe reduction.

While abiotic and biotic Fe reduction have similar effects on the release of sorbed nutrients and trace metals through dissolution of Fe minerals, there are certain differences in the

effects of biotic and abiotic Fe reduction on the carbon cycle. In microbially-mediated Fe reduction, soil bacteria utilize Fe^{III} as a terminal electron acceptor in respiration. Under most circumstances, the soil bacteria use organic carbon as the electron donor. This links Fe reduction to carbon respiration, and CO_2 release from soil, with wide-reaching implications on the soil carbon cycle. On the other hand, abiotic Fe reduction does not necessarily couple with organic carbon oxidation. Consequently, a high fraction of Fe removed from a Steel IRIS Probe cannot be directly linked to carbon oxidation. However, high fractions of Fe removal from a Steel IRIS Probe can be linked to nutrient, colloid, and trace metal release that is associated with reductive dissolution of Fe minerals, biotic or abiotic.

Fenton Chemistry and Removal of Fe-Oxides from Steel IRIS Probes

There was evidence in experiment 1 and 3 that Fenton Chemistry could potentially play a role in the removal of Fe^{III} oxides from the Steel IRIS Probe surface, so we designed experiment 4 to track Fenton reactions. Under oxic conditions and in the presence of Fe^{+2} and Fe^{+3}, Fe is either oxidized or reduced to form a hydroxyl or hydroperoxyl free radical. These free radicals are strong oxidants that go on to take part in other oxidation reactions. The hydroperoxyl free radical can be quenched through reduction of Fe^{III} to Fe^{+2} and the production of oxygen and a proton. The continuous creation and then quenching of free radicals could be driving Fe removal from the Steel IRIS Probes as both Fe^{+2} and Fe^{III} redox states are present.

We used treatments that had been used in the previous studies (100% and 25% WFPS) in addition to a water only treatment. We used Steel IRIS Probes, and also Steel IRIS Probes with no exposed Fe^0 (rusted ends) to determine whether Fe^0 exposed on the ends of the Steel IRIS Probe was acting as an electron source for abiotic Fe reduction to Fe^{+2} ($Fe^0 + 2\ Fe^{+3} \rightarrow 3\ Fe^{+2}$).

To test the Fenton Chemistry hypothesis, monitored hydrogen peroxide presence in all treatments. We used modified IRIS tubes (Fe Oxides painted on PVC) as a control, since on Fe^{III} is introduced to the system with this method.

In terms of Fe removal from the various passive redox probes, we found expected results that provide similar information as the previous experiments (Fig A.4). Hydrogen peroxide was detected in the water and saturated soil treatments of Steel IRIS Probes with and without rusted ends (Figs A.5 and A.6). We found hydrogen peroxide persistently in the water-only treatments (Figs. A.5 and A.6). That we detected hydrogen peroxide in both the autoclaved and live treatments indicates that this hydrogen peroxide presence was not due to enzymatic processes, but abiotic Fenton Chemistry.

While hydrogen peroxide was produced in the high water-content soils, it is not as likely that Fenton Chemistry is a major source of rust removal from the Steel IRIS Probes in field soil conditions. The experimental design provided no means by which the reactive free radicals could leave the system. Therefore, the free radicals persisted, potentially removing more Fe from the Steel IRIS Probe surface, creating a greater potential for more free radical production. However, this positive feedback loop would not exist in most natural soils, as drainage would inhibit any free radicals produced from continuously chipping away at the Steel IRIS surface. Fenton Chemistry may obscure the results of a Steel IRIS Probe installation if they are to be installed in continuously saturated soils with low hydraulic conductivities. This could be the case in depressions and wetlands, but probably not floodplains.

Soil Moisture and Fe Reduction – Reducing Conditions in Unsaturated soil

In experiments in which we varied soil water content (WFPS), we observed that there was Fe removed from the Steel IRIS Probes under unsaturated conditions. These findings corroborate well with other studies which indicate that anaerobic processes are potentially harbored within soil aggregates under unsaturated conditions due to low oxygen diffusion through water-filled micropores. Additionally, in-field studies have indicated that while nitrate and manganese reduction are more energetically favorable for microbial respiration, multiple respiration pathways are utilized simultaneous in the soil environment (Fe^{III}, Mn^{IV}, and NO_3^- reduction most likely occur in concert). The results from experiment 2 indicate that the Steel IRIS Probes successfully record Fe reduction that occurs under unsaturated conditions. This makes the probes especially well-suited to the study of upland soil profiles, which rarely undergo complete saturation, but often still have high potential to reduce iron.

CONCLUSIONS

We conducted a series of in-lab experiments to explore the mechanisms of Fe removal from Steel IRIS Probes. The experiments were designed to better understand the roles of microbially-mediated Fe reduction, chelation by DOM, abiotic Fe reduction (stimulated by various reducing agents), and Fenton Chemistry as a means of removing Fe-Oxides (rust) from the surface of the Steel IRIS Probes. We additionally sought to better define the role of moisture in mediating Fe reduction in soils, and determine whether Steel IRIS Probes successfully track Fe reduction under different moisture regimes. From our experiments we conclude that Fe removal is mainly due to microbial reduction, but there is some removal that could be attributed to Fe reduction by functional groups on DOM, or other reactive species in soil. The results also

indicate that chelation is not a predominant process in removing Fe from the Steel IRIS Probes. Our final experiment indicated that Fenton Chemistry could act as a means of removing Fe from the Steel IRIS Probes, but only in cases in which soil is saturated/the Steel IRIS is installed in stagnant water, and transport is limited for long periods of time allowing for formation and perpetuation of the peroxide free radicals. Finally, our experiments provided more evidence for high potential for Fe Reduction in upland soils under a range of soil moisture conditions. Indeed, the results of experiment 2 indicated that even at low soil moistures, some Fe reduction can occur in this Hawaiian soil. In summary, our results show that Fe removal from the Steel IRIS Probes is most closely linked to microbial Fe reduction, although it does take into account some abiotic Fe reduction, and, in very rare and specific cases uncommon to upland soils, Fenton Chemistry.

FIGURES

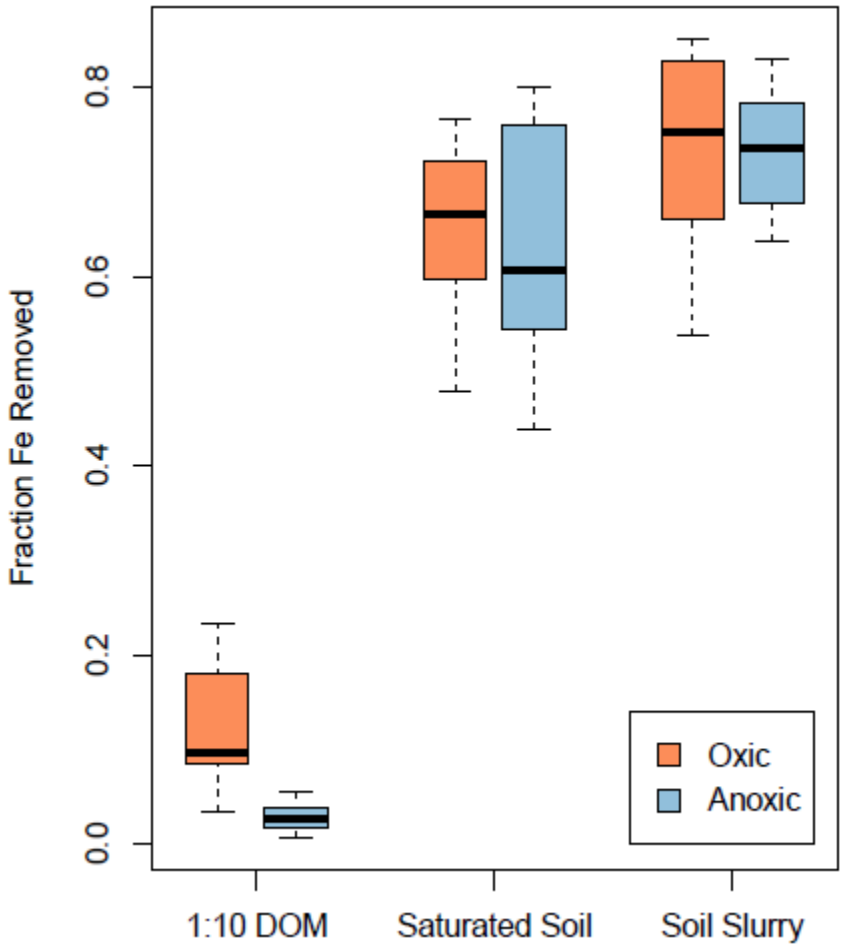

Figure A.1: Results from the first experiment examining the effect of 1:10 dissolved organic matter solution, saturated soil conditions, and slurried soil on Fe removal from the steel IRIS probes under oxic and anoxic conditions. The box represents the middle 25-75% of the distribution, the outer whiskers represent the minimum and maximum, and the heavy middle line represents the median. The darker shade is the oxic treatment that was left exposed to ambient conditions. The lighter shade was kept inside an anoxic glovebox throughout the experiment. Both DOM treatments are significantly lower than the saturated and slurry soil conditions. The was no difference between the oxic and anoxic results within treatments.

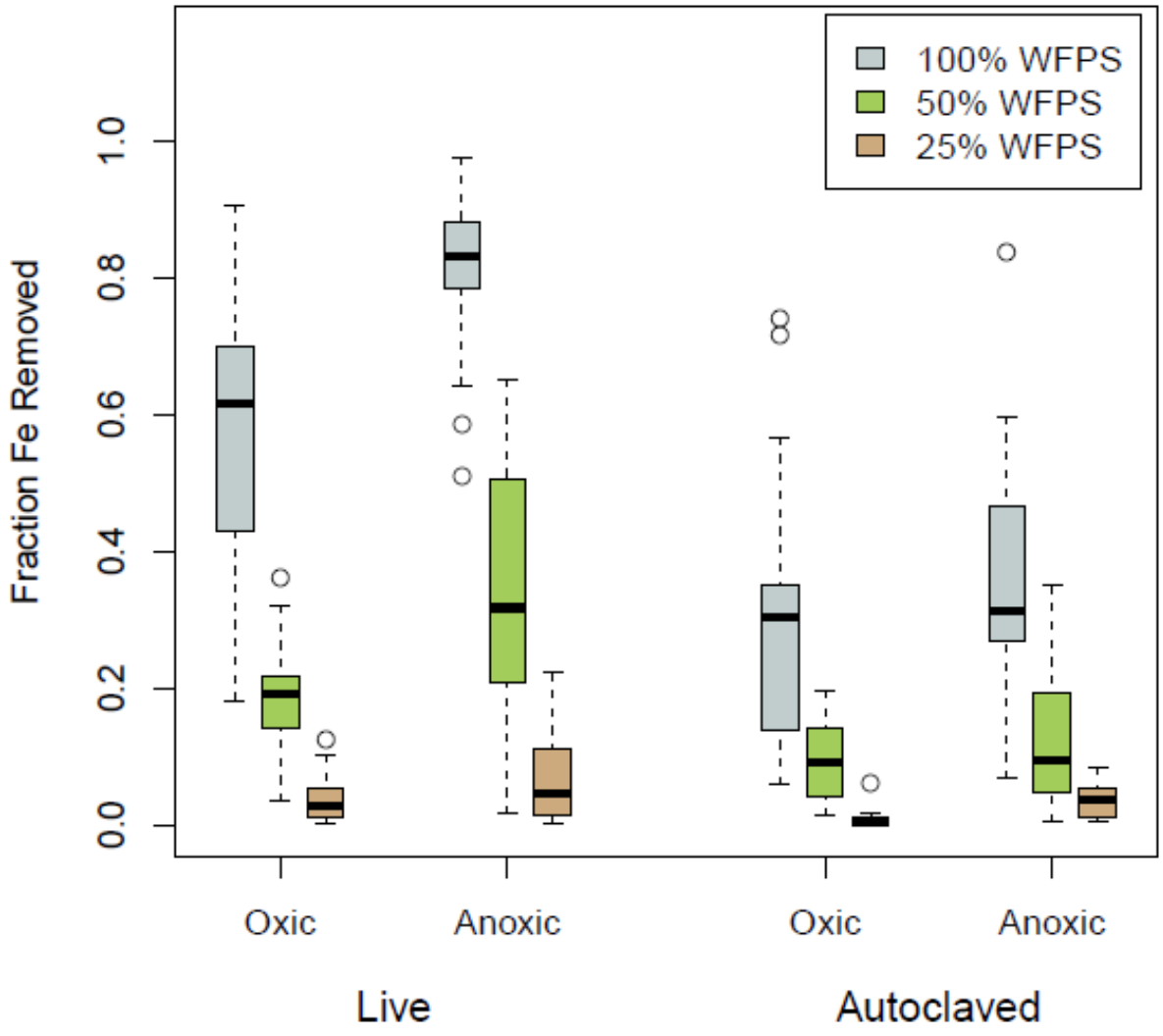

Figure A.2: Results from the second experiment examining the effect of soil water content (WFPS), soil microorganisms, and ambient oxygen conditions on Fe removal from the steel IRIS probes. Blue represents 100% WFPS (saturation), the green represents 50% WFPS, and the pink represents 25% WFPS. The box represents the middle 25-75% of the distribution, the outer whiskers represent the minimum and maximum, and the heavy middle line represents the median. Circles represent outliers. Generally, the anoxic, wetter, and live treatments generated more Fe removal than the other treatments.

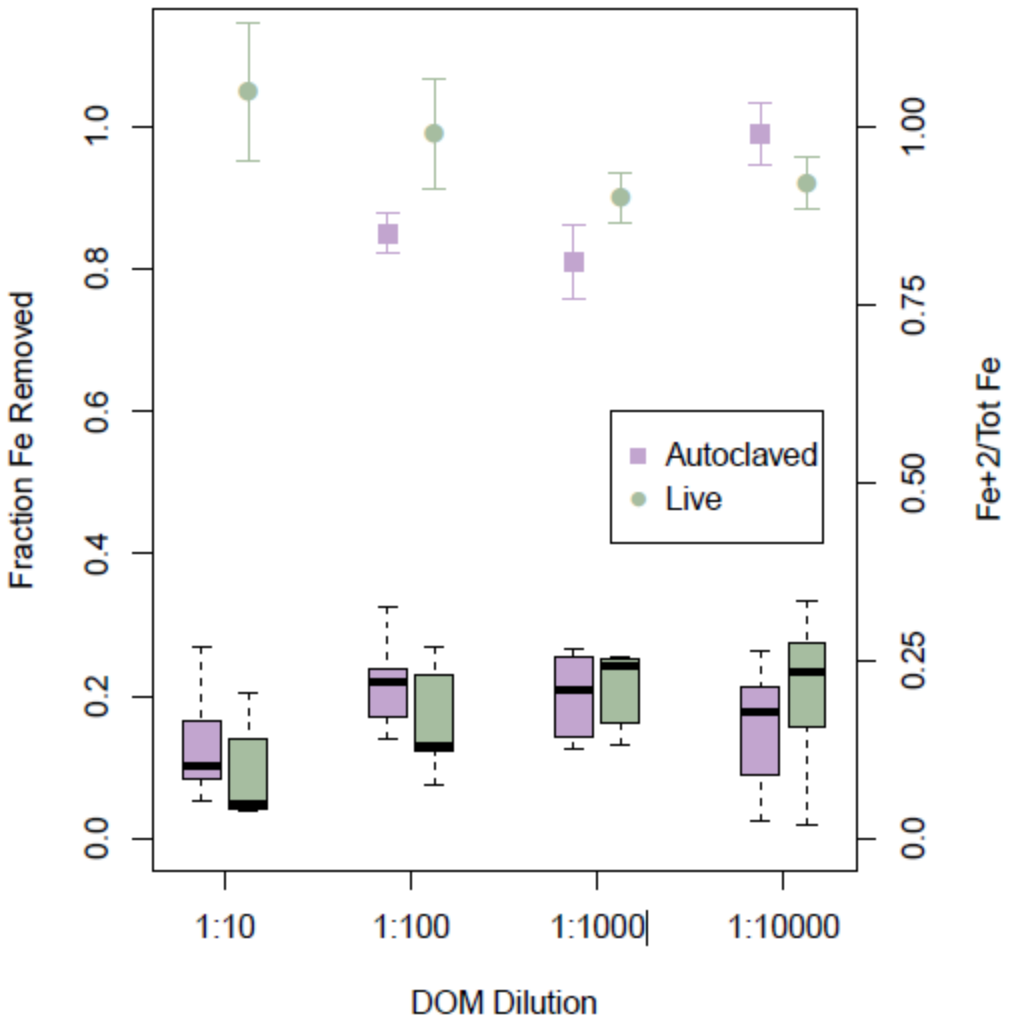

Figure A.3: Next experiment examining the effect of DOM concentration on Fe removal from Steel IRIS rods along with Fe redox state in solution after removal. Boxplots represent the fraction of Fe removed from the Steel IRIS probes, and the points represent the average Fe^{+2}/Fe^{tot} ratio of the DOM solutions after the two week experimental period. . The box represents the middle 25-75% of the distribution, the outer whiskers represent the minimum and maximum, and the heavy middle line represents the median. Whiskers out of the Fe redox state points represent one standard error from the mean. There was no treatment effect with DOM concentration, and all measured treatment Fe ratios indicate predominately Fe^{+2} in solution.

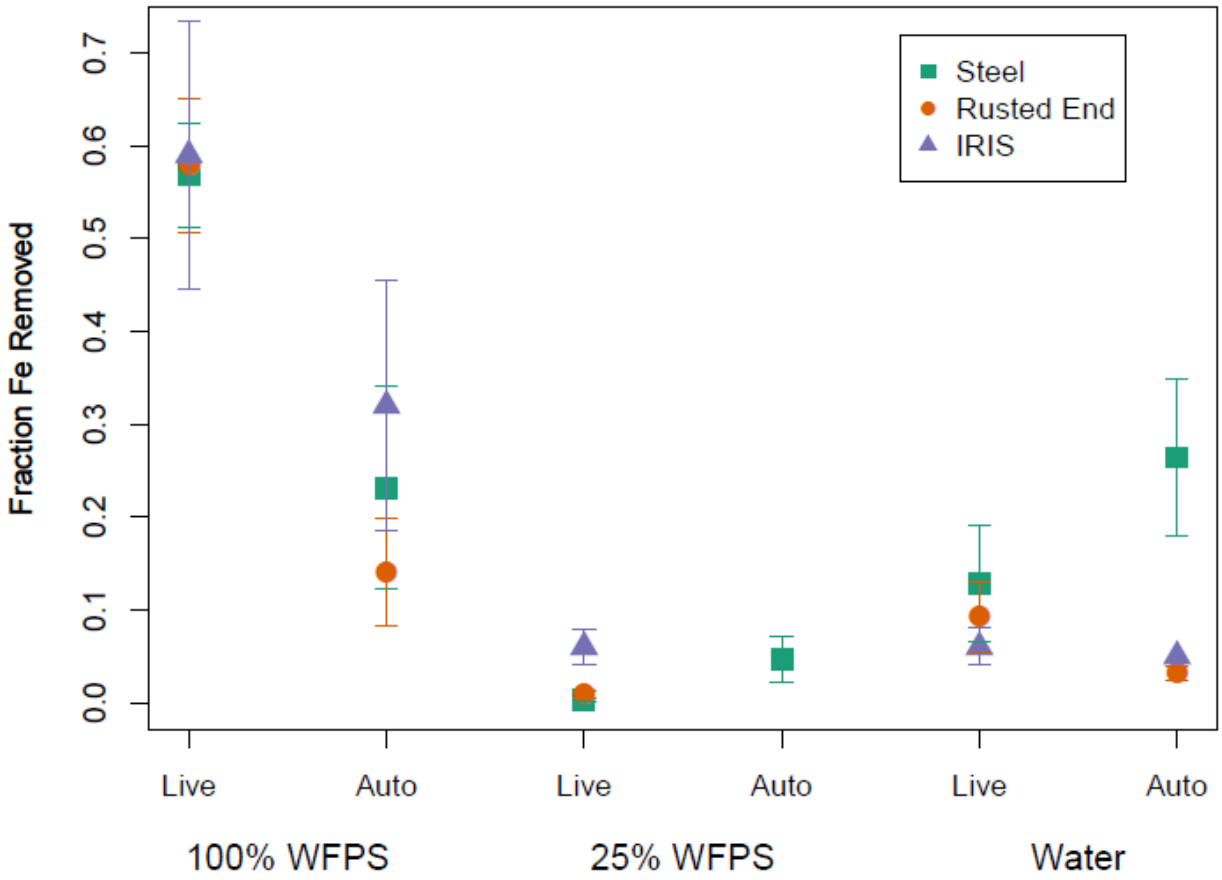

Figure A.4: Fraction of Fe removed from the treatments of experiment 4 comparing Fe removal from Steel Iris Probes (square), Steel IRIS Probes with rusted ends (circle), and modified IRIS Tubes (triangle), in live and autoclaved (auto) soil with 100%, 25% WFPS, and in water. Points represent the mean of the measurements made in triplicate. Error bars represent one standard error from the mean. The different passive probes are not significantly different, except for in the autoclaved water treatment in which the steel IRIS without rusted ends is significantly higher than the others. The IRIS Tube treatments in 100% WFPS have much more variability.

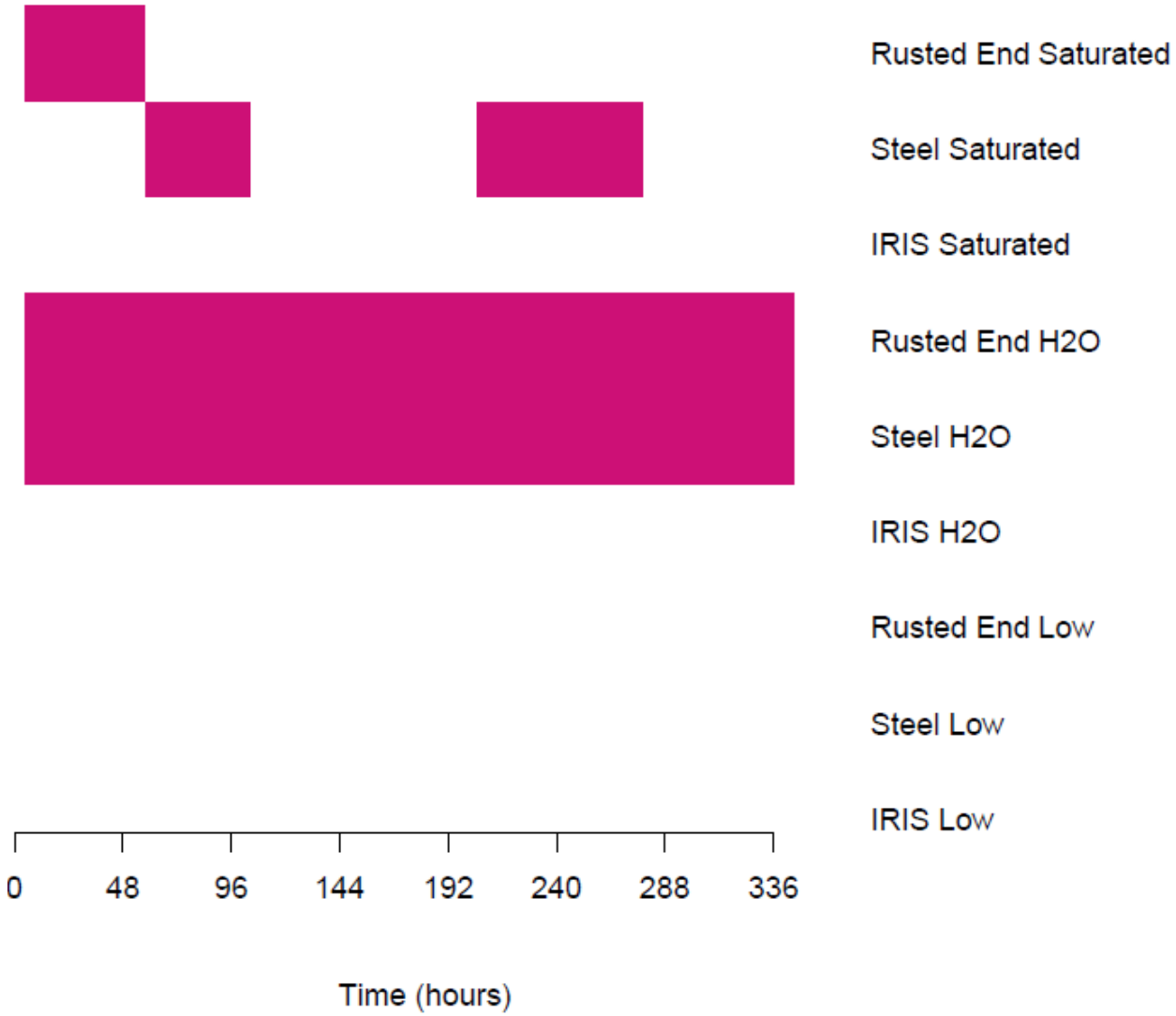

Figure A.5: Presence of hydrogen peroxide in the solution of each live treatment over the two week sampling period. Pink indicates presence of Hydrogen peroxide. Measurements were taken at hour 0, 6, 18, 45, 72, 120, 168, 216, 288, and 336 (end point). Hydrogen peroxide persisted in the treatments with steel IRIS (rusted and unrusted ends) in water. This indicates that hydroxide free radicals were created that could facilitate the removal of Fe oxide from the steel surface.

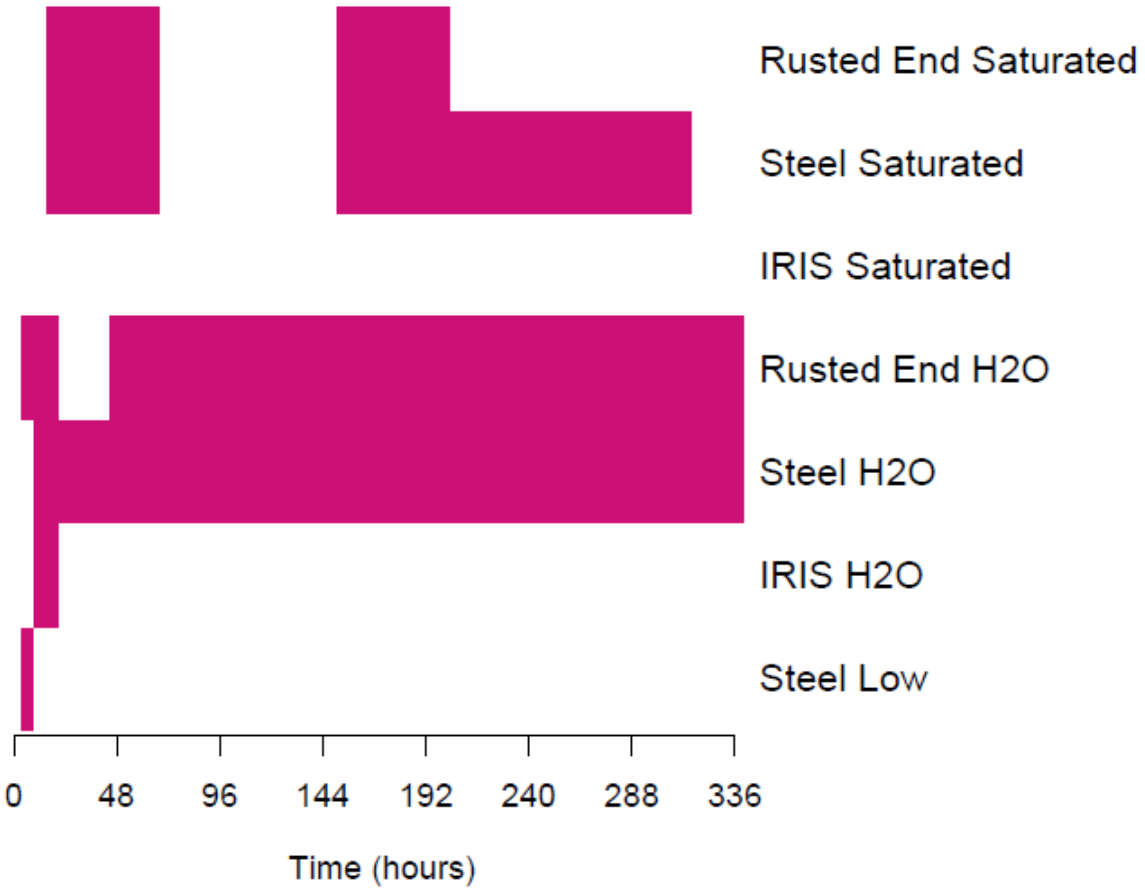

Figure A.6: Presence of hydrogen peroxide in the solution of each autoclaved treatment over the two week sampling period. Pink indicates presence of Hydrogen peroxide. Measurements were taken at hour 0, 6, 18, 45, 72, 120, 168, 216, 288, and 336 (end point). Hydrogen peroxide persisted in the treatments with steel IRIS (rusted and unrusted ends) in water. This indicates that hydroxide free radicals were created that could facilitate the removal of Fe oxide from the steel surface.

APPENDIX B

MULTIPLE LINEAR REGRESSION MODELS DESCRIBING FE REMOVAL FROM STEEL IRIS PROBES

Table B.1 October 2015 0-60+ cm MLR

	Model A		Model B	
	Coefficient	Probability Statistic	Coefficient	Probability Statistic
Intercept	0.2197	0.2359	0.07139	$1.07 * 10^{-8}$
HCP Mean	0.03056	0.1273		
PRP Mean	$-3.005 * 10^{-3}$	0.8364		
Plan Curvature	$-1.226 * 10^{-3}$	0.2883		
Profile Curvature	$-3.164 * 10^{-3}$	0.0729	-0.00238	0.144
Aspect	$-1.499 * 10^{-3}$	0.1024		
Elevation	$-6.636 * 10^{-5}$	0.9486		
R Squared	0.2889		0.08357	
Adjusted R Squared	0.07558		0.04691	
p-value	0.2803		0.1436	

Table B.2 October 2015 0-10 cm MLR

	Model A		Model B	
	Coefficient	Probability Statistic	Coefficient	Probability Statistic
Intercept	0.08164	0.2435	0.00169	0.7861
HCP Mean	$-5.069 * 10^{-3}$	0.4928		
PRP Mean	0.01488	0.0126	0.01015	0.0164
Plan Curvature	$-8.74 * 10^{-5}$	0.8390		
Profile Curvature	$-1.285 * 10^{-4}$	0.8409		
Aspect	$2.823 * 10^{-5}$	0.4034		
Elevation	$-4.657 * 10^{-4}$	0.2239		
R Squared	0.3284		0.2094	
Adjusted R Squared	0.127		0.1778	
p-value	0.1907		0.0164	

Table B.3 October 2015 10-20 cm MLR

	Model A	
	Coefficient	Probability Statistic
Intercept	0.3004	0.297
HCP Mean	-0.02796	0..362
PRP Mean	0.03376	0.147
Plan Curvature	$-8.990 * 10^{-4}$	0.613
Profile Curvature	$-3.99 * 10^{-3}$	0.142
Aspect	$-1.618 * 10^{-4}$	0.250
Elevation	$-1.010 * 10^{-3}$	0.517
R Squared	0.1986	
Adjusted R Squared	-0.04186	
p-value	0.5634	

Table B.4 October 2015 20-30 cm MLR

	Model A		Model B	
	Coefficient	Probability Statistic	Coefficient	Probability Statistic
Intercept	0.2662	0.3190	0.3683	0.000698
HCP Mean	-0.06312	0.0345	-0.05490	0.0221
PRP Mean	0.0136	0.5207		
Plan Curvature	$-8.477 * 10^{-4}$	0.608		
Profile Curvature	$3.362 * 10^{-4}$	0.8910		
Aspect	$-3.839* 10^{-4}$	0.00665	$-3.424 * 10^{-4}$	0.006557
Elevation	$7.568 * 10^{-4}$	0.6006		
R Squared	0.3417		0.2877	
Adjusted R Squared	0.1442		0.2283	
p-value	0.1656		0.01707	

Table B.5 October 2015 30-40 cm MLR

	Model A		Model B	
	Coefficient	Probability Statistic	Coefficient	Probability Statistic
Intercept	0.6376	0.0402	0.3907	0.00119
HCP Mean	-0.08151	0.0162	-0.06958	0.01078
PRP Mean	0.01445	0.5406		
Plan Curvature	$-1.734 * 10^{-3}$	0.3513		
Profile Curvature	$-1.665 * 10^{-3}$	0.5446		
Aspect	$-2.995 * 10^{-4}$	0.470	$-2.739 * 10^{-4}$	0.04436
Elevation	$-1.427 * 10^{-3}$	0.3792		
R Squared	0.3166		0.2519	
Adjusted R Squared	0.1116		0.1896	
p-value	0.215		0.03072	

Table B.6 October 2015 40-50 cm MLR

	Model A		Model B	
	Coefficient	Probability Statistic	Coefficient	Probability Statistic
Intercept	0.0137	0.9617	0.06702	$7.88 * 10^{-5}$
HCP Mean	-0.0182	0.553		
PRP Mean	-0.0375	0.1113		
Plan Curvature	$-3.341 * 10^{-3}$	0.0721	$-3.723 * 10^{-3}$	0.0464
Profile Curvature	$-4.78 * 10^{-3}$	0.0827	$-5.057 * 10^{-3}$	0.0697
Aspect	$-5.898 * 10^{-5}$	0.6715		
Elevation	$1.158 * 10^{-3}$	0.4600		
R Squared	0.3816		0.2015	
Adjusted R Squared	0.1961		0.1349	
p-value	0.1049		0.0672	

Table B.7 October 2015 50-60+ cm MLR

	Model A		Model B	
	Coefficient	Probability Statistic	Coefficient	Probability Statistic
Intercept	0.4546	0.2795	0.0821	$2.57 * 10^{-4}$
HCP Mean	-0.03392	0.4466		
PRP Mean	-0.02655	0.4261		
Plan Curvature	$-2.377 * 10^{-3}$	0.3636		
Profile Curvature	$-8.89 * 10^{-3}$	0.0299	$-7.99 * 10^{-3}$	0.0335
Aspect	$-6.835 * 10^{-5}$	0.7350		
Elevation	$-1.306 * 10^{-3}$	0.5654		
R Squared	0.3816		0.1683	
Adjusted R Squared	0.1961		0.135	
p-value	0.1049		0.0336	

Table B.8 March 2016 0-60+ cm

	Model A	
	Coefficient	Probability Statistic
Intercept	0.2175	0.115
HCP Mean	0.00394	0.558
PRP Mean	0.004189	0.773
Plan Curvature	0.001906	0.117
Profile Curvature	0.001575	0.274
Aspect	$-7.43 * 10^{-5}$	0.211
Elevation	$-8.34 * 10^{-4}$	0.325
PRP Pre	-0.00425	0.772
HCP Pre	0.00502	0.701
R Squared	0.08412	
Adjusted R Squared	-0.01765	
p-value	0.582	

Table B.9 March 2016 0-10 cm

	Model A	
	Coefficient	Probability Statistic
Intercept	0.339	0.0478
HCP Mean	0.00471	0.5708
PRP Mean	0.00966	0.5903
Plan Curvature	$-1.28 * 10^{-4}$	0.9316
Profile Curvature	$1.688 * 10^{-3}$	0.3412
Aspect	$-2.066 * 10^{-5}$	0.7772
Elevation	$-1.296 * 10^{-3}$	0.2152
PRP Pre	$6.988 * 10^{-3}$	0.6999
HCP Pre	-0.1202	0.4570
R Squared	0.0744	
Adjusted R Squared	-0.02844	
p-value	0.6702	

Table B.10 March 2016 10-20 cm

	Model A		Model B		Model C	
	Coefficient	Probability Statistic	Coefficient	Probability Statistic	Coefficient	Probability Statistic
Intercept	0.1865	0.3355	0.1068	$2 * 10^{-16}$	0.109	$2 * 10^{-16}$
HCP Mean	$-5.62 * 10^{-3}$	0.5538				
PRP Mean	$3.042 * 10^{-3}$	0.1403				
Plan Curvature	$4.57 * 10^{-3}$	0.00862	0.004621	0.00705	0.00351	0.0261
Profile Curvature	$3.532 * 10^{-3}$	0.08358	0.003217	0.09982		
Aspect	$-1.248 * 10^{-4}$	0.1376				
Elevation	$-6.819 * 10^{-4}$	0.5665				
PRP Pre	$-3.299 * 10^{-2}$	0.1142				
HCP Pre	$2.107 * 10^{-2}$	0.2553				
R Squared	0.1548		0.09334		0.06911	
Adjusted R Squared	0.0609		0.07009		0.04921	
p-value	0.1265		0.0219		0.02611	

Table B.11 March 2016 20-30 cm

	Model A		Model B		Model C	
	Coefficient	Probability Statistic	Coefficient	Probability Statistic	Coefficient	Probability Statistic
Intercept	$-4.254 * 10^{-3}$	0.9824	0.06029	0.2373	0.150	$2.18 * 10^{-11}$
HCP Mean	$-7.451 * 10^{-3}$	0.4331				
PRP Mean	$8.721 * 10^{-3}$	0.6703				
Plan Curvature	$3.502 * 10^{-3}$	0.04216	0.003558	0.0349	2.299	0.02419
Profile Curvature	$5.445 * 10^{-3}$	0.00855	0.005051	0.0100	$5.33 * 10^{-3}$	0.00744
Aspect	$-1.623 * 10^{-4}$	0.05483	$-1.617 * 10^{-4}$	0.0464	$-1.617 * 10^{-4}$	0.05010
Elevation	$3.565 * 10^{-4}$	0.7643				
PRP Pre	$-1.265 * 10^{-2}$	0.5418				
HCP Pre	$3.517 * 10^{-2}$	0.0596	0.0245	0.0598		
R Squared	0.1917		0.1793		0.1399	
Adjusted R Squared	0.1019		0.1361		0.1064	
p-value	0.0432		0.00428		0.00869	

Table B.12 March 2016 30-40 cm

	Model A		Model B	
	Coefficient	Probability Statistic	Coefficient	Probability Statistic
Intercept	0.2803	0.1368	0.05148	0.04427
HCP Mean	0.0196	0.03556	0.0171	0.02192
PRP Mean	$-8.034 * 10^{-3}$	0.6854		
Plan Curvature	$4.844 * 10^{-3}$	0.00421	0.00478	0.00409
Profile Curvature	$3.872 * 10^{-3}$	0.0508	0.00396	0.03912
Aspect	$-6.673 * 10^{-5}$	0.4099		
Elevation	$-1.561 * 10^{-3}$	0.1777		
PRP Pre	-0.01431	0.4763		
HCP Pre	0.01367	0.4447		
R Squared	0.2216		0.1725	
Adjusted R Squared	0.1351		0.1402	
p-value	0.01619		0.00212	

Table B.13 March 2016 40-50 cm

	Model A		Model B	
	Coefficient	Probability Statistic	Coefficient	Probability Statistic
Intercept	0.3633	0.0242	0.3568	0.0177
HCP Mean	0.0132	0.0927	2.513	0.0140
PRP Mean	0.01259	0.4546		
Plan Curvature	$3.211 * 10^{-3}$	0.0236	0.00293	0.210
Profile Curvature	$8.603 * 10^{-4}$	0.6041		
Aspect	$-9.666 * 10^{-5}$	0.1608		
Elevation	$-2.088 * 10^{-3}$	0.0350	-0.00203	0.0296
PRP Pre	-0.01093	0.5206		
HCP Pre	$6.607 * 10^{-3}$	0.6625		
R Squared		0.207		0.1772
Adjusted R Squared		0.1189		0.1451
p-value		0.02641		0.001725

Table B.14 March 2016 50-60+ cm

	Model A		Model B	
	Coefficient	Probability Statistic	Coefficient	Probability Statistic
Intercept	0.03998	0.8121	0.02871	0.2369
HCP Mean	0.01892	0.0245	0.016932	0.0112
PRP Mean	0.01890	0.2909		
Plan Curvature	$-5.470 * 10^{-4}$	0.7116		
Profile Curvature	$-1.149 * 10^{-3}$	0.5143		
Aspect	$6.145 * 10^{-5}$	0.3988		
Elevation	$2.72 * 10^{-4}$	0.7927		
PRP Pre	$-4.279 * 10^{-3}$	0.8125		
HCP Pre	$-2.501 * 10^{-2}$	0.1225		
R Squared	0.1515		0.0786	
Adjusted R Squared	0.05726		0.06693	
p-value	0.1378		0.01124	

Table B.15 March 2016 WS3 0-60+ cm MLR

	Model A		Model B	
	Coefficient	Probability Statistic	Coefficient	Probability Statistic
Intercept	$-1.4 * 10^{-1}$	0.3943	$6.221 * 10^{-2}$	0.00027
HCP Mean	$-5.542 * 10^{-3}$	0.7931		
PRP Mean	$-1.695 * 10^{-2}$	0.2224		
Plan Curvature	$-1.530 * 10^{-3}$	0.2800		
Profile Curvature	$-1.139 * 10^{-5}$	0.9941		
Aspect	$1.899 * 10^{-4}$	0.0506	$1.227 * 10^{-4}$	0.043
Elevation	$1.183 * 10^{-3}$	0.2566		
PRP Post	$-4.196 * 10^{-3}$	0.7587		
HCP Post	$2.595 * 10^{-3}$	0.8225		
PRP Pre	$2.072 * 10^{-2}$	0.1233		
HCP Pre	$3.001 * 10^{-3}$	0.8670		
R Squared	0.3068		0.115	
Adjusted R Squared	0.02946		0.08901	
p-Value	0.3953		0.04301	

Table B.16 March 2016 WS3 0-10 cm MLR

	Model A		Model B	
	Coefficient	Probability Statistic	Coefficient	Probability Statistic
Intercept	$6.121 * 10^{-2}$	0.818	$4.179 * 10^{-2}$	0.09106
HCP Mean	$-4.225 * 10^{-3}$	0.903		
PRP Mean	$-5.948 * 10^{-3}$	0.790		
Plan Curvature	$2.001 * 10^{-4}$	0.930		
Profile Curvature	$-2.250 * 10^{-4}$	0.929		
Aspect	$2.894 * 10^{-4}$	0.067	$3.1795 * 10^{-4}$	0.0014
Elevation	$5.013 * 10^{-5}$	0.976		
PRP Post	$-1.773 * 10^{-2}$	0.430		
HCP Post	$1.619 * 10^{-2}$	0.395		
PRP Pre	$2.773 * 10^{-2}$	0.203		
HCP Pre	$-1.304 * 10^{-2}$	0.657		
R Squared	0.3719		0.2613	
Adjusted R Squared	0.1206		0.2396	
p-value	0.2048		0.0014	

Table B.17 March 2016 WS3 10-20 cm MLR

Model A		
	Coefficient	Probability Statistic
Intercept	-0.2678	0.318
HCP Mean	-0.0179	0.603
PRP Mean	0.00504	0.821
Plan Curvature	0.00108	0.636
Profile Curvature	0.00362	0.156
Aspect	0.000211	0.173
Elevation	0.00185	0.274
PRP Post	-0.0145	0.514
HCP Post	-0.0198	0.298
PRP Pre	-0.0114	0.595
HCP Pre	0.0468	0.117
R Squared	0.3234	
Adjusted R Squared	0.05274	
p-value	0.3403	

Table B.18 March 2016 WS3 20-30 cm MLR

Model A		
	Coefficient	Probability Statistic
Intercept	-0.310	0.183
HCP Mean	-0.000790	0.790
PRP Mean	-0.0135	0.485
Plan Curvature	-0.000263	0.893
Profile Curvature	0.00335	0.129
Aspect	0.0000141	0.286
Elevation	0.00169	0.248
PRP Post	-0.00512	0.789
HCP Post	0.00513	0.751
PRP Pre	0.00325	0.859
HCP Pre	0.0399	0.121
R Squared	0.3429	
Adjusted R Squared	0.08	
p-value	0.2811	

Table B.19 March 2016 WS3 30-40 cm MLR

	Model A		Model B	
	Coefficient	Probability Statistic	Coefficient	Probability Statistic
Intercept	-0.0855	0.232	0.1109	$1.64 * 10^{-6}$
HCP Mean	0.0273	0.370		
PRP Mean	-0.0416	0.042	-0.0168	0.198
Plan Curvature	0.000450	0.823		
Profile Curvature	0.00253	0.258		
Aspect	$1.95 * 10^{-4}$	0.153		
Elevation	$2.93 * 10^{-3}$	0.843		
PRP Post	0.0120	0.543		
HCP Post	-0.00631	0.703		
PRP Pre	0.0137	0.467		
HCP Pre	0.00642	0.803		
R Squared	0.2586		0.04834	
Adjusted R Squared	-0.03796		0.02035	
p-Value	0.5699		0.1976	

Table B.20 March 2016 WS3 40-50 cm MLR

	Model A		Model B	
	Coefficient	Probability Statistic	Coefficient	Probability Statistic
Intercept	0.0659	0.7229	$5.688 * 10^{-2}$	0.00405
HCP Mean	0.0166	0.4917		
PRP Mean	-0.0116	0.4578		
Plan Curvature	-0.00319	0.0538	$-1.637 * 10^{-3}$	0.2211
Profile Curvature	-0.00219	0.2184		
Aspect	0.000186	0.0895	$4.94 * 10^{-5}$	0.4821
Elevation	-0.000263	0.8226		
PRP Post	0.02306	0.1461		
HCP Post	-0.01225	0.3557		
PRP Pre	0.02436	0.1118		
HCP Pre	-0.0240	0.2461		
R Squared	0.2754		0.05154	
Adjusted R Squared	-0.01441		-0.00594	
p-Value	0.5073		0.4176	

Table B.21 March 2016 WS3 50-60+ cm MLR

	Model A		Model B		Model C	
	Coefficient	Probability Statistic	Coefficient	Probability Statistic	Coefficient	Probability Statistic
Intercept	-0.542	0.1231	-0.2661	0.4020	-0.252	0.4261
HCP Mean	0.0154	0.7297				
PRP Mean	0.00973	0.7354				
Plan Curvature	-0.00667	0.0308	-0.00575	0.0552	-0.004306	0.0933
Profile Curvature	-0.00640	0.0565	-0.00274	0.3300		
Aspect	0.000142	0.4732				
Elevation	0.00418	0.0623	0.00345	0.0892	0.003381	0.0952
PRP Post	-0.0155	0.5894				
HCP Post	0.0344	0.1651				
PRP Pre	0.0312	0.2648				
HCP Pre	-0.0679	0.0808	-0.0550	0.0532	-0.0551	0.0525
R Squared	0.2754		0.2323		0.208	
Adjusted R Squared	-0.01441		0.1332		0.1338	
p-Value	0.5073		0.07644		0.05562	

Table B.22 June 2016 0-60+ cm MLR

	Model A		Model B		Model C	
	Coefficient	Probability Statistic	Coefficient	Probability Statistic	Coefficient	Probability Statistic
Intercept	-0.0891	0.2262	-0.0533	0.3287	0.04777	$9.17 * 10^{-6}$
HCP Mean	$8.568 * 10^{-3}$	0.0342	$5.463 * 10^{-3}$	0.0726		
PRP Mean	$-4.450 * 10^{-3}$	0.4420				
Plan Curvature	$8.66 * 10^{-5}$	0.8572				
Profile Curvature	$-1.858 * 10^{-4}$	0.66-19				
Aspect	$1.782 * 10^{-5}$	0.5003				
Elevation	$8.791 * 10^{-4}$	0.0806	$6.219 * 10^{-3}$	0.0732		
PRP Post	$-3.122 * 10^{-3}$	0.3738				
HCP Post	$-5.349 * 10^{-3}$	0.0436	$-5.885 * 10^{-3}$	0.0152	$-3.088 * 10^{-3}$	0.117
PRP Pre	$-1.197 * 10^{-3}$	0.4448				
HCP Pre	$-7.152 * 10^{-4}$	0.6710				
R Squared	0.1528		0.107		0.03252	
Adjusted R Squared	0.02443		0.07034		0.01962	
p-Value	0.3136		0.03984		0.1166	

Table B.23 June 2016 0-10 cm MLR

	Model A	
	Coefficient	Probability Statistic
Intercept	$-1.962 * 10^{-3}$	0.960
HCP Mean	$5.518 * 10^{-4}$	0.794
PRP Mean	$-1.47 * 10^{-3}$	0.632
Plan Curvature	$1.631 * 10^{-4}$	0.524
Profile Curvature	$-1.928 * 10^{-4}$	0.394
Aspect	$6.541 * 10^{-6}$	0.641
Elevation	$1.759 * 10^{-4}$	0.506
PRP Post	$-1.797 * 10^{-3}$	0.336
HCP Post	$-8.516 * 10^{-4}$	0.540
PRP Pre	$1.474 * 10^{-4}$	0.859
HCP Pre	$-1.006 * 10^{-3}$	0.263
R Squared	0.09075	
Adjusted R Squared	-0.04702	
p-Value	0.7579	

Table B.24 June 2016 10-20 cm MLR

	Model A	
	Coefficient	Probability Statistic
Intercept	$-4.662 * 10^{-3}$	0.869
HCP Mean	$1.088 * 10^{-3}$	0.482
PRP Mean	$1.689 * 10^{-3}$	0.452
Plan Curvature	$-2.703 * 10^{-4}$	0.151
Profile Curvature	$-1.653 * 10^{-4}$	0.318
Aspect	$1.067 * 10^{-5}$	0.299
Elevation	$8.472 * 10^{-5}$	0.661
PRP Post	$9.837 * 10^{-4}$	0.470
HCP Post	$-5.833 * 10^{-4}$	0.565
PRP Pre	$-2.375 * 10^{-4}$	0.695
HCP Pre	$-5.593 * 10^{-4}$	0.393
R Squared	0.1081	
Adjusted R Squared	-0.02709	
p-Value	0.6295	

Table B.25 June 2016 20-30 cm MLR

	Model A		Model B		Model C		Model D	
	Coef.	Prob. Stat.	Coef.	Prob. Stat.	Coef.	Prob. Stat.	Coef.	Prob. Stat.
Intercept	-0.06100	0.3369	-0.06269	0.2756	0.03216	0.000342	0.01923	$8.31 * 10^{-11}$
HCP Mean	$1.956 * 10^{-3}$	0.5707						
PRP Mean	$-4.650 * 10^{-3}$	0.3543						
Plan Curvature	$-1.007 * 10^{-3}$	0.0180	$-1.266 * 10^{-3}$	0.00208	$-1.231 * 10^{-3}$	0.002976	$-1.203 * 10^{-3}$	0.00392
Profile Curvature	$4.072 * 10^{-4}$	0.2707						
Aspect	$9.524 * 10^{-6}$	0.6772						
Elevation	$7.549 * 10^{-4}$	0.0833	$6.823 * 10^{-4}$	0.09708				
PRP Post	$3.946 * 10^{-4}$	0.8965						
HCP Post	$-1.790 * 10^{-3}$	0.4298						
PRP Pre	$-1.670 * 10^{-3}$	0.2199						
HCP Pre	$-2.719 * 10^{-3}$	0.0657	$-2.884 * 10^{-3}$	0.02354	$-1.484 * 10^{-3}$	0.1183		
R Squared	0.2483		0.1671		0.1348		0.1056	
Adjusted R Squared	0.1344		01328		0.1115		0.09372	
p-Value	0.02985		0.003785		0.004705		0.003923	

Table B.26 June 2016 30-40 cm MLR

	Model A		Model B	
	Coefficient	Probability Statistic	Coefficient	Probability Statistic
Intercept	-0.1445	0.1595	0.0382	0.000855
HCP Mean	$4.374 * 10^{-3}$	0.4316		
PRP Mean	$-6.405 * 10^{-3}$	0.4279		
Plan Curvature	$-4.692 * 10^{-4}$	0.4855		
Profile Curvature	$-4.179 * 10^{-4}$	0.4815		
Aspect	$8.139 * 10^{-5}$	0.0300	$6.185 * 10^{-5}$	0.06303
Elevation	$1.094 * 10^{-3}$	0.1186		
PRP Post	$9.486 * 10^{-4}$	0.8461		
HCP Post	$9.227 * 10^{-4}$	0.8001		
PRP Pre	$-3.627 * 10^{-3}$	0.0997	$-3.330 * 10^{-3}$	0.05124
HCP Pre	$-3.554 * 10^{-4}$	0.8797		
R Squared	0.1597		0.08744	
Adjusted R Squared	0.03233		0.06277	
p-Value	0.2747		0.03386	

Table B.27 June 2016 40-50 cm MLR

	Model A		Model B	
	Coefficient	Probability Statistic	Coefficient	Probability Statistic
Intercept	-0.05212	0.4853	0.0203	0.02343
HCP Mean	$7.915 * 10^{-3}$	0.0544	0.005186	0.06125
PRP Mean	$-7.572 * 10^{-3}$	0.2016		
Plan Curvature	$-1.962 * 10^{-4}$	0.6896		
Profile Curvature	$1.206 * 10^{-4}$	0.7809		
Aspect	$-7.966 * 10^{-6}$	0.7674		
Elevation	$4.293 * 10^{-3}$	0.3990		
PRP Post	$2.981 * 10^{-3}$	0.4052		
HCP Post	$-1.321 * 10^{-3}$	0.6202		
PRP Pre	$-3.199 * 10^{-3}$	0.0481	$-3.692 * 10^{-3}$	0.00798
HCP Pre	$9.440 * 10^{-4}$	0.5830		
R Squared	0.1597		0.09793	
Adjusted R Squared	0.03233		0.07355	
p-Value	0.2747		0.02208	

Table B.28 June 2016 50-60+ cm MLR

	Model A		Model B	
	Coefficient	Probability Statistic	Coefficient	Probability Statistic
Intercept	0.1783	0.2365	0.0382	0.0664
HCP Mean	0.0143	0.0828	0.0130	0.0371
PRP Mean	$8.126 * 10^{-4}$	0.9453		
Plan Curvature	$9.518 * 10^{-4}$	0.3363		
Profile Curvature	$6.091 * 10^{-4}$	0.4850		
Aspect	$-7.185 * 10^{-5}$	0.1871		
Elevation	$-9.967 * 10^{-4}$	0.3302		
PRP Post	$-4.592 * 10^{-3}$	0.5229		
HCP Post	-0.01002	0.0647	$-8.667 * 10^{-3}$	0.0767
PRP Pre	$1.054 * 10^{-3}$	0.7423		
HCP Pre	$3.717 * 10^{-3}$	0.2834		
R Squared	0.1235		0.06268	
Adjusted R Squared	-0.009284		0.03735	
p-Value	0.5118		0.09117	

APPENDIX C

MOSSBAUER AND SEM CHARACTERIZATION OF STEEL IRIS PROBES

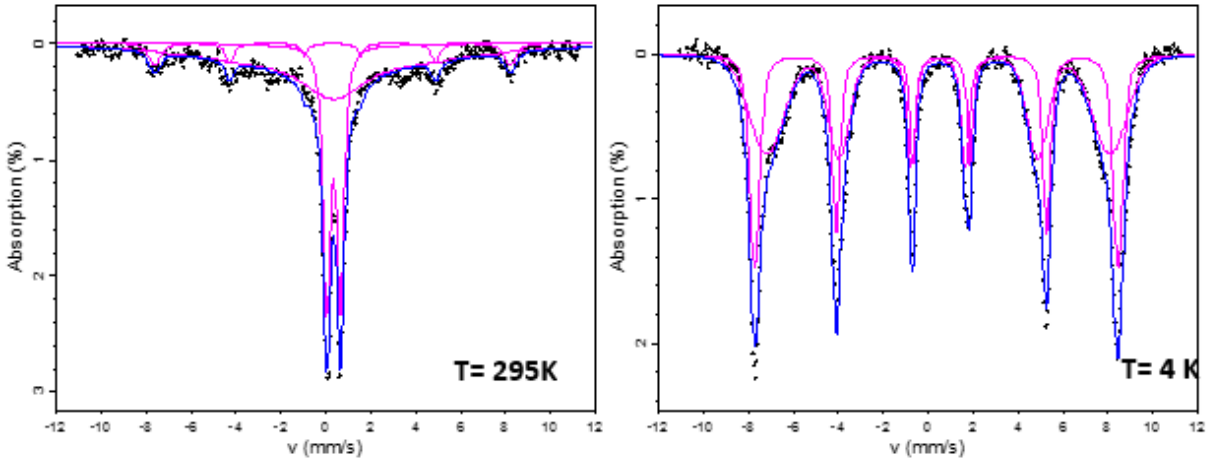

Figure C.1: Mossbauer spectra of shavings from a Steel IRIS Probe surface. Nano-goethite (43% of the spectral area) is the wide sextet at 4K with a quadruple splitting value of -0.12 mm s-1, and hyperfine field strength of 50.2 T; ferrihydrite (57% of spectral area) is the inner sextet at 4K with a quadruple splitting value of 0.002 mm s-1, and hyperfine field strength of 47.4 T.

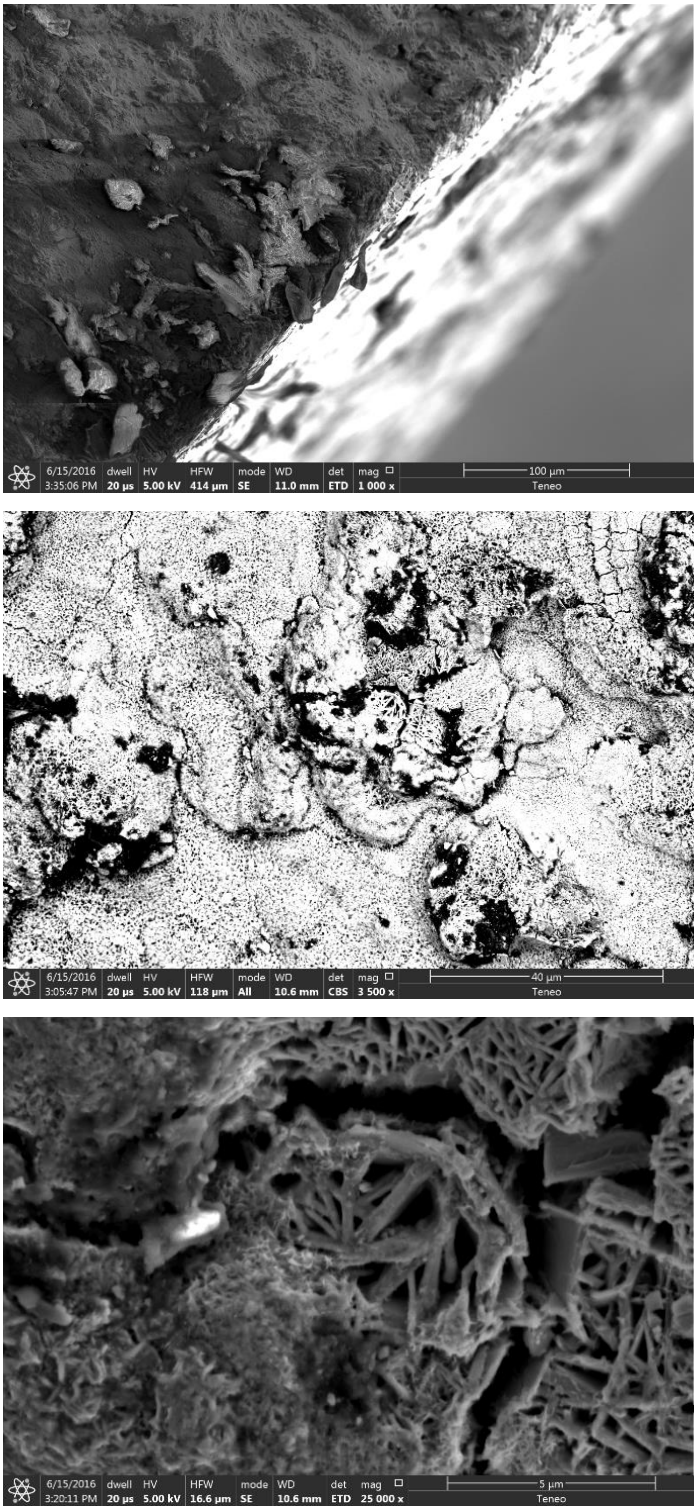

Figure C.2: SEM images of Steel IRIS Probes displaying crystalline structure and Fe oxide coating thickness.